JPL NO. 9950-396

AeroChem TP-392

DOE/JPL 954862-79/8
Distribution Category UC-63

(NASA-CR-163515) DEVELOPMENT OF A MODEL AND COMPUTER CODE TO DESCRIBE SOLAR GRADE SILICON PRODUCTION PROCESSES Final Report, 21 Sep. 1977 - 30 Sep. 1979 (AeroChem Research Labs., Inc.) 126 p HC A07/MF A01 CSCL G3/44

N80-31873

Unclas
28571

DEVELOPMENT OF A MODEL AND COMPUTER CODE TO DESCRIBE SOLAR GRADE SILICON PRODUCTION PROCESSES

FINAL REPORT

R. K. GOULD AND R. SRIVASTAVA

DECEMBER 1979

The JPL Low-Cost Solar Array Project is sponsored by the U. S. Department of Energy and forms part of the Solar Photovoltaic Conversion Program to initiate a major effort toward the development of low-cost solar arrays. This work was performed for the Jet Propulsion Laboratory, California Institute of Technology by agreement between NASA and DoE.

AeroChem Research Laboratories, Inc.
Princeton, New Jersey

AeroChem TP-392

DOE/JPL 954862-79/8
Distribution Category UC-63

DEVELOPMENT OF A MODEL AND COMPUTER CODE TO DESCRIBE SOLAR GRADE SILICON PRODUCTION PROCESSES

FINAL REPORT

R. K. GOULD AND R. SRIVASTAVA

DECEMBER 1979

JPL Contract No. 954862
DRL Item No.6, DRD No. DT
LSA Silicon Material Task

Approved by

Hartwell F. Calcote
Director of Research

AeroChem Research Laboratories, Inc.
Princeton, New Jersey

FOREWORD AND ACKNOWLEDGMENTS

This report covers the period 21 September 1977 to 30 September 1979. Dr. D.B. Olson and P.J. Howard contributed to the program. Helpful discussions with Professor D.E. Rosner of Yale University are gratefully acknowledged.

The code listings and user instructions (Appendixes B-H) are published in a separate supplementary volume, DOE/JPL-954862-79/8A.

ABSTRACT

This report describes models and computer codes which may be used to describe flow reactors in which high purity, solar grade silicon is produced via reduction of gaseous silicon halides. A prominent example of the type of process which may be studied using the codes developed in this program is the $SiCl_4/Na$ reactor currently being developed by the Westinghouse Electric Corp.

During this program two large computer codes were developed. The first is the CHEMPART code, an axisymmetric, marching code which treats two-phase flows with models describing detailed gas-phase chemical kinetics, particle formation, and particle growth. This code, based on the AeroChem LAPP (Low Altitude Plume Program) code can be used to describe flow reactors in which reactants mix, react, and form a particulate phase. Detailed radial gas-phase composition, temperature, velocity, and particle size distribution profiles are computed. Also, deposition of heat, momentum, and mass (either particulate or vapor) on reactor walls is described. The second code is a modified version of the GENMIX boundary layer code which is used to compute rates of heat, momentum, and mass transfer to the reactor walls. This code lacks the detailed chemical kinetics and particle handling features of the CHEMPART code but has the virtue of running much more rapidly than CHEMPART, while treating the phenomena occurring in the boundary layer in more detail than can be afforded using CHEMPART.

These two codes have been used in this program to predict particle formation characteristics and wall collection efficiencies for $SiCl_4/Na$ flow reactors. It is found that large input enthalpies (large H-atom inputs) are required to prevent $Si(\ell)$ droplet formation. (This enthalpy is supplied by introducing large quantities of arc-heated hydrogen in the Westinghouse reactor.) On the other hand, large hydrogen flows mean short transit times of gas through the reactor and hence short times for wall collection of Si. It is anticipated that an important application of these codes will be their use in finding operating conditions where droplet formation may be minimized and high collection efficiencies may still be realized in reactors of the Westinghouse type.

NOMENCLATURE: SECTIONS II-V

A^+	damping constant in Van Driest's mixing length formula
C_f	wall skin friction coefficient
D_i	mass diffusivity of species i (Fickian for vapor, Brownian for particles)
g	number of monomer units (approximate measure of particle size); see Eq. (24), Section II.
j_i''	mass flux of species i (kg m^{-2} s)
k_T, k_T'	"thermal diffusion ratios" defined in Eqs. (32) and (33), Section II.
K	pseudo "specific rate constant" defined by Eq. (45), Section IV (due to thermophoresis)
Kn_i	Knudsen number of species i ($\equiv 1/R_i$)
ℓ	mean free path of gas; also used for turbulence mixing length
M_c	molecular weight of "carrier gas"
M_i	molecular weight of species i
M_1	molecular weight of diffusing vapor (i.e., silicon monomer)
Nu	Nusselt number
p	pressure
r	radial distance measured from reactor tube centerline
R_i	radius of ith species (molecular or particle radius)
Re	Reynolds number
Sc_i	Schmidt number ($\equiv \mu/\delta\ D_i$) of species i
St	Stanton number
T	temperature
u	streamwise component of gas velocity in the developing boundary layer (downstream reactor region)
v	radial component of gas velocity in the developing boundary layer (downstream reactor region)
$\vec{V}_T$	thermal settling velocity (Section II)
x	streamwise distance along reactor tube length
x_i	mole fraction of species i

y	downstream distance measured from reactor tube wall
y_i	mass fraction of species i

Greek

α_d	fraction of molecules undergoing "diffuse reflection" from particle surface
α_i	thermal diffusion of thermophoretic factor for species i
α_m	momentum accommodation coefficient
α_o	value of α_i in the continuum limit ($Kn_i = 0$)
α_∞	value of α_i in the free-molecule limit ($Kn_i = \infty$)
Γ_h	exchange coefficient for heat transport
$\Gamma_{i,eff}$	effective exchange coefficient for mass transport
δ_m, δ_T	species and thermal boundary layer thicknesses
ε_p	eddy diffusivity
ε_i/k	energy-well-depth parameter in Lennard-Jones potential law
λ_i, λ_e	thermal conductivity of particle and carrier gas
μ	dynamic viscosity of gas
ν	kinematic viscosity of gas
ρ	density of gas
ρ_i	density of particle
σ_i	diameter of particle of species i

Subscripts

b	bulk property
c	centerline of carrier gas
CE	Chapman-Enskog
eff	effective
h	pertaining to heat transfer
i	species
m	pertaining to mass transfer; also used to indicate conditions at edge of species layer

mp	melting point
o	initial condition
r	radial or reference quantity
SEM	Stokes-Einstein-Millikan
W	quantity evaluated at the reactor tube wall
1	referring to monomer

NOMENCLATURE: SECTIONS VI-VIII*

$a_{1/2}$	defined by Eq. (71), Section VI.
A	constant in expression for k_f (see Eq. (61)) (RC(K,1))
$b_{1/2}$	defined under Eq. (63), Section VI.
B	activation energy (see Eq. (61)) (RC(K,3))
c_p	specific heat of mixture $(\sum_i X_i c_{p_i})$(CPBAR(K))
c_{p_i}	specific heat of ith species (CPTB(I,K))
D_i	diffusion (Brownian) coefficient for particles, ith mass class
E_o	turbulence energy dissipation (TURDIS)
f_{p_i}	ratio of actual drag coefficient to Stokes flow drag coefficient for particles, ith mass class
F_i	moles of ith species per gram of fluid (ALPHA(I,K), RALPHA(I,K))
F_{p_i}	number of particles per gram of fluid, ith mass class
g_i	Gibbs free energy of ith species at standard state (1 atm) (GTB(I,K))
g_{p_i}	ratio of actual heat transfer coefficient to that for Stokes flow, ith mass class particles
ΔG	change in standard Gibbs free energy for a reaction, $\sum_i (g_i)$ products $- \sum_i (g_i)$ reactants
ΔG°	Gibbs free energy of formation
G_{ij}	particle thermal velocity (GPP(I,J))
h	static enthalpy of mixture (H,STATEN)
h_i	enthalpy of ith species (HTB(I,K))
h_{298_i}	heat of formation of ith species at T = 298 K (HF(I))
H	stagnation enthalpy of mixture (HSTAG, STAGEN)

* Where a FORTRAN variable in the CHEMPART code exists corresponding exactly to the tabulated quantity, the FORTRAN name is given in parentheses.

ΔH°	enthalpy of formation
k_B	Boltzmann's constant
k_f	forward rate coefficient (RATE)
k_r	backward rate coefficient
K	eddy viscosity coefficient
$\overline{K}$	eddy viscosity coefficient for Donaldson/Gray Model (see Eq. (70))
K_{ij}	coagulation rate coefficient (RATEP(I,J))
Kn_i	Knudsen number of particles, ith mass class (XKNUN(I))
K_p	equilibrium constant (K)
L	latent heat of vaporization
Le	Lewis number (laminar or turbulent) (XLE(K))
m_i	mass of particles, ith mass class (MASSP(I))
$M_{1/2}$	Mach number at half radius, defined under Eq. (70) (QQ300)
N	temperature exponent in reaction rate equation (Eq. (61)) (RC(K,2))
NPG	number of particle mass classes
N_A	Avogadro's number (AV)
Nu	particle Nusselt number
p	static pressure
Pr	Prandtl number (laminar or turbulent) (SIGMA(K))
r	radial coordinate normal to jet or reactor centerline (Y(K))
r_i	particle radius, ith mass class (RZ(I))
r_{in}	inner mixing zone radius (QQ200)
$r_{1/2}$	defined under Eq. (66b) (QQ100)
$\overline{r}_{1/2}$	defined under Eq. (65) (QQ100)
R	universal gas constant (R)
R_w	reactor radius (RWALL)
Re	Reynolds number
Re_{p_j}	particle Reynolds number, ith mass class (REP)
s	supersaturation ratio
St	particle Stokes number
T	static temperature (T(I),RT(I))
T_{p_i}	particle temperature for ith mass class (UP(I,K))

T_w	wall temperature (TWALL)
u	x component of velocity (U(K),RU(K))
u_{p_i}	x component of particle velocity, ith mass class (UP(I,K))
v	r component of velocity
$\dot{w}_i$	rate of production, of ith species (WDOT(I))
$\dot{w}_{p_i}$	rate of particle production, ith mass class (QXP(I,K))
$\dot{w}^{(j)}$	rate of production from jth reaction
W	molecular weight of mixture $(\sum_i F_i)^{-1}$ (inverse of WTMIX(K)
W_i	molecular weight of ith species (WTMOLE(I))
x	coordinate parallel to jet centerline (X)
X_i	mole fraction of ith species
y	distance from wall, $(r_w - r)$
Y_i	mass fraction of ith species

Greek

α	constant for external control of eddy viscosity (see Eqs. (63) to (69) (XK2)
β_{ij}	particle capture efficiency
γ	surface tension
δ_i	particle mean free path, ith mass class
ε	eddy diffusivity for turbulent flow; defined as μ/ρ
ε	emissivity (EPS)
η	defined by Eq. (63)
λ	molecular mean free path
μ	effective viscosity for turbulent flow (XMU(K))
μ_g	molecular viscosity (UM(K))
μ_t	eddy viscosity
ν	kinematic viscosity
ρ	gas density (RHOG(K))
ρ_p	particle density (RHS)
σ	Stefan-Boltzmann constant

Ψ	stream function (PSI)

Subscripts

e	evaluated at edge of mixing layer (free stream)
i	ith species
j	value at nozzle (jet) exit
p_i	particle mass class i
o	evaluated at axis of symmetry, r = 0
w	evaluated at wall

Miscellaneous

$\lvert\ \rvert$	absolute value
$\left(\frac{\partial}{\partial\beta}\right)_\gamma$	partial derivative with respect to β; γ being held constant
$\sum_i$	summation over i species
[ ]	concentration of gaseous species

TABLE OF CONTENTS

LIST OF TABLES

LIST OF FIGURES

I. INTRODUCTION

This report covers the development of models and associated computer codes which describe processes and phenomena involved in novel methods for the production of high purity silicon. A prominent example[1] of such a process is one undergoing development by the Westinghouse Electric Corp. in which the production of silicon is performed via a chemical reaction between gaseous silicon tetrachloride and sodium jet streams, carried out in an arc-heated, turbulent flow tube reactor. In this process the reaction between $SiCl_4$ and Na is completed in an upstream reactor section and silicon vapor and/or droplet formation occurs. The process then strives for efficient separation and collection of the silicon in a downstream section by the collection of silicon on the reactor walls. In order to provide a reasonably complete description of processes such as this the following computer codes were developed or adapted:

GENMIX[2] - Solves the developing, turbulent boundary layer problem encountered in the downstream reactor section due to the flow of silicon-containing hot product gases through this cooled-wall portion. Deposition of silicon on the walls is taken to be controlled by convective-diffusive processes. Thus separation/collection of silicon vapor can be described by this code. The code accounts for variable fluid properties but neglects radiation and thermophoretic (Soret) effects in computing the reactor's vapor collection efficiency.

MPDEU - Solves the particle transport equation in the downstream reactor section. This equation describes the mass transfer rate of silicon droplets controlled by convection, Fick and eddy diffusion, as well as the Soret effects. Since the gas-phase velocity and temperature fields in the developing tubular flow of the reactor govern the abovementioned transport processes, GENMIX is coupled to MPDEU.

CHEMPART - Solves the turbulent, jet mixing problem including detailed gas-phase chemistry and particle formation. This code also treats mass, momentum, and energy flux to the walls. This code is an extension of the well-known LAPP[3] code for rocket plume exhaust studies.

The development of these codes is based on a rationale best explained with the help of Figs. 1 and 2. Figure 1 shows an $SiCl_4$/Na flow reactor with a simple reactant input geometry. The significant phenomena occurring within the reactor are specified, along with rough values for the temperatures prevailing in each region. Specifically, the following phenomena must be described if

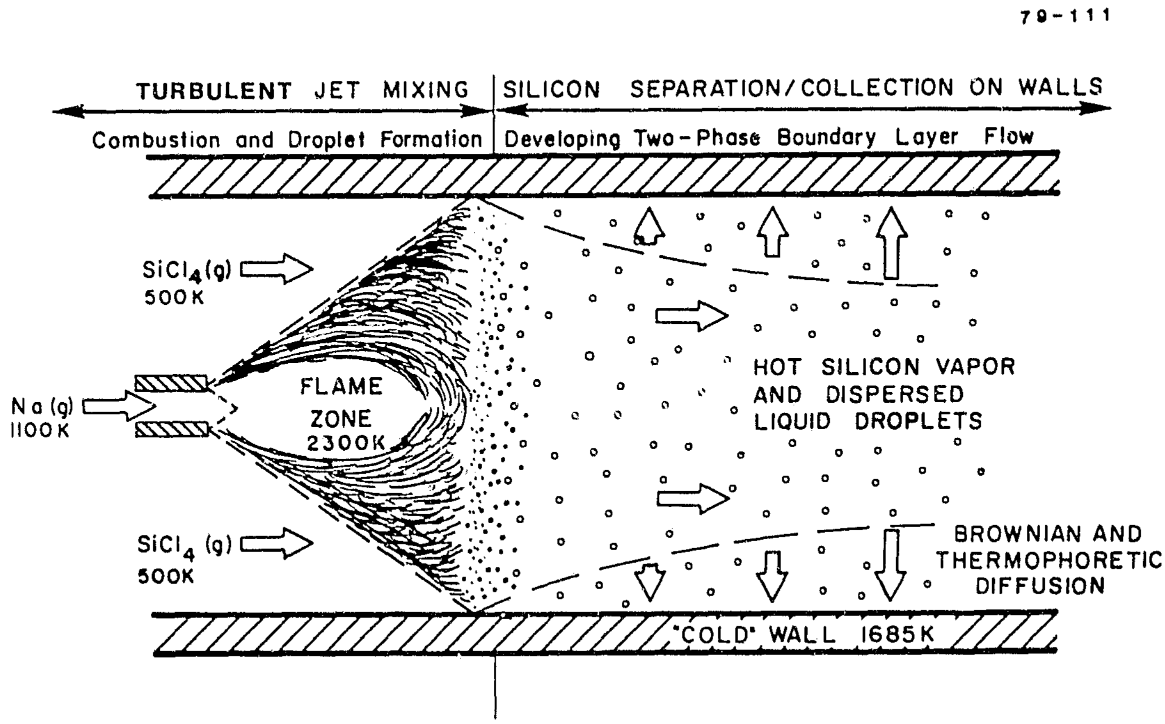

FIGURE 1 SCHEMATIC OF THE REACTOR CONSIDERED

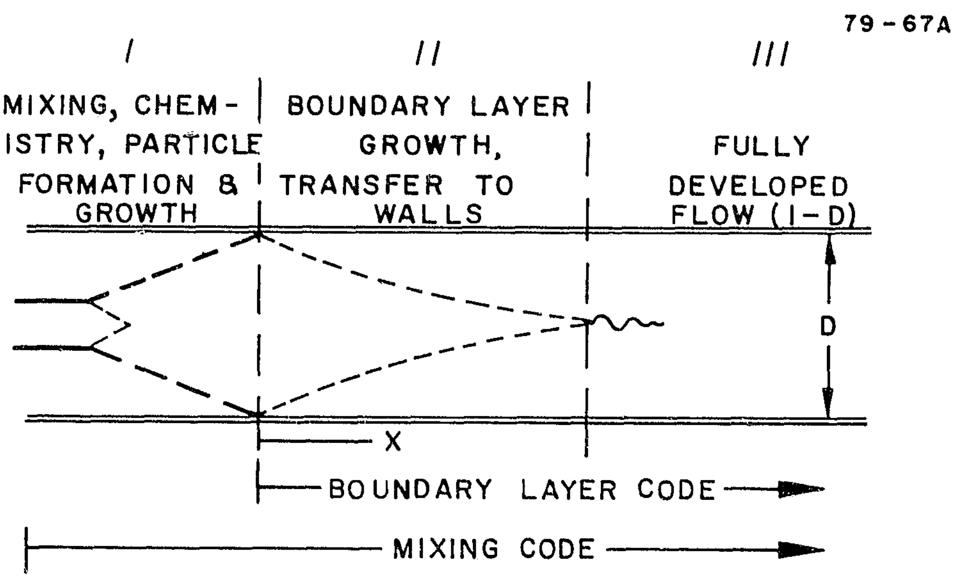

FIGURE 2 SCHEMATIC OF THE VARIOUS REGIMES WITHIN A SILICON REACTOR

the fate of the silicon produced in the reactor is to be computed; (i) in the upstream mixing region, rate of mixing and reaction, (ii) also in the upstream region, rate of Si droplet formation, (iii) in the downstream, developing flow region, rate of boundary layer growth, (iv) also in the downstream region, rate of particle growth via agglomeration and heterogeneous condensation, and (v) also in the downstream region, rate of diffusion and thermophoretic transport of Si vapor and droplets to the reactor walls.

In order to describe the situation of Fig. 1, the scheme indicated in Fig. 2 has been employed. In this schematic, three regions are indicated: In the first, upstream region in which the jet of Na vapor is mixed with the silicon halide, the CHEMPART code is used to extract detailed information concerning the mixing and rate of reaction. Particle formation, if supersaturation occurs, is also computed. In the next section, where boundary layer development occurs, CHEMPART is again used to follow particle growth rates, slow gas-phase chemistry, and wall deposition. However, due to the size and expense of running this code, it was felt that another smaller code would be desirable. Hence, a boundary layer code was developed, based on the GENMIX code, which could treat the boundary layer problems without detailed chemistry, but with a mass transport model to compute wall deposition rates. Finally, some 50 or more diameters downstream, a fully-developed flow occurs. At this point, one-dimensional calculations could be used to compute wall deposition rates. CHEMPART tests for this situation and once a uniform core flow develops, detailed calculations are performed only at the centerline and within the boundary layer. Although not in fact a one-dimensional calculation, this technique results in much the same result in terms of economy. (GENMIX runs rapidly enough that such modification is unnecessary.)

In the sections which follow, the theoretical background needed for the use of these codes is described. Then the code themselves are explained. Finally, their use in studying $SiCl_4$/Na flow reactors is described. Listings of the codes and examples of input and output are given in Appendices.

II. MODELING OF THE REACTOR BOUNDARY LAYER

A major problem faced in the production of silicon via gas-phase reaction of silicon halide in flow reactors is the collection of the Si vapor or droplets formed by the reaction. One means of collecting the silicon is to allow enough residence time within the reactor for diffusion of the silicon to reactor walls followed by condensation of vapor (or capture of droplets) on the walls. Such a condensation method is being employed by Westinghouse.[1]

In view of the potential significance of this condensation process, a major effort in this program has been the adaptation of a powerful boundary layer code to permit the calculation of rates of transport of Si through the growing boundary layers of such flow reactors. In this section the theory of mass transport through such boundary layers is described. Since it is envisioned that flow reactors that depend on Si vapor wall deposition[1] will operate above the Si dew point, emphasis will be on the calculation of vapor transport. However, since droplet formation may occur in the boundary layer or in the downstream part of the core flow within the reactor, the transport of a particulate phase is also fully examined.

A. THE BOUNDARY LAYER MODEL

The basic tool used for study of mass transport through the reactor wall boundary layer is the well-known GENMIX code.[2] This code is used to obtain the information concerning the velocity and temperature distributions near the reactor wall needed to compute rates of mass transport through the boundary layer. The code is applied to the downstream section of the reactor where it is assumed that chemical reaction is complete and the gases are thus effectively inert. The physical problem thus involves an analysis of a hot, turbulent developing flow field within a circular pipe with cooled walls. Due to the large temperature variation between the reactor core flow and the walls, it is essential to include the effects of non-uniform fluid properties and the possible formation of silicon droplets due to condensation (caused by cooling silicon vapor). However, for simplicity, at present we restrict attention to the case with no condensation. That is, silicon is assumed to exist only in the vapor state.

Yet another simplification is rendered in this analysis by viewing the overall product gas mixture as an effective binary system, with silicon as one species and all other gases (mainly NaCl, Ar, H_2) as the only other species (referred to subsequently as the "carrier" gas). The molecular weight and other properties of the carrier gas are taken to be a weighted average of the properties of the individual components. On this basis, the diffusional behavior of silicon vapor through the surrounding gas can be uniquely described in terms of the appropriate mass diffusivities (or mass transport coefficients). On the other hand, the thermal diffusivity (or heat transport coefficient) of the overall product gas mixture will be nearly equal to that of the carrier gas alone, since silicon concentrations are typically low. In the case of silicon vapor deposition, the relative importance of heat and mass transfer processes inside a typical reactor is nearly equal. That is, the Lewis number for the system is close to unity. The effect of turbulence, as treated in the model considered, lies mainly in enhancing the diffusive transport of heat, mass, and momentum.* The enhancement due to the so-called turbulent counterparts of the abovementioned diffusivities will be assumed to be such that the "effective Lewis number" remains close to unity. That is, turbulence enhances heat and mass transfer rates equally. However, according to current belief and experimental data the enhancement of momentum transfer rates due to turbulence is somewhat less (a fact represented by setting the turbulent Prandtl number† equal to 0.9).

It is clear, therefore, that a good description of turbulent transport coefficients is pivotal to the success of the present model. For now, a mixing length approach to turbulence modeling has been adopted. The chief drawback of this approach is that it relies heavily on an empirical determination of several constants, some of which might vary from one flow situation to another. This handicap will have to be overcome by the use of more sophisticated (differential) models of turbulence. This latter class of turbulence models, which describe the mixing length via differential equations (rather than alge-

---

* The diffusive transport of momentum (or vorticity) is analogously controlled by the kinematic viscosity (ν), or momentum diffusivity.

† The Prandtl number is the ratio of momentum diffusivity to thermal diffusivity.

braic ones, as done here), can, of course, be blended into the present formulation. However, we believe that since turbulent heat/mass transfer predictions using even the most elaborate approaches sometimes incur errors of up to 15%,[4] retaining the mixing length model would at least give us the advantage of greater simplicity with relatively little loss of achievable accuracy. Moreover, the mixing length model has been extensively studied and tested in pipe flow configurations against both experimental data[5] and the predictions of more sophisticated models.[6,7]

In view of the abovementioned assumptions and recognizing that the developing pipe flow processes of interest are characterized by comparable changes in the radial and axial directions (i.e., two-dimensional, axisymmetric) one may adopt the Patankar and Spalding[5] turbulent boundary layer formulation for the conservation of overall mass, momentum, energy (or stagnation enthalpy) and silicon vapor species.* No attempt will be made to reproduce these well-established parabolic, partial differential equations here since they have been fully detailed in Refs. 2 and 5. Instead here we choose to discuss aspects not immediately obvious from their discussion.

Implicit in the governing equations used by these authors[2,5] are the following assumptions:

(i) The densit, fluctuations caused by turbulence are of insignificant importance compared to the flux contributions of other fluctuating quantities (e.g., velocity, temperature, concentration).

(ii) The dissipation rate of turbulent kinetic energy (due to velocity fluctuations interacting with the mean velocity) is negligible compared to the viscous dissipation rate of mean kinetic energy.

Under these assumptions, it is possible to reduce the otherwise complicated turbulent boundary layer equations to a form similar to the better-understood steady, compressible, laminar boundary layer equations, provided one defines suitable "effective" values for the momentum, thermal, and mass diffusivities

---

* It can be estimated from the magnitudes of the various diffusivities that the velocity, temperature, and species boundary layers will all develop at nearly the same rate. The "fully-developed" state is not reached until some 40-60 diam downstream from the pipe inlet.

discussed earlier. These have been defined by the following flux-gradient relationships (assuming Newtonian behavior)*:

$$\tau \equiv \mu_{eff} \frac{\partial u}{\partial y} \qquad \text{(shear stress)} \qquad (1)$$

$$q'' \equiv -\Gamma_{h,eff}\, C_p \frac{\partial T}{\partial y} \qquad \text{(heat flux)} \qquad (2)$$

$$j_i'' \equiv -\Gamma_{i,eff} \frac{\partial Y_i}{\partial y} \qquad \text{(mass flux of species i)} \qquad (3)$$

where μ_{eff} is the effective viscosity, $\Gamma_{h,eff}$ the ratio of effective thermal conductivity (λ_{eff}) to the constant pressure specific heat of the carrier gas (C_p), and $\Gamma_{i,eff}$ the product of the mean gas density (ρ) and the effective mass diffusivity ($D_{i,eff}$) of silicon vapor in the carrier gas. u, T, and Y_i denote the time-averaged streamwise velocity, absolute temperature, and mass fraction of silicon, respectively.

Each of the effective transport coefficients above is the sum of a laminar (or molecular) contribution and a pseudo, turbulence-induced contribution. The latter may be greater by some two orders of magnitude in fully turbulent (i.e., nearly inviscid) regions, such as the reactor core flow. However, closer to the reactor walls turbulence energy is rapidly depleted due to the dissipating influence of molecular viscosity, and transport is affected mainly by the laminar (molecular) mechanism. As a result the turbulent parts of the transport coefficients can vary significantly across the reactor cross-section. The motivation for introducing a "mixing-length," or any other turbulence model, is to describe this variation realistically.

In the present analysis the following radial variation of mixing length, from the reactor axis (or centerline) to the wall, was prescribed:

$$\ell = \begin{cases} \lambda\delta \quad , \quad y > \dfrac{\lambda\delta}{K} & \text{(core layer region)} \\ Ky[1-\exp(-y^+/A^+)], \quad 0 \leq y \leq \dfrac{\lambda\delta}{K} & \text{(near wall region)} \end{cases} \qquad (4)$$

---

* We neglect for the moment (see the next section) thermophoretic transport.

where y is the distance from the wall, δ is the thickness of the turbulent boundary layer, and λ, K, and $A^{+\dagger}$ are taken to have the constant values 0.09, 0.435, and 26.0, respectively. Physically, such a distribution of mixing length distinguishes regions of high local Reynolds number, $y^{+} \equiv yu_{*}/\nu$,‡ (or nearly inviscid flow) from those regions near the wall which are governed by the progressively increasing effect of molecular viscosity (i.e., a "damping" of the mixing length with decreasing y^{+}, according to Van Driest's[10] exponential law). Note that this permits a viscous sublayer region next to the reactor walls so that the influence of even weak turbulent fluctuations is felt. Just outside the viscous sublayer the mixing length obeys an undamped, "defect law" behavior (i.e., $\ell = Ky$).

Using the above mixing length distribution it is possible to express the effective viscosity as:

$$\mu_{eff} = \mu_{turbulent} + \mu_{laminar} \tag{5}$$

$$= \rho \ell^2 \left|\frac{\partial u}{\partial y}\right| + \mu \tag{6}$$

where $\left|\frac{\partial u}{\partial y}\right|$ is the magnitude of the time-averaged velocity gradient normal to the reactor wall. Since this quantity decreases away from the wall (becoming zero at the boundary layer edge) turbulence is operative only in regions in which the velocity gradient exceeds a small critical value. If, in any flow region the turbulence velocity scale $\left|\ell \frac{\partial u}{\partial y}\right|$ falls below a certain fraction of the local velocity, this quantity is set to the local prevailing velocity. Such a circumstance tends to occur in the fully-turbulent core flow region of the reactor.

---

† It has been shown[8,9] more recently that A^{+} is a sensitive function of pressure gradient and wall blowing or suction. This parameter determines the thickness of the "viscous sublayer" region.

‡ u_{*} is the so-called "friction velocity" defined here in terms of the local shear stress by the relation $u_{*} \equiv (\tau/\rho)^{1/2}$

B. COMMENTS ON THE NUMERICAL SOLUTION PROCEDURE

Since the governing equations to be solved are parabolic partial differential equations, their solution requires the specification of appropriate initial and boundary conditions. In the present study the initial conditions at the pipe entrance were specified as uniform (corresponding to centerline values) profiles of u, T, and Y_i across the pipe cross-section. The domain of integration was taken to be the region between the pipe centerline and the wall. Boundary conditions on u, T, and Y_i were specified at the wall as:

$$u = 0 \tag{7}$$

$$T = T_w \text{(constant)} = 1700 \text{ K} \tag{8}$$

$$Y_i = Be^{-A/T_w} \approx 0^* \tag{9}$$

The last condition is a consequence of assuming that silicon vapor is in equilibrium at the wall (i.e., the partial pressure equals the saturated vapor pressure). The centerline boundary conditions on these variables were taken to correspond to the symmetry conditions:

$$\frac{\partial u}{\partial y} = 0, \quad \frac{\partial T}{\partial y} = 0, \quad \frac{\partial Y_i}{\partial y} = 0 \tag{10}$$

Using the above initial and boundary conditions, GENMIX produced solutions at specific downstream stations along the reactor by marching forward in steps (whose size was proportional to the local boundary layer thickness). At each step the solution to the coupled system of conservation equations is carried out using a fully implicit, 6-point, finite difference algorithm (based on an integral approach that ensures conservation, rather than the usual Taylor series expansion). The algorithm uses a substitution method for solving the resulting system of coupled algebraic equations (with a tri-diagonal matrix), thus avoiding the time-consuming and unreliable operation of inverting the coefficient matrix. It was found in this study, as in others, that GENMIX is

---

* A and B are constants with the values 46710.0 K and 7.3166×10^{10} N m^{-2}, respectively.

extremely efficient as a code. For instance, the full solution for a 9 m reactor length with some 80 to 100 radial gridpoints is completed in about 17 s (CP time on CDC 7600 computer).

The remarkable efficiency of GENMIX is really a result of the many different time-saving features built into the code. While the program chooses its own forward marching step size, the cross-stream grid spacing is specified as input. In the present problem, the gridpoints were so chosen as to be unequally spaced over the pipe radius, with a greater resolution capability near the wall, where gradients were steep. Furthermore, it must be noted that the solution in GENMIX is not carried out in physical space (x,y) but rather in the transformed von Mises[11] coordinates (x,ω). In this latter coordinate system, the normalized stream function ω always provides a fixed integration domain: $0 \leq \omega \leq 1$. In general, the advantage of working in this transformed space is the greater solution accuracy and ease that results from imposing boundary conditions at fixed extremities. However, in the solution of constant radii pipe flows (such as the present case), this advantage is not fully realized since the two extremities remain fixed even in physical space. Of course, an alternative solution tactic may have been to solve the problem between the wall and the edge of the developing boundary layer. In this latter case, working in the transformed stream function ordinates may be a definite advantage.

A major disadvantage of the GENMIX solution procedure may be its handling of the near-wall flow. The reactor wall is a point of singularity in the (x,ω) space because the flow velocity there is zero and it multiplies the highest derivatives of the transformed equations. This disconcerting feature also tends to render the transformation process back to physical space somewhat inaccurate for gridpoints close to the wall. In order to circumvent some of the difficulties associated with this singular point, the Patankar-Spalding procedure generates solutions for the region next to the wall using a turbulent Couette flow analysis (further simplified using a constant property assumption). Thus one does not obtain a rigorous finite difference solution of the two-dimensional boundary layer equations in the region close to the wall. However, this device greatly enhances the numerical solution efficiency since wider grid spacings can be used. Moreover, by arranging the region of Couette flow very close to the wall, the error due to this approximation may be rendered acceptable.

C. SILICON TRANSPORT LAWS

Using GENMIX a description of the boundary layer flow field can be generated. The transport of Si to the walls may then be generated once the diffusion constant describing its Fick and Soret transport properties are obtained.

The mechanism of transport of silicon particles (including, as the smallest particles, vapor molecules) onto reactor walls is dependent on the size of the particles. For particles larger than about a micron, deposition is controlled by turbulence-induced inertial impaction; sub-micron sized silicon droplets deposit by a convective-diffusion process. In order to predict the mass flux to the reactor wall of the latter class of droplets it is necessary to recognize two separate contributions to the time-averaged diffusional flux: (i) a concentration gradient-driven (Fick) flux and (ii) a temperature gradient-driven (Soret) flux. The relative importance of these contributions itself varies with particle size, the former being dominant for the smaller sub-micron sizes while the latter controls the behavior of particles with sizes closer to a micron, as shown qualitatively in Fig. 3. Thus, in general,[12-14]

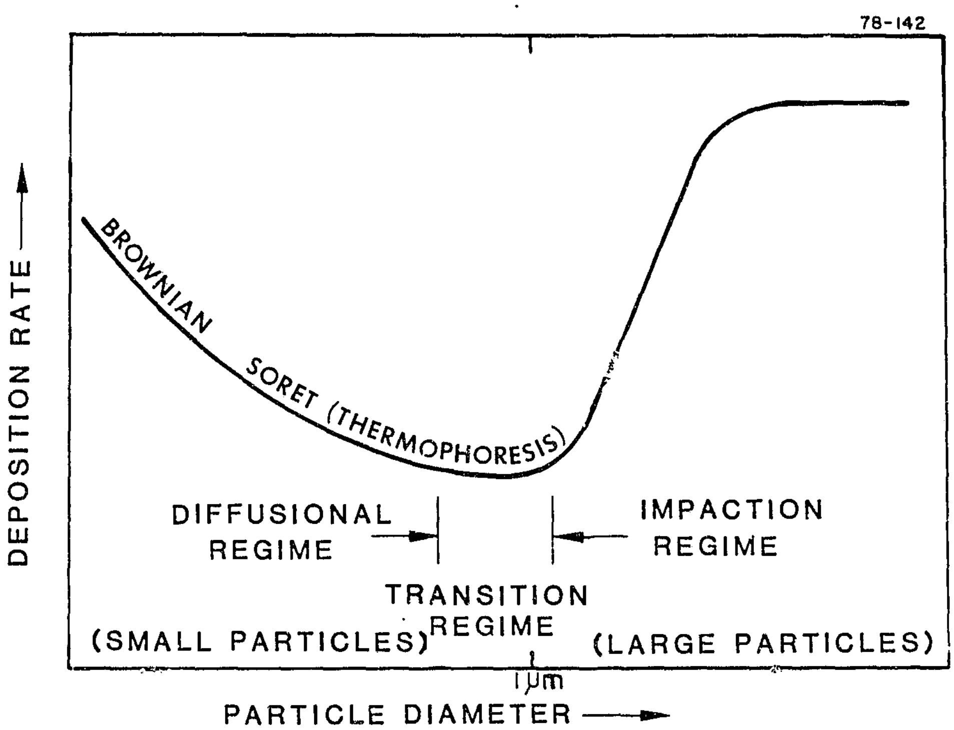

FIGURE 3 VARIATION OF DEPOSITION RATE OF SILICON PARTICLES WITH SIZE

for a species i (vapor or particle) that is dilute in a carrier gas the diffusional mass flux (per unit area, per unit time) at any point, $\vec{j}_i''$, (corresponding to a particular pressure and temperature) is given by[12,13]:

$$\vec{j}_i'' = -\rho D_i \left[(\vec{\nabla Y}_i) + \alpha_i Y_i (1 - Y_i) \frac{1}{T} (\vec{\nabla T}) \right] + \vec{j}_{turb}'' \quad (11)$$

where ρ is the local mass density of the carrier gas, Y_i the local mass fraction of the diffusion species, T the local absolute temperature (with the operator ∇ denoting gradient of the particular scalar, temperature or concentration). The first two terms in Eq.(11) represent the diffusional mass fluxes due to concentration and temperature gradients, respectively. The third term, $\vec{j}_{turb}''$, is the mass flux contribution due to turbulent or "eddy diffusion." Assuming, as is customary, that the turbulent diffusion also has a Fickian nature, one can write,

$$\vec{j}_{turb}'' = -\rho \varepsilon_p (\vec{\nabla Y}_i) \quad (12)$$

where ε_p is the so-called "eddy diffusivity." Particles larger than about a micron would inevitably be deposited on the walls due to inertial impaction caused by turbulent velocity fluctuations normal to the wall. Hence, for such large particles the overall mass flux to the wall would be dominated by $\vec{j}_{turb}''$. However, the sub-micron size particles will be driven close to the wall by turbulence eddies before the concentration and temperature gradient driven fluxes (i.e., Fick and Soret effects) become important in the final stages of deposition, within a nearly laminar (viscous) sublayer next to the wall.

However, before deposition rate (or mass flux) can be calculated, one needs to establish the Fick (or Brownian) diffusion coefficient D_i, the dimensionless thermal (Soret) diffusion or "thermophoretic" factor α_i, and the "eddy" diffusivity ε_p. The former two transport property coefficients depend upon the molecular nature of the species present in a given "effective" binary mixture (e.g., silicon-argon, in the case considered later in this report), and on the prevailing pressure and temperature.* In addition, they are both strong func-

---

* Under typical silicon reactor operating conditions the concentration dependence of these transport coefficients will be negligible, due to the diluteness of silicon in the carrier gas.

tions of particle size, changing by several orders of magnitude (as shown later) in traversing the particle size spectrum from molecular diameters* to about a micron.

Interestingly enough, while the values of the Fick diffusivities (i.e., D_i and ε_p) are always positive, ensuring that Brownian and turbulent transport of Si always occur in the direction of decreasing concentration (towards the reactor walls), the value of α_i may sometimes be negative. The latter circumstance is usually characteristic of diffusing species that are lighter than the carrier gas (e.g., silicon vapor (28.09) diffusing through argon (39.94)). Thus the Soret flux has the potential to drive silicon vapor towards higher temperatures, away from the "cool" walls, and thereby reduce the overall collection efficiency of Si. Fortunately, as shown later, the value of α_i for Si particles (defined here as any molecular cluster exceeding roughly twice the mass of a single vapor molecule) is invariably positive, since the particles are heavier than the surrounding gas. That is, while condensed Si droplets will always be driven towards the reactor walls, uncondensed Si vapor could actually be driven away from the walls due to the Soret effect. Therefore, in addition to considering the mechanisms of Brownian and turbulent transport of silicon, we investigate the conditions under which Soret, or temperature gradient-driven diffusion, can be important. Although this latter effect has been ignored in the past in the belief that its contribution to the overall mass flux would be negligible, we conclude that the Soret effect can indeed play a crucial role in the Si (particle/vapor) separation process, under typical reactor conditions. Fortuitously, the Soret flux for condensed Si droplets will always favor deposition onto the walls.

For the sake of comparison, it is necessary to define the "eddy" diffusivity, ε_p, for mass transport. In general, by viewing turbulence as the random agitated movement of small packets of fluid, it is possible to define ε_p in terms of a "mixing length" (in much the same spirit as the "viscous mean-free-path" in the kinetic theory of gases represents an average distance for effective transfer of momentum by molecules). Thus,

---

* Particle size is described in terms of diameter or radius since it will be assumed here that the particles (silicon liquid droplets) are perfectly spherical.

$$\varepsilon_p \sim u'\ell_1 \sim \ell_1^2 \left|\frac{dU}{dy}\right| \tag{13}$$

where ℓ_1 is a mixing length, u' the large scale turbulent velocity fluctuations present in the core flow of the reactor, and $\left|\frac{dU}{dy}\right|$ the magnitude of the time-averaged (steady) normal velocity gradient. Both ℓ_1 and $\left|\frac{dU}{dy}\right|$ will vary with distance above a wall, y, with ℓ_1 being zero at the wall since turbulence is precluded (i.e., the "no-slip" condition). While the many available models of turbulence provide different expressions for the variation of ℓ_1 with distance normal to a wall, accurate estimates of ℓ_1 and the proportionality constant in the above expression, for any given flow situation, usually result from experiments. Lin et al[15] suggest the following expression, valid in the viscous sublayer flow, next to a wall:

$$\varepsilon_p = \nu\left(\frac{y^+}{14.5}\right)^3, \; y^+ < 5 \tag{14}$$

where ν is the kinematic viscosity and y^+ is a non-dimensional normal distance from the wall defined as:

$$y^+ \equiv \left[y\, U(f/2)^{1/2}\right]/\nu \tag{15}$$

with U the average velocity and f the Fanning friction factor. For particles small enough to follow the small-scale eddy motions close to a wall, the eddy diffusivity does not depend upon particle size.

Although silicon particles of widely varying sizes must be considered in the modeling of the deposition processes within any proposed reactor, reliable information about the "molecular" transport coefficients (i.e., D_i and α_i) is available only at the two extremes of the size spectrum. For particle sizes much smaller than the mean-free-path of the carrier gas, the well-known kinetic theory results of Chapman and Enskog[16] (CE) apply. In this limit of "free-molecule" flow, surrounding gas molecules do not suffer appreciable changes in their distribution functions upon collision with the particle. Furthermore, since expressions for α_i are an outcome of CE theory using second-order terms of the perturbation series, while the D_i expressions come out of first-order terms, one concludes that α_i will be more sensitive to interactions between colliding molecules. Thus more sophisticated molecular

potential models than the Lennard-Jones 12:6 (e.g., the exponential model)[17,18] might ultimately be necessary to accurately determine α_i in this limit, although the Lennard-Jones might suffice for engineering purposes.

For particles much larger than the mean-free-path of the surrounding gas, the gas structure becomes "invisible" and the behavior can be described by the Navier-Stokes equations for a "continuum," subject to the usual "no-slip" boundary conditions at the particle surface (e.g., the Stokes-Einstein (SE) expression for particle diffusivity[19]).

The main difficulty in specifying transport properties is encountered for particles in the intermediate size range, on the order of a mean-free-path. This presents the notorious unsolved problem of the "transition regime." Although several attempts have been made to extend the continuum results into the transition regime, by imposing "slip" or jump-type boundary conditions at the particle surface, these are at best heuristic. Understanding of the real transition mechanisms involved is altogether insufficient. However, the transition regime experimental data of Millikan[20] and others have made it possible to establish various empirical correction factors (as discussed later) that cover a wide portion of the transition regime. Unfortunately, even such widely used interpolation formulae as the Stokes-Einstein-Millikan (SEM) expression are unsatisfactory since they do not exactly match the predictions of CE theory when extended to the "free-molecule" limit.

Crucial to the accurate modeling of silicon deposition, therefore, is a proper description of the abovementioned transport coefficients. Since present knowledge regarding the "transition regime" is insufficient, it would be justifiable to suggest universal interpolation formulae for these coefficients, covering the entire particle size (or Knudsen number*) range. Moreover, mathematically continuous functions that blend together the known results in different regions would be both physically and computationally more desirable.

---

* The particle Knudsen number (Kn_i) will be defined here as the ratio of the mean-free-path (ℓ) in the surrounding gas to the particle radius (R_i) (i.e., $Kn_i \equiv \frac{\ell}{R_i}$). Thus $Kn_i \to 0$ corresponds to the "continuum" limit while $Kn_i \to \infty$ refers to the "free-molecule" limit. It is sometimes assumed[19] that the range $0 < Kn_i < 0.25$ represents the region of "slip-flow" while $0.25 < Kn_i < 10$ is the region of "transition-flow."

In what follows, a novel rational approach[13] to creating such "universal" descriptions of the Fick diffusivity (i.e., D_i) and the Soret factor (i.e., α_i) is outlined.

1. Universal Formula for D_i

The expression for diffusivity adopted in this report blends the near-continuum SEM relation (valid for small Kn_i values) with the free-molecule CE expression (valid for large values of Kn_i, > 10) according to the following universally valid relationship[19]:

$$D_i = D_{SEM} + \frac{D_{CE} - D_{SEM}}{[1 + \exp\{- C(Kn_i - Kn_o)\}]} \tag{16}$$

where C and Kn_o are constants. The magnitude of C controls the abruptness of the transition from D_{SEM} to D_{CE} as the Kn_i is increased. Kn_o is the Knudsen number value at the "point of inflection" of D_{SEM}. Figure 4 illustrates the rationale behind choosing such an interpolation function to describe the diffusivity of particles in a gas.

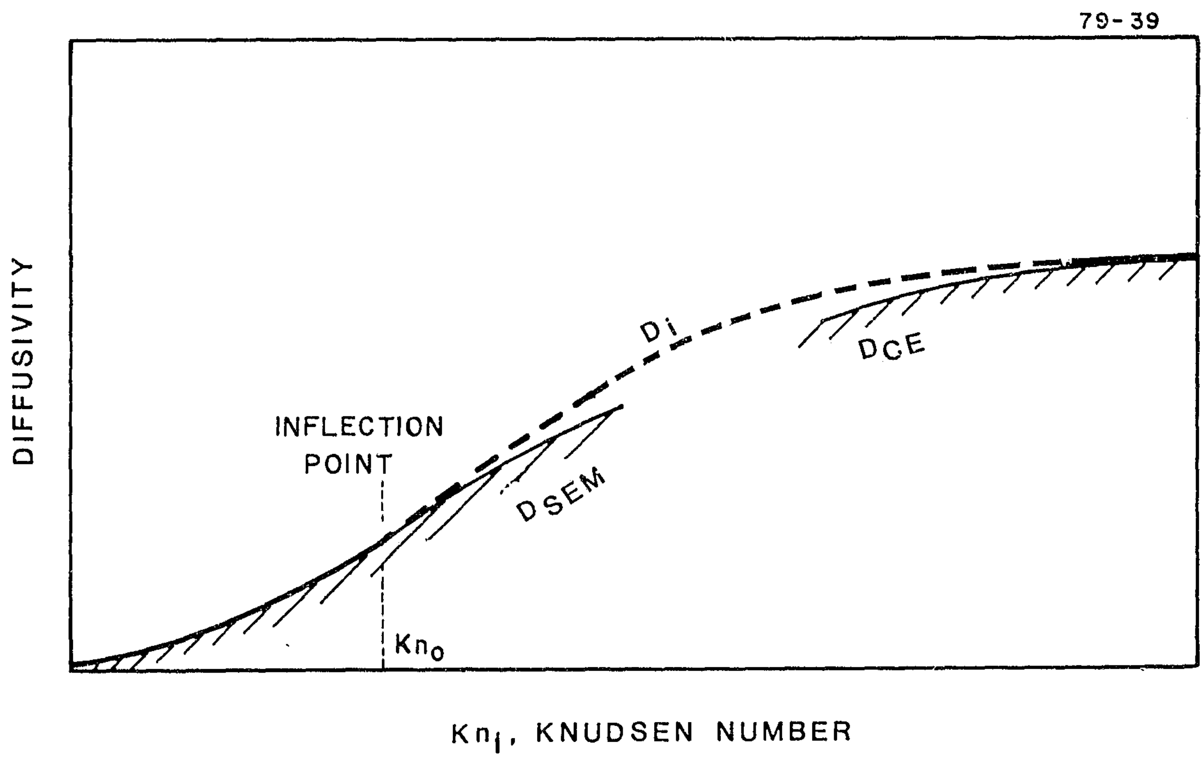

FIGURE 4 RATIONALE FOR THE DIFFUSIVITY FORMULA (EQ. 16))

The Stokes-Einstein-Millikan expression for diffusivity, D_{SEM}, is based on Millikan's[20] famous oil-drop experiments which permitted measurement of the isothermal drag force on particles of various sizes moving through a gas. Using a stochastic analysis of Brownian motion, Einstein[21] had earlier related the particle diffusivity to the "mobility," or relative velocity per unit force, through the reaction:

$$D_i = kTB \tag{17*}$$

the mobility, B, being given by the Stokes formula for low Reynolds number continuum flow around a sphere:

$$B = \frac{1}{6\pi\mu R_i} \tag{18}$$

where μ is the dynamic viscosity of the gas. Recognizing that as the particle size approaches the gas mean-free-path, the drag for a given velocity becomes less (due to "slip") than predicted by Stokes law (i.e., the mobility increases), Millikan suggested the following expression for mobility, which is a well-accepted correction of the Stokes result:

$$B = \frac{1}{6\pi\mu R_i \beta} \tag{18a}$$

where

$$\beta \equiv [1 + C_m Kn_i + C_d Kn_i \exp(-0.88/Kn_i)]^{-1} \tag{18b}$$

$$C_m \equiv (2 - \alpha_m)/\alpha_m \tag{18c}$$

$$C_d \equiv \left\{\frac{\pi}{8}\alpha_m^2 + \left(\frac{13-\pi}{4}\right)\alpha_m + 2\right\} \Big/ \left\{\alpha_m + \frac{\pi}{8}\alpha_m^2\right\} \tag{18d}$$

with α_m denoting the so-called momentum accommodation coefficient, a measure of the efficiency of momentum transfer between the particle and the surrounding

---

* k is the Boltzmann constant.

gas molecules.* Combining Eqs. (17) through (18d) yields the needed expression for diffusivity, valid at least for small departures from $Kn_i = 0$:

$$D_{SEM} = \frac{kT}{6\pi\mu R_i} \left[1 + C_m Kn_i + C_d Kn_i \exp(-0.88/Kn_i)\right] \tag{19}$$

At the other extreme, for particles much smaller than the gas mean-free-path (but not necessarily as small as molecules) the diffusivity D_{CE} should be given by the Chapman-Enskog relation[22]:

$$D_{CE} = 1.8583 \times 10^{-3} \left(\frac{T^{3/2}}{p}\right) \left(\frac{1}{M_c} + \frac{1}{M_i}\right)^{1/2} \left(\frac{1}{\sigma_{ci}{}^2 \Omega}\right) \tag{20}$$

where p is the pressure (atm), M_c and M_i the molecular weights of the carrier gas, c, and diffusing molecular species, i, respectively, σ_{ci} the effective collision diameter (angstroms) and Ω the reduced collision integral. Equation (20) is strictly valid only for molecules with spherically symmetric potential force fields, with the supplementary relations:

$$\sigma_{ci} = \frac{1}{2} (\sigma_c + \sigma_i)$$

$$\Omega = \text{fn}\left(\frac{kT}{\varepsilon_{ci}}\right) \quad \text{(See Ref. 23 for a tabulation of this function.)} \tag{21}$$

$$\varepsilon_{ci} = (\varepsilon_c \varepsilon_i)^{1/2}$$

where σ_{ci} and ε_{ci} can be taken to represent the size and energy-well depth in, say, the Lennard-Jones molecular interaction model.

To generalize Eq. (20) for the case of small particles, we need to redefine only the molecular weight M_i and the molecular diameter σ_i. Treating the particle as a "heavy molecule," g times the mass of the corresponding molecule, its "molecular weight" can be expressed as:

---

* Values of α_m depend on the nature of the particle and the surrounding gas. Experimentally determined values for various substances[19] usually lie in the range $0.9 < \alpha_m < 1.0$. In this report $\alpha_m = 1$ (perfect accommodation) is assumed for the results presented later.

$$M_i = g\,M_1 = \left[\left(\frac{4}{3}\pi R_i^3\right)\left(\frac{N_A\rho_i}{M_1}\right)\right] M_1 \qquad (22)^*$$

where M_1 is the molecular weight of the substance constituting the particle, g is the ratio of the particle volume to the molecular volume (i.e., $\frac{M_1}{N_A\rho_i}$) of the substance, and ρ_i is the particle density. The "molecular" diameter of a particle is simply

$$\sigma_i = (2R_i) \times 10^8 \ (\mathring{A}) \qquad (23)$$

if the particle radius R_i is expressed in centimeters. Combining Eqs. (20) through (23) yields the following expression for the diffusivity of very small particles:

$$D_{CE} = 1.8583 \times 10^{-3}\left(\frac{T^{3/2}}{p}\right)\left(\frac{1}{M_c} + \frac{1}{gM_1}\right)^{1/2}\left(\frac{1}{\sigma_{ci}^2\Omega}\right) \qquad (24)$$

where

$$\sigma_{ci}^2 \cong \frac{1}{4}(\sigma_c + 2 \times 10^8 \ R_i)^2 \qquad (24a)$$

$$\Omega \simeq 1.22\left(\frac{kT}{\varepsilon_i}\right)^{-0.16} \qquad (24b)$$

$$g = \left(\frac{4}{3}\pi R_i^3\right)\left(\frac{N_A\rho_i}{M_1}\right) \qquad (24c)$$

Incorporating the expressions for D_{SEM} and D_{CE}, given by Eqs. (19) and (24), into Eq. (16) yields the required, universally valid, equation for the diffusivity D_i. The value of Kn_0 was taken to be 0.44 so that the point of inflection in Eq. (16) coincided with the inflection point of the SEM formula (i.e., Eq. (19)). The value of C was chosen to be 1.5 for the results presented below.

---

* N_A is the Avogadro number.

2. Universal Formula for α_i

Using a rationale similar to the one adopted for D_i, but necessarily different because entirely different (and more complicated) expressions usually describe α_i, we propose the following universally valid formula for the Soret factor:

$$\alpha_i = \left(\frac{A\ Kn_i}{1 + A\ Kn_i}\right)\alpha_\infty + \left(\frac{1}{1 + A\ Kn_i}\right)\alpha_o \tag{25}$$

where α_∞ is the "thermal diffusion factor" predicted by CE theory for $Kn_i \to \infty$ and α_o is the value of the Soret factor as $Kn_i \to 0$. The constant A is determined by forcing the prediction of Eq. (25), in the transition regime, to agree with established experimental data for some value of Kn_i of order unity.

It is known that a particle suspended in a gas with a uniform temperature gradient will drift through the gas under the action of a thermal force. When this "thermophoretic" force just balances the opposing drag force on the particle, a constant thermal settling velocity is achieved. Using Millikan's oil-drop apparatus, modified to provide for a temperature gradient, Phillips[24] was able to accurately describe the thermal settling velocity up to $Kn_i \approx 0(1)$, for particles of widely varying thermal conductivities (including the coupling that usually exists between the velocity and temperature fields surrounding a moving particle). We have incorporated[13] the Phillips formulae into a computer program that predicts the thermal settling velocity ($\vec{V}_T$) at some value of the Knudsen number (say, $Kn_i = 1$) and used this to find the corresponding Soret factor (α_P). Knowing α_∞ and α_o, as shown below, A can then be determined as:

$$A = \frac{1 - \alpha_o}{\alpha_\infty - \alpha_P} \tag{26}$$

for a given particle-carrier gas combination and given flow conditions.

Since the CE expression for α_∞ is extremely complicated, we utilize the analysis of Waldmann and Schmitt[25] which yields the following expression for $\vec{V}_T$ valid for small particles whose drift in a temperature gradient can be associated with the stronger bombardment by higher energy molecules from the "hot side":

$$\frac{\vec{V}_T}{\left|-\frac{1}{T}(\vec{\nabla}T)\right|} \equiv \alpha_i D_i = \frac{3}{4}\nu\left(\frac{1}{1+\frac{\pi}{8}\alpha_d}\right) = \alpha_\infty D_i \tag{27}$$

where D_i is the diffusivity already discussed, ν the kinematic viscosity, and α_d the fraction of molecules that undergo "diffused reflection" from the particle surface. It turns out that the above result for α_i does not exactly match the CE result for molecular sized particles. In order to achieve this match a new constant correction factor σ_{corr} is introduced as follows:

$$\alpha_\infty = \frac{3}{4}\left(\frac{\nu}{D_i}\right)\frac{1}{(1+\frac{\pi}{8}\alpha_d)}\frac{1}{\sigma_{corr}} \tag{28}$$

Physically, the effect of σ_{corr} is to account for the variation in α_d with increasing particle size.* The ratio (ν/D_i) is the particle Schmidt number (Sc_i). It is a measure of the relative importance of momentum to mass transfer. Since the diffusivity of large particles is small, unlike gas molecules, Sc_i is typically large (as seen later, Table I).

Here α_o is taken to be related to the thermophoretic velocity deduced by Epstein,[25] for particles much larger than the gas mean-free-path (using a slip-flow procedure). Using Epstein's result one can write:

$$\alpha_o = \frac{3}{4} Sc_i\left[\frac{1}{1+0.5(\lambda_i/\lambda_c)}\right] \tag{29}$$

where λ_i and λ_c are the thermal conductivities of the particle and gas, respectively.

Equations (26), (28), and (29) when incorporated into Eq. (25) provide the required universal formula for the Soret factor α_i.

3. Transport Properties

The analysis just presented for the evaluation of the transport properties of particles dilute in a carrier gas, was first applied to the case of silicon particles in argon, under typical reactor operating condi-

---

* When $(\alpha_i)_{CE}$ is negative, $\sigma_{corr} \approx 1$ may be assumed.

tions. Figures 5 and 6 show the numerically computed values of α_i and D_i over a wide range of Knudsen number (Kn_i). Table I is provided to gain an idea of the corresponding particle size in terms of the other possible size variables: g, R_i, or Sc_i. Note that while g and R_i are absolute measures of particle size, Kn_i and Sc_i depend strongly upon the prevailing pressure and temperature. Table II gives the values of input constants and the computed values of some useful quantities. The following features regarding Figs. 5 and 6 are also noteworthy:

(i) Both D_i and α_i change rapidly by orders of magnitude, in going from very small ($g = 1$, $R_i = 1.58$ Å, $Kn_i = 4.4 \times 10^3$, $Sc_i = 0.73$) to large particles ($g=10^{18}$, $R_i = 157$ μm, $Kn_i = 4.4 \times 10^{-3}$, $Sc_i = 4.6 \times 10^9$). In this connection it should be mentioned that particles of about 1 μm diam (see Fig. 3 and Table I), which lie within the "transition regime," correspond to the size ranges:

$$10^{10} < g < 10^{11}$$

$$3.4 \times 10^{-5} \text{ cm} < R_i < 7.3 \times 10^{-5} \text{ cm}$$

$$2.04 > Kn_i > 0.95$$

$$1.1 \times 10^6 < Sc_i < 5.35 \times 10^6$$

(ii) As expected physically, the diffusivity D_i of large particles is small, increasing significantly as particles approach molecular dimensions. On the other hand, the magnitude of the Soret factor α_i shows an opposite trend in this case. The physical implication[12] of this is better understood from Eq. (11) which gives the net mass flux. Since D_i is always positive a negative α_i (or temperature gradient) tends to reduce the flux. In this case, the usually large α_i when D_i is small, and vice versa, leads to the conclusion that the Soret flux will dominate the Brownian flux only for larger particles.

Figure 7 reveals the pressure and temperature dependences of the transport coefficients. Due to the complicated functional dependence of α_i and D_i on Kn_i and Sc_i, simple representations may not be possible for all particle sizes. It is clear, however, that over the range of temperatures (≈ 1700 to 3500 K) and pressures (≈ 0.5 to 1.0 atm) of interest in silicon reactors, D_i retains approximately the same characteristics as described by the CE expression (i.e., $T^{3/2}/p$), at least for particle diameters up to about

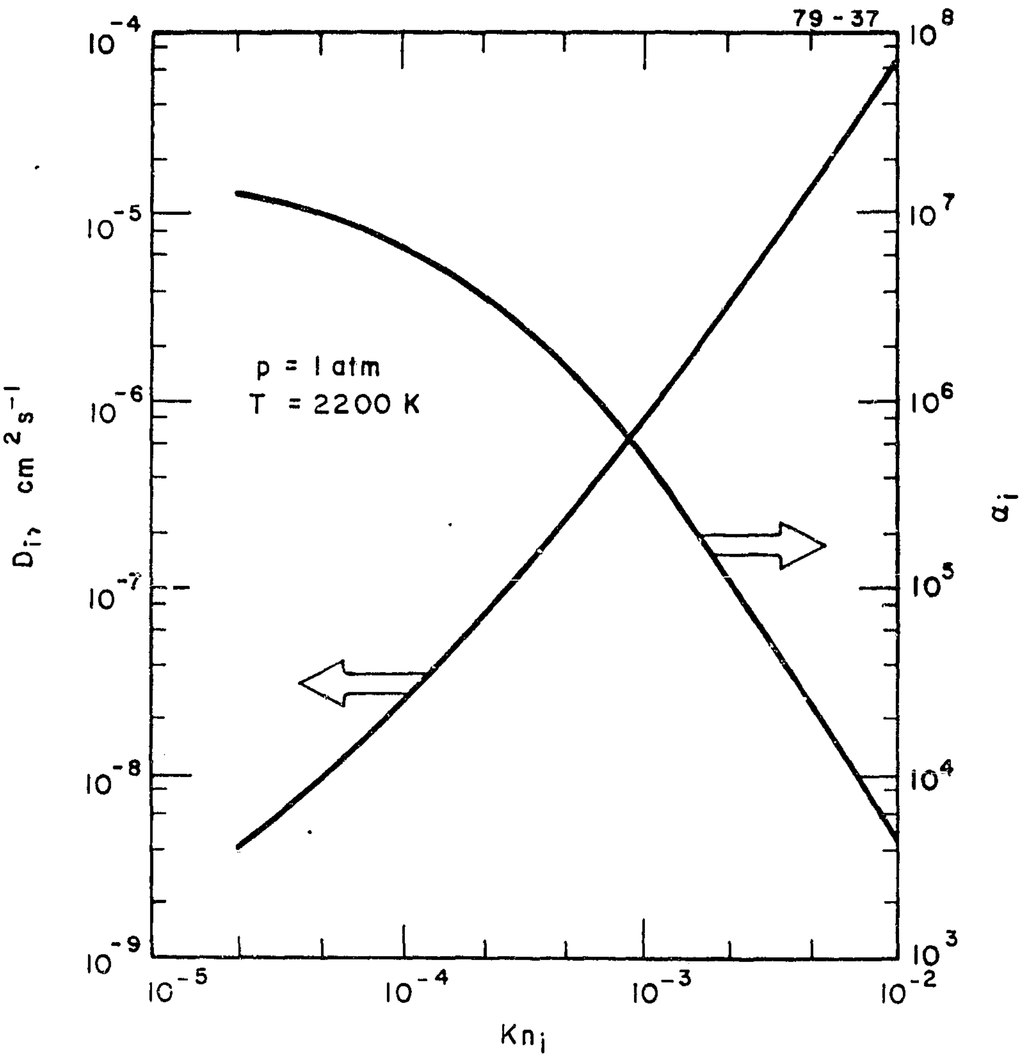

FIGURE 5 VARIATION OF α_i AND D_i FOR "LARGE" PARTICLES

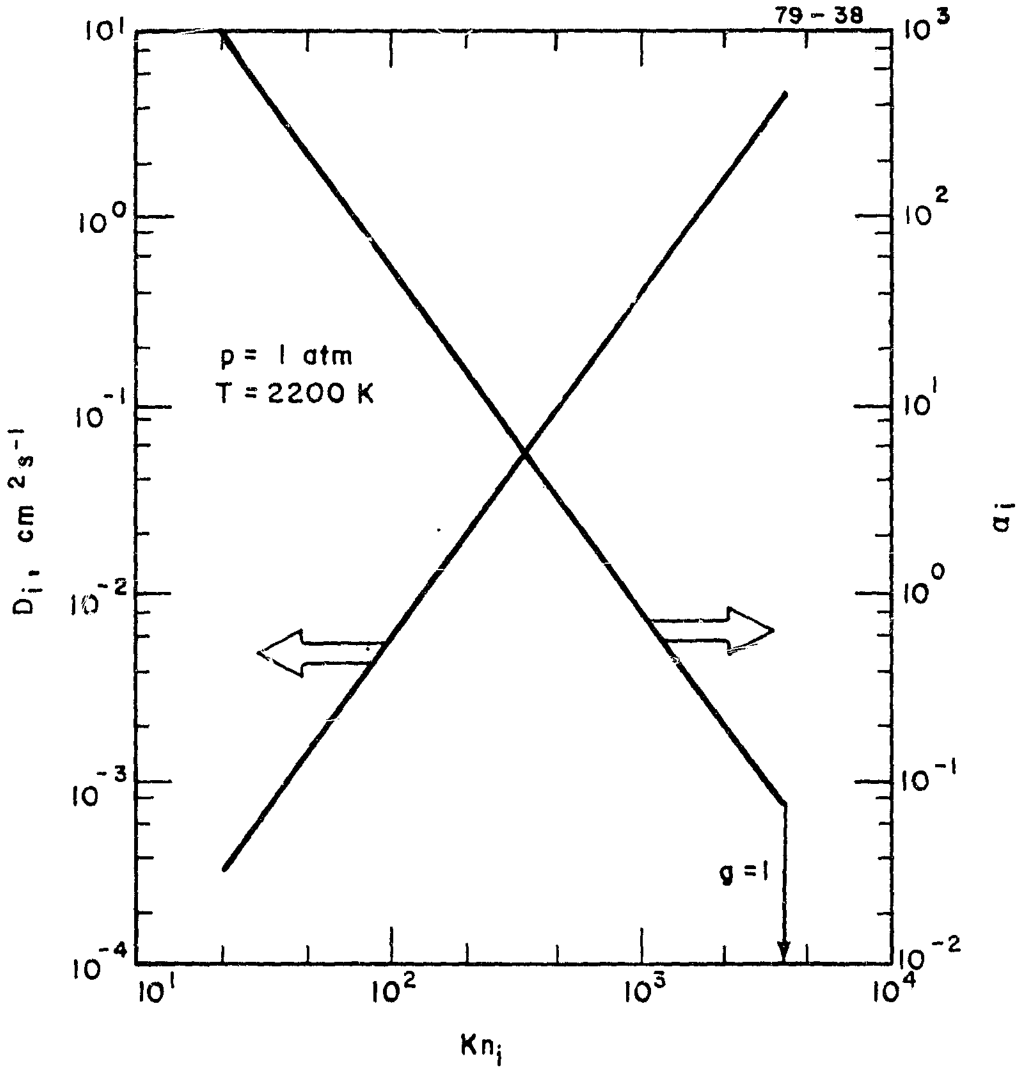

FIGURE 6 VARIATION OF α_i AND D_i FOR "SMALL" PARTICLES (Note the apparent discontinuity in α_i in going from vapor to particles).

TABLE I

COMPARISON OF VARIOUS SIZE RELATED VARIABLES FOR Si-Ar

(p = 1 atm, T = 2200 K)

g	R_i (cm)	Kn_i	Sc_i
1.00	1.58 (-08)	4.39 (03)	7.2 (-01)
1.00 (01)	3.39 (-08)	2.04 (03)	2.4
1.00 (02)	7.31 (-08)	9.50 (02)	7.8
1.00 (03)	1.57 (-07)	4.41 (02)	2.8 (01)
1.00 (04)	3.39 (-07)	2.04 (02)	1.1 (02
1.00 (05)	7.31 (-07)	9.50 (01)	5.2 (02)
1.00 (06)	1.57 (-06)	4.41 (01)	2.3 (03)
1.00 (07)	3.39 (-06)	2.04 (01)	1.0 (04)
1.00 (08)	7.31 (-06)	9.50	4.9 (04)
1.00 (09)	1.57 (-05)	4.41	2.3 (05)
1.00 (10)	3.39 (-05)	2.04	1.1 (06)
1.00 (11)	7.31 (-05)	9.50 (-01)	5.3 (06)
1.00 (12)	1.57 (-04)	4.41 (-01)	2.1 (07)
1.00 (13)	3.39 (-04)	2.04 (-01)	6.8 (07)
1.00 (14)	7.31 (-04)	9.50 (-02)	1.7 (08)
1.00 (15)	1.57 (-03)	4.41 (-02)	4.2 (08)
1.00 (16)	3.39 (-03)	2.04 (-02)	9.5 (08)
1.00 (17)	7.31 (-03)	9.50 (-03)	2.1 (09)
1.00 (18)	1.57 (-02)	4.41 (-03)	4.5 (09)

TABLE II

VALUES OF SOME INPUT AND COMPUTED CONSTANTS

INPUT CONSTANTS (Si-Ar)

p	$= 1$ atm	
T	$= 2200$ K	
α_m	$= 1.0$	
α_d	$= 1.0$	
M_i	$= 28.09$	gm/gm-mol
M_c	$= 39.94$	gm/gm-mol
α_∞	$= -0.10279$ (CE theory estimate)	
N_A	$= 6.023 \times 10^{23}$ molecules/gm-mol	
k	$= 1.3805 \times 10^{-16}$ ergs K^{-1}	
σ_i	$= 2.910$ Å	
(ε_i/k)	$= 3036.0$ K	
σ_c	$= 3.542$ Å	
(ε_c/k)	$= 93.3$ K	
λ_i/λ_c	$= 350$	
C	$= 1.5$	(See Eq. (16)
Kn_o	$= 0.44$	(See Eq. (16)

Particle density: $\rho_i = \rho_{mp} \, [1 - Z(T - T_{mp})]$

ρ_{mp}	$= 3.025$ gm cm^{-3}
Z	$= 1.175 \times 10^{-4}$
T_{mp}	$= 1685$ K

Gas Viscosity: $\dfrac{\mu}{\mu_r} = \left(\dfrac{T}{T_r}\right)^{\omega}$

μ_r	$= 8.021 \times 10^{-4}$ poise
T_r	$= 2000$ K
ω	$= 0.35$

COMPUTED CORRECTION FACTORS

C_m	$= 1.0$	(see Eq. (19))
C_d	$= 0.61557$	(see Eq. (19))
A	$= 1.9182$	(see Eq. (25))

COMPUTED VALUES OF SOME VARIABLES

ν	$= 3.7498$ cm^2 s^{-1}
ρ	$= 2.2116 \times 10^{-4}$ gm cm^{-3}
ℓ	$= 6.9572 \times 10^{-5}$ cm
λ_c	$= 1.5472 \times 10^{-4}$ cals/(cm-s-K)

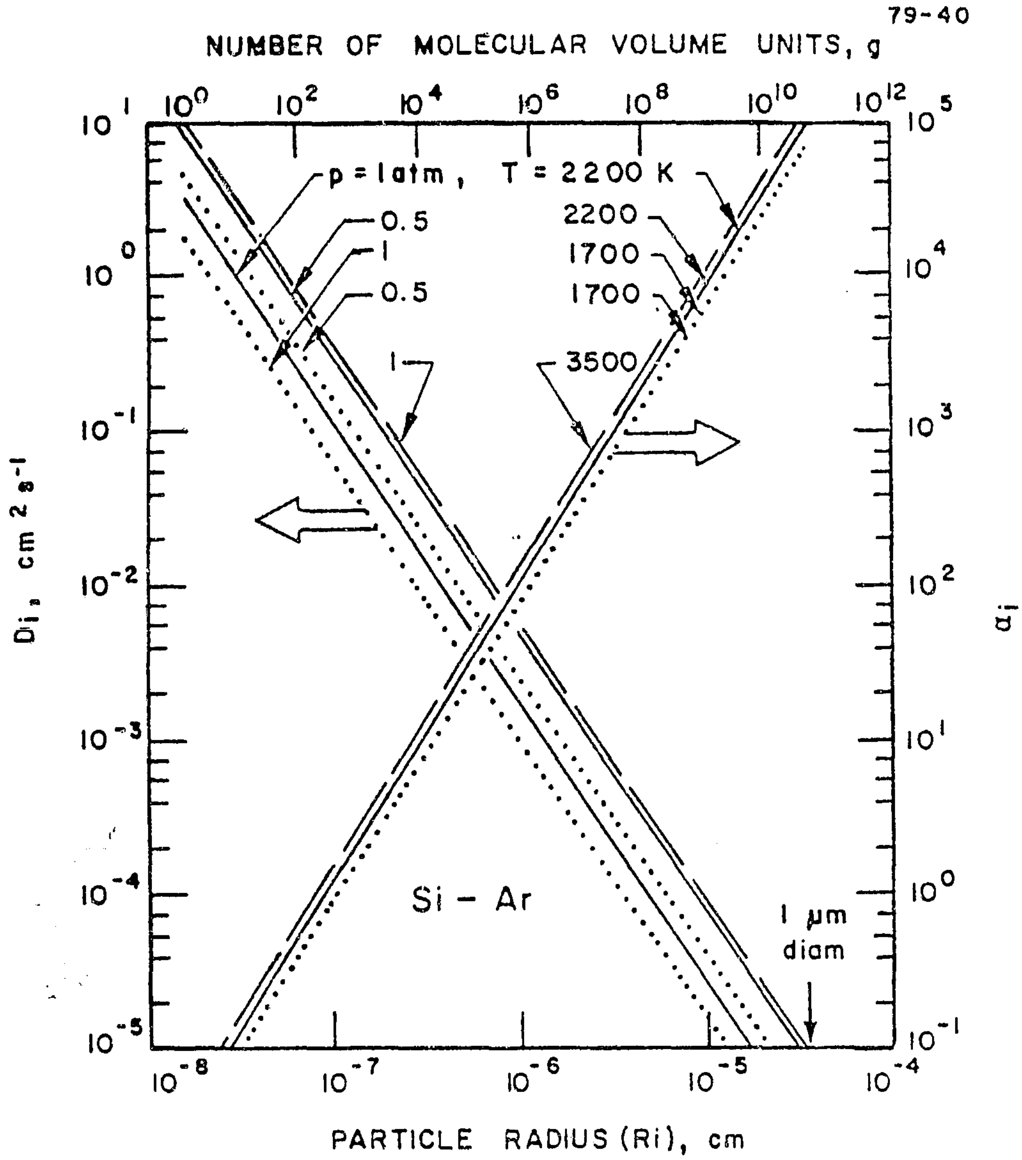

FIGURE 7 VARIATION OF α_i AND D_i WITH PRESSURE AND TEMPERATURE

1 μm. On the other hand, α_i is nearly insensitive to temperature and pressure. Figure 7 is restricted to particle diameters up to about a micron since it is generally true that the Soret effect (thermophoresis) may not be as significant as inertial forces for very large particles.

Figure 8 compares the case of a negative α_i (e.g., Si vapor in Ar) versus one with a positive α_i (e.g., Si vapor in H_2).* In order to increase the separation (or collection) efficiency of silicon, it is clear that α_i should be positive so that the Soret flux is directed towards the "cold" reactor walls. Since a multicomponent mixture of gases is actually present an "effective" Soret factor must be considered such that

$$\alpha_{i,eff} = \left[\sum_{j \neq i} \alpha_{ij} x_j \right] \Big/ (1 - x_i) \tag{30}$$

where x_i is the mole fraction of species i and α_{ij} the Soret factor for species i diffusing in a carrier gas j. It is to be noted that the "effective" Soret factor depends both on the relative concentrations of the various gaseous species present as well as on the magnitude and sign of their individual Soret factors. Typically, as in the Westinghouse process,[1] for instance, one can expect a mixture of silicon in mainly sodium chloride vapor, argon, and hydrogen gases. The various mole fractions would be roughly

$$x_{Si} = 0.08$$
$$x_{H_2} = 0.5$$
$$x_{Ar} = 0.12$$
$$x_{NaCl} = 0.3$$

If the effective carrier gas is a mixture of H_2, Ar, and NaCl its average molecular weight would be

$$M_{avg} = \sum_j x_j M_j = 23.34 \tag{31}$$

---

* Note, the value of α_i for Si particles in both Ar and H_2 is positive.

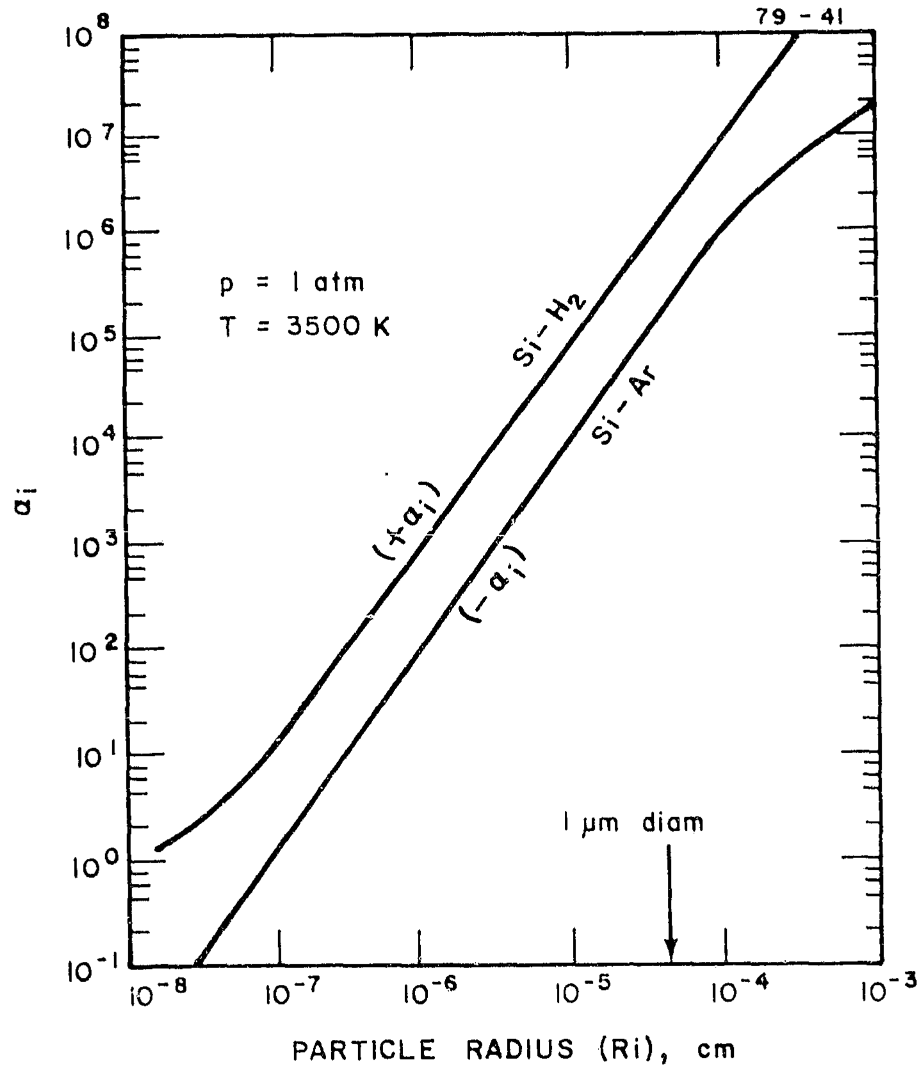

FIGURE 8 COMPARISON OF THE SORET FACTOR α_i FOR TWO DIFFERENT TYPES OF CARRIER GASES

Since the molecular weight of Si vapor molecules is larger than this ($M_{Si} \cong 28$) one would expect a positive value of $\alpha_{i,eff}$ to govern the Soret diffusion of silicon vapor in a mixture of the abovementioned gases. Indeed, using the above mole-fraction estimates together with the following approximate values of α (deduced from CE theory) applicable to Si vapor:

$$\alpha_{Si,H_2} = 0.7$$

$$\alpha_{Si,NaCl} = -0.3$$

$$\alpha_{Si,Ar} = -0.1$$

one obtains $\alpha_{i,eff} \cong 0.27$. Thus the net Soret flux of vapor should normally be directed towards the wall. Using this it was estimated that the Soret mass flux for Si vapor to the reactor wall may not exceed 15-20% of the corresponding Fick flux. However, the sign of $\alpha_{i,eff}$ is sensitive to the prevailing product concentrations. It is conceivable, therefore, that in certain portions, near the reactor walls, the concentration of H_2 may be locally small enough for $\alpha_{i,eff}$ to become negative and lead to a detrimental flux of Si vapor away from the walls.* To eliminate the occurrence of such a possibility we would recommend maintaining a H_2 rich atmosphere near the reactor walls at all times.

It is worth pointing out that the real problem, as mentioned earlier, involves (besides vapor) some silicon droplets that may be treated as "heavy molecules" (i.e., the submicron size class). In the context of the above discussion, pertaining to vapor, it is clear that the effective "molecular weight" of this "heavy-molecule-gas" will always be considerably greater than that of Si vapor (see Eq. (22)). Hence, one can, in fact, expect a huge (but favorable) Soret contribution to the overall mass flux for particles in the "transition regime."

Finally, one needs to gain some idea of the relative importance of the three mechanisms of diffusion (i.e., Brownian, Soret, and turbulent) studied in this report. Brownian and turbulent diffusion are known to be

---

* Our more exact boundary layer calculations in the future will also be aimed at determining the extent of this possibility.

important for very small and very large particles, respectively. However, the importance of Soret diffusion for particles of about a micron diameter is easily seen from Fig. 7. Typically, α_i is large ($\approx 10^5$) while D_i is small ($\approx 10^{-5}$). Recalling that α_i, the Soret factor, is related to a thermal diffusion coefficient $D_{T,i}$ (which is really the appropriate counterpart of D_i), the following useful "thermal diffusion ratios" may be defined:

$$k_T \equiv \frac{D_{T,i}}{\rho D_i} \cong \alpha_i Y_i (1 - Y_i) \tag{32}$$

$$k_T' \equiv \frac{D_{T,i}}{\rho (D_i + \varepsilon_p)} \cong \frac{D_{T,i}}{\rho \varepsilon_p} \cong \frac{\alpha_i D_i Y_i (1 - Y_i)}{\varepsilon_p} \tag{33}$$

The former compares the extent of Soret and Brownian diffusion, whereas the latter expresses the importance of Soret vs overall Fickian (i.e., Brownian + turbulent) diffusion. Since, as seen above, $\alpha_i D_i \cong 1$, $Y_i \cong 0.1$, and $\varepsilon_p \approx 10^{-2}$ (from Eq. (14)), close to the wall,* one finds:

$$k_T \approx 10^4$$

$$k_T' \approx 10$$

That is, Soret transport of silicon particles will predominate all the other forms of diffusion for particles about 1 μm diam, in a viscous sublayer region close to the reactor wall.

It is of interest to determine here the particle size "window" (see Fig. 3) for which Soret diffusion dominates. An upper limit is approximately set by the physical requirement that particles exceeding about 1 μm diam will be controlled solely by their inertia.[19] However, the condition $k_T = 1$ (see Eq. (32)) determines the lower size limit at which Soret diffusion becomes as important as Brownian diffusion. It is interesting to note that this lower limit is sensitive to the prevailing Si concentration (or mass fraction).

---

* Note that since $\varepsilon_p \approx y^3$, the value of ε_p drops rapidly as the wall is approached. For $0 < y^+ < 5$, the variation in ε_p corresponds to $0 < \varepsilon_p < 0.15$ (see Table II).

Using $Y_i \cong 0.1$, one obtains $\alpha_i \cong 10$, which (from Fig. 7) corresponds to a particle diameter of 0.01 μm, under typical reactor conditions. With $k_T = 10$ one can expect Soret diffusion to outweigh Brownian diffusion, a condition which here would correspond to $\alpha_i = 100$ and a particle diam of 0.02 μm. Thus one can safely say that Soret diffusion (i.e., thermophoresis) will be the dominant transport mechanism, near the reactor walls, for silicon droplets in the size range: 0.01 μm to 1.0 μm diam. Note that this is a much wider size range than the one usually quoted in the literature on a somewhat ad hoc basis.

In summary, the analysis just presented emphasizes the following aspects relevant to modeling the silicon separation processes within a reactor:

(i) It is essential that the model describe the transport to the reactor walls of a whole size distribution of silicon particles, from vapor molecules to droplets of several microns in diameter. As a first step to determining the average mass flux due to a statistical particle size distribution, the universally valid transport coefficient formulae, developed in this report, will be needed.

(ii) Very small or large silicon droplets will be deposited on the reactor walls by Brownian and turbulent diffusion, respectively. However, the often ignored transport mechanism of Soret diffusion (or thermophoresis), due to large temperature gradients, will control the deposition of silicon droplets in the diameter range 0.01 μm to 1.0 μm, within a viscous sublayer region close to the walls.

III. SILICON VAPOR DEPOSITION

Using the GENMIX code we focus attention here on results of calculations which pertain to the mechanism of silicon vapor deposition and may thus help us improve the performance of a given silicon reactor.

A. CROSS-STREAM PROFILES

The structure of the developing, turbulent flow in the "downstream" section is characterized by the velocity, temperature, and silicon mass fraction profiles across the reactor tube radius. Figure 9 shows the variations in normalized (with respect to the centerline values) velocity, temperature, and concentration vs the normalized radial distance from the pipe centerline. The operating conditions and pipe geometry were chosen to match the Westinghouse reactor design.[1] As expected from the prescribed mixing length distribution discussed earlier, it is possible to discern at least three regions of distinctly different behavior. Near the pipe centerline ($r/R = 0$) the fully turbulent core flow tends to even out all gradients due to rapid mixing. On the other hand, near the wall ($r/R = 1$) the steepest gradients are established under the influence of the molecular diffusivities for momentum, heat, and mass competing with residual (damped) turbulent diffusivities. Within this "viscous sublayer" the turbulent fluctuations decay rapidly (according to the Van Driest hypothesis) as the wall is approached. Thus, in the immediate vicinity of the wall, the final deposition of silicon may occur primarily by molecular mechanisms (i.e., a nearly laminar flow condition). Joining these two extremes is the outer turbulent (defect law) layer where transport occurs mainly due to diffusive turbulent fluctuations, characterized by a mixing length that varies linearly with distance from the wall. Note that in this region, unlike the viscous sublayer, there is negligible damping due to viscosity. Rather, the length and velocity scales of turbulence are smaller than in the core flow.

Although in reality the abovementioned zones blend continuously into each other, it has been customary to view turbulent pipe flows in terms of at least three different layers (with respect to the velocity profile)[26]: the laminar sublayer, the buffer layer, and the fully turbulent layer. Such a model is especially true of fully developed pipe flows. However, even Fig. 9 (for a developing flow) reveals these zones. The profiles are nearly linear

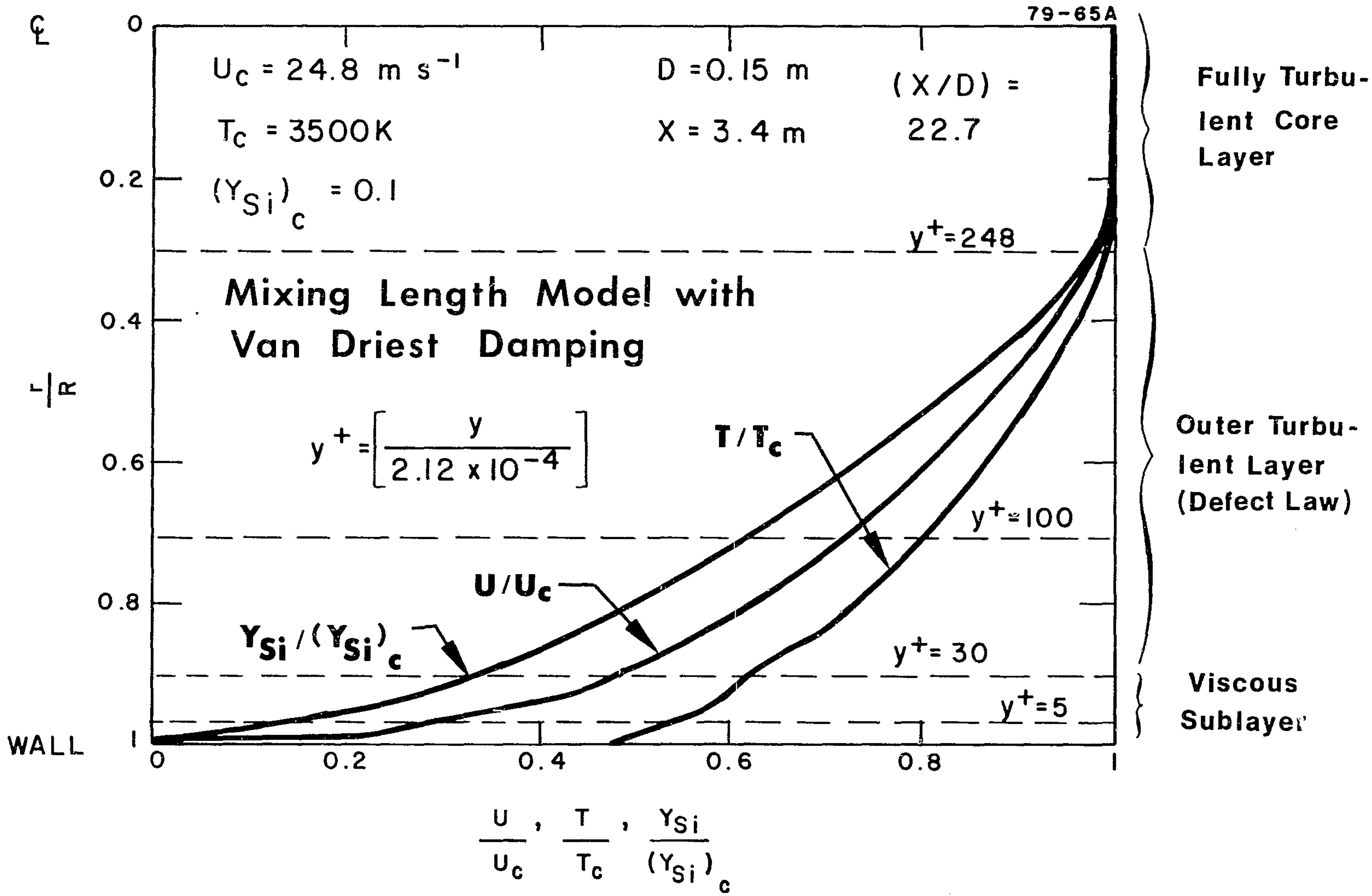

FIGURE 9. COMPUTED CROSS-STREAM PROFILES IN THE DEVELOPING, TURBULENT REACTOR FLOW

next to the wall, implying that the laminar sublayer is a region of constant fluxes of momentum, heat, and mass. It is also interesting to note that the thicknesses of these three laminar sublayers are different, with the temperature and mass fraction layer thickness being equal and larger than the velocity layer thickness. Such a behavior is dictated by the input values of the laminar Prandtl and Schmidt numbers. In this case Pr = Sc = 0.7 was used. On the other hand, the buffer layer region is also seen to be one of nearly constant fluxes, even though the fluxes here are less than those in the laminar sublayer. Based on the prevailing wall shear stress, these two zones are expected to correspond to regions of the velocity profile that lie in the ranges $0 \leq y^+ \leq 5$ (laminar sublayer) and $5 < y^+ \leq 30$ (buffer layer). Both these zones fall within the viscous sublayer. Elsewhere in the boundary layer, the fluxes decrease with distance away from the wall and the final boundary layer thicknesses are nearly all equal. This is a consequence of the assumption that the effective Lewis and Prandtl numbers are nearly unity.

B. STREAMWISE VARIATION OF FLUXES

Figure 10 shows the variation of the non-dimensional momentum, heat, and mass fluxes along the reactor length, X (non-dimensionalized with respect to the reactor diameter, D). The flow and other conditions are identical to those used for Fig. 9. The following definitions of the Stanton numbers for heat (St_h) and mass (St_m) transfer, and the skin-friction coefficient (C_f), were employed:

$$St_h \equiv - \frac{\dot{q}''_w}{\rho_b U_b (\tilde{h}_b - \tilde{h}_w)} \tag{34}$$

$$St_m \equiv - \frac{j''_w}{\rho_b U_b (Y_{i_b} - Y_{i_w})} \tag{35}$$

$$C_f \equiv \frac{\tau_w}{\frac{1}{2} \rho_b U_b^2} \tag{36}$$

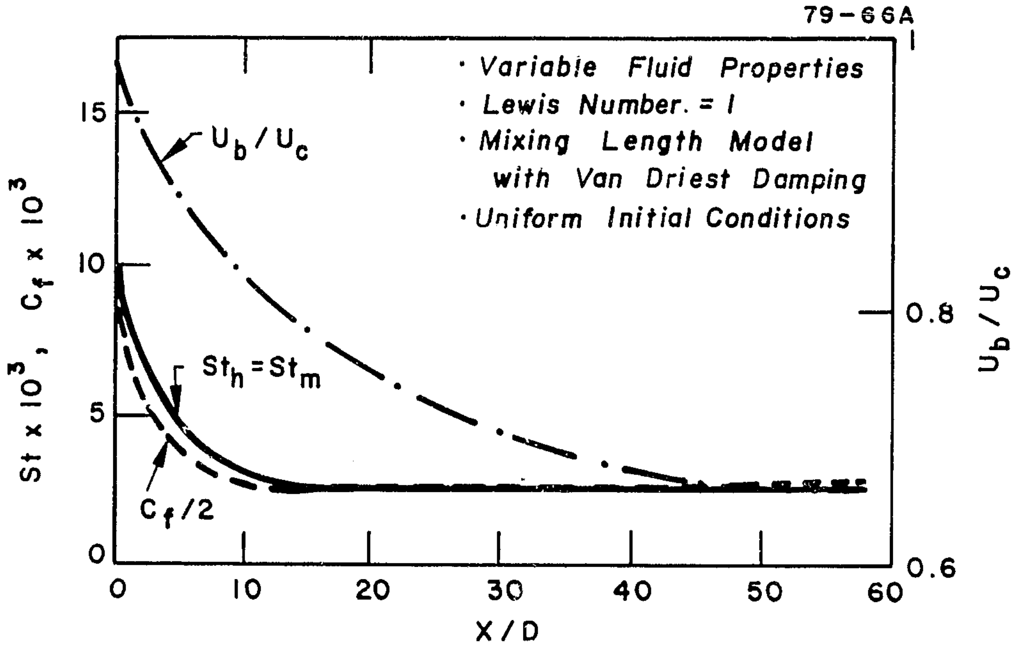

FIGURE 10 COMPUTED STREAMWISE VARIATION OF HEAT, MASS, AND MOMENTUM FLUXES TO THE REACTOR WALLS

where the subscript "b" refers to bulk (average) quantities and "w" refers to quantities evaluated at the reactor wall. $\tilde{h}$ is the stagnation enthalpy which may be defined in terms of the temperature and flow velocity as

$$\tilde{h} \equiv c_p T + \frac{u^2}{2} \tag{37}$$

In the present analysis $St_h = St_m$ due to the assumption of unity effective Lewis number. Furthermore, the closeness of the St and $C_f/2$ curves in Fig.10. suggests that under these conditions a Reynolds analogy of the type:

$$St \cong C_f/2 \tag{38}$$

might be valid within the reactor since the effective Prandtl (and Schmidt) numbers are close to unity and the pressure variation in the downstream direction is small due to a low inlet velocity (in this case $U_{c,inlet} = 20 \text{ m s}^{-1}$). In the other cases studied, it was found that greater deviations from this Reynolds analogy occurred with increasing inlet velocity due to more significant pressure gradients. Table III summarizes some of these results. It

TABLE III

NON-DIMENSIONAL FLUXES

$U_{c,inlet} = 20 \text{ m s}^{-1}$

X/D	$C_f/2$	$St_h (= St_m)$	$Nu_h (= Nu_m)$[a]	Re_b[b]	U_c/U_b[c]
2.5000E-03	8.3427E-02	1.1552E-01	3.5594E+02	4.4018E+03	1.0008E+00
2.5004E-01	1.1321E-02	1.2953E-02	4.0070E+01	4.4191E+03	1.0188E+00
2.7492E+00	4.7148E-03	5.1492E-03	1.5839E+01	4.3943E+03	1.0781E+00
5.2479E+00	4.0373E-03	4.3114E-03	1.3119E+01	4.3468E+03	1.1201E+00
7.7466E+00	3.6458E-03	3.8325E-03	1.1549E+01	4.3048E+03	1.1567E+00
1.0245E+01	3.4007E-03	3.5314E-03	1.0543E+01	4.2650E+03	1.1903E+00
1.2744E+01	3.2230E-03	3.3122E-03	9.8011E+00	4.2273E+03	1.2219E+00
1.5243E+01	3.0874E-03	3.1455E-03	9.2280E+00	4.1910E+03	1.2520E+00
1.7742E+01	2.9807E-03	3.0147E-03	8.7699E+00	4.1558E+03	1.2810E+00
2.0241E+01	2.8945E-03	2.9094E-03	8.3941E+00	4.1217E+03	1.3091E+00
2.2740E+01	2.8237E-03	2.8232E-03	8.0798E+00	4.0885E+03	1.3365E+00
2.5239E+01	2.7646E-03	2.7516E-03	7.8132E+00	4.0565E+03	1.3633E+00
2.7738E+01	2.7146E-03	2.6916E-03	7.5856E+00	4.0261E+03	1.3895E+00
3.0237E+01	2.6726E-03	2.6415E-03	7.3936E+00	3.9985E+03	1.4151E+00
3.2736E+01	2.6369E-03	2.5995E-03	7.2345E+00	3.9758E+03	1.4395E+00
3.5235E+01	2.6058E-03	2.5638E-03	7.1107E+00	3.9621E+03	1.4621E+00
3.7734E+01	2.5807E-03	2.5352E-03	7.0416E+00	3.9679E+03	1.4800E+00
4.0233E+01	2.5590E-03	2.5100E-03	7.0139E+00	3.9920E+03	1.4926E+00
4.2732E+01	2.5397E-03	2.4875E-03	7.0170E+00	4.0298E+03	1.5009E+00
4.5231E+01	2.5227E-03	2.4675E-03	7.0405E+00	4.0761E+03	1.5059E+00
4.7731E+01	2.5075E-03	2.4496E-03	7.0768E+00	4.1271E+03	1.5087E+00
5.0230E+01	2.4939E-03	2.4334E-03	7.1205E+00	4.1801E+03	1.5101E+00
5.2729E+01	2.4817E-03	2.4188E-03	7.1682E+00	4.2337E+03	1.5106E+00
5.5228E+01	2.4708E-03	2.4053E-03	7.2184E+00	4.2871E+03	1.5106E+00
5.7727E+01	2.4609E-03	2.3930E-03	7.2703E+00	4.3402E+03	1.5102E+00
6.0000E+01	2.4522E-03	2.3832E-03	7.3196E+00	4.3876E+03	1.5076E+00

[a] Nu is the Nusselt number.

[b] Re_b is the bulk Reynolds number based on pipe diameter.

[c] U_c/U_b is the ratio of centerline to bulk velocity.

TABLE III (Continued)

$U_{c,inlet} = 50$ m s^{-1}

X/D	$C_f/2$	$St_h (= St_m)$	$Nu_h (= Nu_m)$[a]	Re_b[b]	U_c/U_b[c]
2.5000E-03	3.6930E-02	5.2027E-02	4.0096E+02	1.1010E+04	1.0003E+00
2.5004E-01	6.7661E-03	7.9653E-03	6.1594E+01	1.1047E+04	1.0108E+00
2.7491E+00	3.2103E-03	3.6452E-03	2.7992E+01	1.0970E+04	1.0495E+00
5.2480E+00	2.7381E-03	3.0468E-03	2.3198E+01	1.0877E+04	1.0783E+00
7.7471E+00	2.4685E-03	2.7058E-03	2.0449E+01	1.0797E+04	1.1035E+00
1.0246E+01	2.2893E-03	2.4799E-03	1.8616E+01	1.0724E+04	1.1265E+00
1.2745E+01	2.1596E-03	2.3170E-03	1.7283E+01	1.0656E+04	1.1479E+00
1.5245E+01	2.0606E-03	2.1926E-03	1.6258E+01	1.0592E+04	1.1683E+00
1.7744E+01	1.9821E-03	2.0945E-03	1.5438E+01	1.0530E+04	1.1877E+00
2.0243E+01	1.9182E-03	2.0146E-03	1.4765E+01	1.0470E+04	1.2065E+00
2.2743E+01	1.8651E-03	1.9483E-03	1.4199E+01	1.0411E+04	1.2248E+00
2.5242E+01	1.8205E-03	1.8931E-03	1.3721E+01	1.0354E+04	1.2426E+00
2.7741E+01	1.7830E-03	1.8469E-03	1.3313E+01	1.0297E+04	1.2600E+00
3.0241E+01	1.7510E-03	1.8077E-03	1.2960E+01	1.0242E+04	1.2771E+00
3.2740E+01	1.7234E-03	1.7741E-03	1.2650E+01	1.0186E+04	1.2940E+00
3.5239E+01	1.6995E-03	1.7452E-03	1.2377E+01	1.0131E+04	1.3107E+00
3.7739E+01	1.6786E-03	1.7202E-03	1.2134E+01	1.0077E+04	1.3272E+00
4.0238E+01	1.6604E-03	1.6985E-03	1.1917E+01	1.0023E+04	1.3436E+00
4.2737E+01	1.6444E-03	1.6797E-03	1.1723E+01	9.9699E+03	1.3598E+00
4.5237E+01	1.6304E-03	1.6636E-03	1.1552E+01	9.9200E+03	1.3758E+00
4.7736E+01	1.6183E-03	1.6497E-03	1.1413E+01	9.8831E+03	1.3909E+00
5.0235E+01	1.6071E-03	1.6376E-03	1.1354E+01	9.9048E+03	1.4037E+00
5.2735E+01	1.5985E-03	1.6286E-03	1.1356E+01	9.9609E+03	1.4068E+00
5.5234E+01	1.5911E-03	1.6206E-03	1.1397E+01	1.0047E+04	1.4095E+00
5.7733E+01	1.5842E-03	1.6129E-03	1.1440E+01	1.0133E+04	1.4113E+00
6.0000E+01	1.5738E-03	1.6071E-03	1.1483E+01	1.0208E+04	1.4126E+00

TABLE III (Continued)

$U_{c,inlet}$ = 100 m s^{-1}

X/D	$C_f/2$	$St_h (= St_m)$	$Nu_h (= Nu_m)$ [a]	Re_b [b]	U_c/U_b [c]
2.5000E-03	1.9136E-02	2.7157E-02	4.1865E+02	2.2023E+04	1.0002E+00
2.5006E-01	4.3963E-03	1.7131E-03	2.6536E+01	2.2128E+04	1.0069E+00
2.7511E+00	2.0307E-03	9.9197E-04	1.5496E+01	2.2316E+04	1.0305E+00
5.2513E+00	1.8244E-03	9.0956E-04	1.4227E+01	2.2345E+04	1.0485E+00
7.7513E+00	1.6919E-03	8.5500E-04	1.3381E+01	2.2358E+04	1.0647E+00
1.0251E+01	1.5985E-03	8.1594E-04	1.2772E+01	2.2361E+04	1.0797E+00
1.2751E+01	1.5281E-03	7.8576E-04	1.2298E+01	2.2358E+04	1.0938E+00
1.5251E+01	1.4724E-03	7.6174E-04	1.1917E+01	2.2350E+04	1.1073E+00
1.7751E+01	1.4273E-03	7.4204E-04	1.1603E+01	2.2337E+04	1.1201E+00
2.0251E+01	1.3899E-03	7.2546E-04	1.1335E+01	2.2320E+04	1.1326E+00
2.2751E+01	1.3583E-03	7.1135E-04	1.1104E+01	2.2300E+04	1.1447E+00
2.5251E+01	1.3312E-03	6.9919E-04	1.0903E+01	2.2277E+04	1.1565E+00
2.7751E+01	1.3080E-03	6.8867E-04	1.0726E+01	2.2250E+04	1.1680E+00
3.0251E+01	1.2880E-03	6.7972E-04	1.0573E+01	2.2220E+04	1.1794E+00
3.2750E+01	1.2710E-03	6.7185E-04	1.0435E+01	2.2188E+04	1.1905E+00
3.5250E+01	1.2561E-03	6.6507E-04	1.0313E+01	2.2153E+04	1.2015E+00
3.7750E+01	1.2432E-03	6.5904E-04	1.0202E+01	2.2115E+04	1.2124E+00
4.0250E+01	1.2319E-03	6.5370E-04	1.0102E+01	2.2076E+04	1.2232E+00
4.2750E+01	1.2220E-03	6.4859E-04	1.0009E+01	2.2034E+04	1.2339E+00
4.5249E+01	1.2132E-03	6.4477E-04	9.9252E+00	2.1991E+04	1.2445E+00
4.7749E+01	1.2055E-03	6.4121E-04	9.8500E+00	2.1945E+04	1.2551E+00
5.0249E+01	1.1988E-03	6.3794E-04	9.7786E+00	2.1898E+04	1.2656E+00
5.2749E+01	1.1930E-03	6.3530E-04	9.7158E+00	2.1848E+04	1.2761E+00
5.5248E+01	1.1876E-03	6.3323E-04	9.6679E+00	2.1811E+04	1.2858E+00
5.7748E+01	1.1804E-03	6.3460E-04	9.6935E+00	2.1819E+04	1.2918E+00
6.0000E+01	1.1243E-03	9.3289E-04	1.4275E+01	2.1860E+04	1.2939E+00

TABLE III (Continued)

$U_{c,inlet}$ = 200 m s^{-1}

X/D	$C_{f/2}$	$St_h (= St_m)$	$Nu_h (= Nu_m)$[a]	Re_b[b]	U_c/U_b[c]
2.5000E-03	9.7242E-03	3.5939E-03	1.1082E+02	4.4050E+04	1.0001E+00
2.4996E-01	6.4262E-03	8.5827E-03	2.6380E+02	4.3909E+04	1.0061E+00
2.7489E+00	2.6766E-03	3.0626E-03	9.3320E+01	4.3530E+04	1.0392E+00
5.2480E+00	2.2268E-03	2.4864E-03	7.5214E+01	4.3215E+04	1.0630E+00
7.7473E+00	1.9831E-03	2.1798E-03	6.5547E+01	4.2957E+04	1.0834E+00
1.0247E+01	1.8267E-03	1.9845E-03	5.9356E+01	4.2727E+04	1.1019E+00
1.2746E+01	1.7221E-03	1.8600E-03	5.5350E+01	4.2512E+04	1.1191E+00
1.5245E+01	1.6467E-03	1.7649E-03	5.2266E+01	4.2307E+04	1.1354E+00
1.7745E+01	1.5995E-03	1.7083E-03	5.0348E+01	4.2105E+04	1.1512E+00
2.0244E+01	1.5919E-03	1.7019E-03	4.9907E+01	4.1892E+04	1.1667E+00
2.2743E+01	1.8083E-03	2.0271E-03	5.8935E+01	4.1533E+04	1.1838E+00
2.5241E+01	1.8984E-03	2.1605E-03	6.1671E+01	4.0778E+04	1.2064E+00
2.7740E+01	1.7884E-03	2.0120E-03	5.6928E+01	4.0421E+04	1.2259E+00
3.0239E+01	1.7579E-03	1.9848E-03	5.5668E+01	4.0068E+04	1.2440E+00
3.2738E+01	1.7717E-03	2.0150E-03	5.6166E+01	3.9820E+04	1.2608E+00
3.5236E+01	1.7937E-03	2.0508E-03	5.8035E+01	4.0427E+04	1.2591E+00
3.7735E+01	1.8130E-03	2.0783E-03	6.0009E+01	4.1249E+04	1.2497E+00
4.0234E+01	1.8257E-03	2.0958E-03	6.1497E+01	4.1919E+04	1.2420E+00
4.2733E+01	1.8348E-03	2.1082E-03	6.2669E+01	4.2467E+04	1.2366E+00
4.5232E+01	1.8419E-03	2.1178E-03	6.3652E+01	4.2937E+04	1.2329E+00
4.7731E+01	1.8474E-03	2.1254E-03	6.4507E+01	4.3358E+04	1.2303E+00
5.0230E+01	1.8520E-03	2.1318E-03	6.5281E+01	4.3747E+04	1.2285E+00
5.2729E+01	1.8581E-03	2.1432E-03	6.6179E+01	4.4112E+04	1.2271E+00
5.5228E+01	1.8652E-03	2.1532E-03	6.7017E+01	4.4464E+04	1.2261E+00
5.7727E+01	1.8733E-03	2.1641E-03	6.7880E+01	4.4809E+04	1.2253E+00
6.0000E+01	1.8799E-03	2.1737E-03	6.8647E+01	4.5116E+04	1.2247E+00

TABLE III (Continued)

$U_{b,inlet} = 400$ m s^{-1}

X/D	$C_f/2$	$St_h (= St_m)$	$Nu_h (= Nu_m)$[a]	Re_b[b]	U_c/U_b[c]
2.5000E-03	1.0918E-02	1.4835E-02	9.1491E+02	8.8103E+04	1.0000E+00
2.4995E-01	5.1554E-03	6.1955E-03	3.8037E+02	8.7705E+04	1.0070E+00
2.7488E+00	2.9634E-03	3.4991E-03	2.1241E+02	8.6720E+04	1.0402E+00
5.2473E+00	2.8199E-03	3.3401E-03	2.0011E+02	8.5579E+04	1.0692E+00
7.7457E+00	2.7730E-03	3.2953E-03	1.9474E+02	8.4424E+04	1.0975E+00
1.0244E+01	2.7626E-03	3.2941E-03	1.9196E+02	8.3250E+04	1.1258E+00
1.2743E+01	2.7586E-03	3.2991E-03	1.8955E+02	8.2079E+04	1.1543E+00
1.5241E+01	2.7605E-03	3.3111E-03	1.8754E+02	8.0915E+04	1.1831E+00
1.7739E+01	2.7681E-03	3.3311E-03	1.8598E+02	7.9757E+04	1.2122E+00
2.0238E+01	2.7807E-03	3.3583E-03	1.8494E+02	7.8672E+04	1.2413E+00
2.2736E+01	2.7982E-03	3.3729E-03	1.8715E+02	7.8800E+04	1.2593E+00
2.5234E+01	2.8020E-03	3.4042E-03	1.9155E+02	8.0386E+04	1.2592E+00
2.7733E+01	2.7930E-03	3.3965E-03	1.9502E+02	8.2026E+04	1.2553E+00
3.0231E+01	2.7800E-03	3.3827E-03	1.9769E+02	8.3485E+04	1.2518E+00
3.2730E+01	2.7656E-03	3.3664E-03	1.9985E+02	8.4811E+04	1.2490E+00
3.5228E+01	2.7507E-03	3.3490E-03	2.0172E+02	8.6048E+04	1.2469E+00
3.7727E+01	2.7358E-03	3.3311E-03	2.0339E+02	8.7228E+04	1.2451E+00
4.0226E+01	2.7211E-03	3.3130E-03	2.0493E+02	8.8367E+04	1.2436E+00
4.2724E+01	2.7067E-03	3.2951E-03	2.0638E+02	8.9475E+04	1.2422E+00
4.5223E+01	2.6926E-03	3.2774E-03	2.0776E+02	9.0560E+04	1.2409E+00
4.7722E+01	2.6789E-03	3.2600E-03	2.0909E+02	9.1624E+04	1.2396E+00
5.0221E+01	2.6655E-03	3.2430E-03	2.1037E+02	9.2671E+04	1.2385E+00
5.2719E+01	2.6526E-03	3.2264E-03	2.1162E+02	9.3701E+04	1.2374E+00
5.5218E+01	2.6400E-03	3.2101E-03	2.1283E+02	9.4715E+04	1.2363E+00
5.7717E+01	2.6277E-03	3.1943E-03	2.1402E+02	9.5715E+04	1.2352E+00
6.0000E+01	2.6141E-03	3.2032E-03	2.1662E+02	9.6609E+04	1.2343E+00

should be pointed out that "bulk" values of properties differ from their corresponding centerline values (denoted by the subscript "c"). This is clear from the variation of U_c/U_b with downstream distance. Typically, the centerline values monotonically exceed the bulk values in the region of developing flow and become constant only when "fully developed" flow conditions are established.*

C. SILICON COLLECTION EFFICIENCY

The ratio of the mass of silicon deposited on the reactor walls, due to the boundary layer convective-diffusion processes, to the total mass of silicon entering a given reactor may be defined as the "collection efficiency." This ratio can readily be calculated by integrating the downstream variation of the silicon mass flux to the walls, j''_w, over the reactor length of interest. Figure 11 shows the results of such a computation. It is seen that the silicon collection efficiency, for a given inlet flow velocity, increases as the reactor length increases. Initially, this increase is slower than in the aft regions (as expected from the mass flux variation shown in Fig. 10). Furthermore, Fig. 11 reveals the important effect of changing flow residence times on the reactor's performance. As expected, faster through-flows reduce the collection efficiency drastically since the flow time is much less than the time for effective silicon vapor diffusion to the reactor walls.

---

* It has been shown[4] that in a pipe, as the developing shear layers merge, U_c exceeds $(U_c)_{\text{fully developed}}$ prior to settling down to a state of equality. Such details of shear layer interaction, however, cannot be predicted by the present mixing length model.

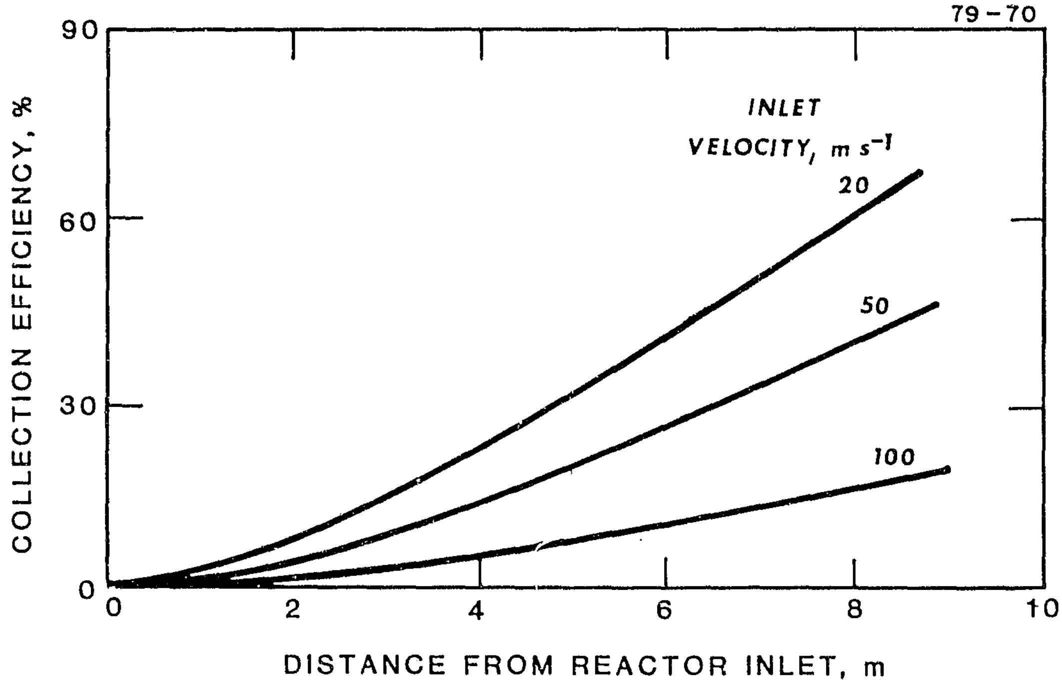

FIGURE 11 COMPUTED VARIATION OF SILICON VAPOR COLLECTION EFFICIENCY OF A REACTOR WITH LENGTH AND INLET VELOCITY

To summarize the results of this section:

(i) Silicon vapor deposition processes were analyzed with due regard to the structure of the developing turbulent flow that prevails over most of a reactor's length.

(ii) The modified GENMIX code was used to provide a computational capability that should be useful to the designer in optimizing a given reactor, with a minimum of experimentation.

(iii) A reliable basis for assessing the silicon vapor collection efficiency of a given reactor has been established.

Finally, it must be mentioned that Soret transport of silicon vapor was intentionally excluded from this analysis, since it is expected to be small in the absence of condensation. The effect, however, will become important when silicon droplets are considered.

IV. A MODEL FOR SILICON PARTICLE COLLECTION

In this section we consider the introduction of particles into the existing GENMIX model[2] for the vapor collection efficiency of silicon reactors of the Westinghouse type.[1] The last section concerned the partial collection onto the reactor walls of silicon vapor present in the reactor's hot core flow (see Fig. 1 for a schematic of the physical situation). While the deposition of vapor was attributed to the processes of convection, Fick diffusion, and turbulent (or eddy) transport to the reactor walls, the deposition of particles (silicon droplets) is expected to be controlled by additional mechanisms. In particular, one expects Brownian diffusion to govern the deposition of small particles (10^{-4}-10^{-2} μm diam) while Soret transport will become more important for larger particles (10^{-2}-1.0 μm diam), especially within the "viscous sublayer" region next to the reactor walls, where large temperature gradients exist. Away from the walls the particles will be transported entirely by diffusive turbulent velocity fluctuations. This later effect will always tend to drive the particles close to the walls. As was shown above (Section II), near the walls the former two molecular mechanisms (i.e., Brownian and Soret effects) will predominate.

In order to describe the overall silicon collection efficiency (generally due to vapor and droplets) of a reactor, it is essential to model the deposition behavior of a distribution of particles[13] varying in size from molecular dimensions to about a micron diameter. In the model considered here it is assumed that the particle size distribution function (PSDF) for the silicon droplets entering the downstream section of the reactor for separation/collection is known. The question, as before, is, "What fraction of the silicon vapor and droplets entering the reactor is collected on the walls?" The model described here attempts to answer this question, with due regard to the various deposition mechanisms mentioned earlier and the two-dimensional developing boundary layer flow within the reactor. In fact, as a result of the slowly developing boundary layers within typical reactors, most of the deposition occurs prior to the establishment of "fully-developed" conditions (i.e., with no streamwise variations). Hence, the available simpler solutions which are valid for fully-developed, or partially developed (Graetz type)[27] flow cannot be used since such analyses only provide an asymptotic limit for the silicon mass transfer rate to the walls. Over the reactor's separation/collection

length, the velocity, temperature, and concentration boundary layers are developing simultaneously. Hence, numerical solution of the coupled system of boundary layer conservation equations is unavoidable in determining the cumulative silicon collection efficiency, which depends upon the variation of the silicon mass flux (at the wall) along the length of the reactor.

This section outlines the general approach adopted in the numerical modeling of the silicon separation/collection processes. Specific complications are isolated in order to show the nature of the problem and the methods used to overcome the difficulties encountered. Insufficient time was available to fully couple a code based on this model to GENMIX. It is hoped that in follow-on work this will be accomplished.

A. PHYSICAL AND MATHEMATICAL ASPECTS

The present two-phase flow model for describing the transport of silicon particles from the hot ($\approx$ 3500 K) core-flow of the reactor to the cooled walls ($\approx$ 1685 K) is based on the assumptions that: (i) the total particle volume is considerably smaller than the volume of the surrounding gas phase so that particle-particle interaction is negligible; (ii) the concentration of the particles is small enough so that their presence does not alter the surrounding gas flow field (i.e., velocity and temperature distributions); (iii) the particles are small enough that they may be treated as "heavy-molecules" in local equilibrium with the gas.

These assumptions are usually justified in the downstream section of the silicon reactor being considered. The diluteness of the silicon droplets can be expected to increase with increasing distance from the droplet source, immediately following combustion. On the other hand, the nature of the processes leading to silicon droplet formation (gas-to-particle conversion via nucleation) ensures that the resulting particles will be of sub-micron sizes.

Under these assumptions, one can write the following particle mass conservation equation suitable to the developing, boundary layer flow within the reactor (axisymmetric):

$$\rho u \frac{\partial Y_i}{\partial x} + \rho v \frac{\partial Y_i}{\partial r} = - \frac{1}{r} \frac{\partial}{\partial r} \left[r \, j_{i_r} \right] \tag{39}$$

where the radial mass flux is given by

$$j_{i_r} \cong j_{i_{laminar}} + j_{i_{turbulent}} \tag{40}$$

$$= -\rho D_i \left[\frac{\partial Y_i}{\partial r} + \alpha_i Y_i (1 - Y_i) \frac{1}{T} \frac{\partial T}{\partial r} \right] - \rho \, \varepsilon_p \frac{\partial Y_i}{\partial r} \tag{41}$$

Expressions for the Brownian diffusivity, D_i, and the dimensionless Soret factor, α_i, were presented above. The turbulent diffusivity, ε_p, is taken to be unaffected by the small particles being considered and hence given by the expressions suggested by Lin et al.[15*] Equation (39) is valid provided the particles do not grow appreciably (via vapor collection on their surfaces) during passage through the particle diffusion layer. Such an assumption may be justifiable in view of the typical thinness of these layers, as seen later. Moreover, Eq. (39) applies to particles of a uniform size, present in the external stream, depositing by convection, Brownian diffusion, and thermophoresis on the reactor walls. In order to describe the deposition of particle size distributions, therefore, one needs to repeatedly solve Eq. (39) with the appropriate boundary condition on concentration at the diffusion layer's edge, corresponding to each particle size class. That is, a PSDF expressing the variation of particle concentration vs size in the external stream is discretized into a finite number of independent size classes, with particles in a given class being characterized by uniquely defined transport coefficients, α_i and D_i. The velocity and temperature fields within the turbulent boundary layers on the reactor walls have to be supplied to the particle diffusion equation. In the present case, for this purpose, the entire velocity and temperature profile history along the reactor tube length is independently computed using a modification of the GENMIX code[2,5] for the finite-difference solution of coupled momentum and energy equations (including variable fluid properties and the damping of turbulence near the reactor walls).

Even in the absence of turbulence, the effects of thermophoresis and Brownian diffusion can immensely complicate the analysis of silicon droplet deposition behavior within the reactor. Physically, one expects thermophoretic effects to be important in regions of the reactor flow field where temperature

---

* This implies that the particles follow the turbulent eddy motions of the gas. Actually, particles near 1 μm diam might break away from the eddies due to their large inertia. Such inertial effects are excluded in the present diffusional model.

gradients are large (i.e., near the walls). On the other hand, the larger particle size class, for which thermophoretic deposition is significant, corresponds to Brownian diffusivities that are extremely small. There exists, therefore, a thin sublayer region next to the walls where both Brownian diffusion and thermophoresis may be important for particle deposition. Outside this sublayer, however, temperature gradients continue to remain strong so that thermophoresis remains important, and diffusion by Brownian motion of particles becomes negligible. Thus one can consider the presence of an "inner layer," next to the walls, where thermophoretic transport of particles balances convection and Brownian diffusion. External to this is an "outer layer" wherein convective transport balances thermophoretic effects in conserving particle mass.* Although Eq. (39) is, in principle, general enough to describe both these layers simultaneously, from the standpoint of computational efficiency it is useful to consider the abovementioned division into different layers (due to their disparate thicknesses).

It has been established that, in analyzing the effects of thermophoresis, it is convenient to visualize the introduction into the boundary layer of additional pseudo "sink" and "suction" behavior.[12] The former will tend to deplete particle concentrations above the reactor walls while the latter acts towards increasing them. The net result of these opposing effects of thermophoresis is to appreciably increase the collection rate for the larger particles.[30]

B. COMMENTS ON THE NUMERICAL SOLUTION PROCEDURE

A few difficulties arise with the numerical solution of the particle transport problem, described in the previous section. They are briefly discussed in this section, together with strategies adopted to overcome them.

---

* It is to be noted that these layers are not related to the "viscous sublayer" region next to the walls where turbulent dissipation of eddies occurs. In fact, both the "inner" and "outer" thermophoretic layers may be embedded within the "viscous sublayer" region. Moreover, the division into "layers" adopted here is different from the asymptotic three-layer model implied by Refs. 28 and 29.

1. The Stiffness Problem

When the characteristic time scales associated with convection, Brownian diffusion, and thermophoresis in Eq. (39) become widely disparate, one is likely to encounter "stiffness" during the numerical solution process. The problem is manifested by unstable numerical solutions if the integration does proceed or by a failure of the integrator to march forward, along the reactor length. The former corresponds to a build-up of truncation error as the solution proceeds (often seen as a wildly fluctuating solution) while the latter shows up as an inability of the integrator to meet the specified local error tolerance.

To overcome this problem, a "stiffness solver," based on Gear's variable order, variable step-size, integration formulae is adopted.[31] A method of lines approach is utilized, suitably discretizing the derivatives along the radial coordinate, in order to solve Eq. (39) as an initial-value, ordinary differential equation. The "solver" employs an implicit scheme for greater stability and to allow marching in larger step sizes. Both these features are crucial to coping with the stiffness problem.

2. The Scaling Problem

Due to the disparate thicknesses of the "inner" and "outer" thermophoretic layers, discussed earlier, one runs into resolution difficulties if the adopted radial grid spacing approaches the thickness of the inner layer, or exceeds it.

In order to deal with this problem the following transformation of the radial coordinate is defined:

$$\tilde{r} = \frac{r_w - r}{r_w - r_m} \tag{42}$$

where r, r_w, and r_m are the radial locations corresponding to the point of interest, the reactor wall, and the edge of the particle diffusion layer. Note that the transformation restricts the domain of integration of Eq. (39) to the range $0 \leq \tilde{r} \leq 1$, regardless of particle size. It is, of course, necessary to specify the approximate thickness of the diffusion layer (i.e., $\delta_m = r_w - r_m$). Since the thickness of the thermal boundary layer (i.e., δ_T), at a given x, is known via prior solution of the energy equation, one may

readily estimate δ_m using the known Lewis number, for that particle size class, from the relation*:

$$\delta_m \cong \delta_T (Le_g)^{1/3} \tag{43}$$

3. Determination of the Variable Edge Boundary Condition

At the above value of δ_m a concentration boundary condition needs to be specified. While the other boundary condition on Eq. (39) is simply specified at the wall as $Y_i = 0$, the one at the "inner layer" edge must be obtained via a degenerate form of Eq. (39). As discussed earlier, the degenerate equation used here ignores the diffusion term and further assumes that the transverse convection of particles in the outer layer is negligible compared to their axial convection. Thus one can write the "outer layer" equation as

$$u \frac{dY_i}{dx} = K\, Y_i \tag{44}$$

where[12]:

$$K \equiv \left[\frac{1}{r}\alpha_i D_i + \frac{1}{\rho}\frac{\partial}{\partial r}\left(\rho D_i \alpha_i\right)\right]\frac{1}{T}\frac{\partial T}{\partial r} + D_i \alpha_i \frac{1}{T}\left\{\frac{\partial^2 T}{\partial r^2} - \frac{1}{T}\left(\frac{\partial T}{\partial r}\right)^2\right\} \tag{45}$$

and analytically solve it to obtain the following expression for the concentration at the outer edge of the "inner layer":

$$Y_i = Y_{i_o} \exp\left[\int_{x_o}^{x} \frac{K}{u}\, dx'\right] \tag{46}$$

where the subscript '$_o$' refers to some specified initial conditions (e.g., at the inlet to the silicon separation/collection section of the reactor).†

---

* A more cumbersome approach could have been to estimate δ_m by solving the boundary layer concentration integral equation.

† A more exact alternative approach to modeling the outer layer would include the transverse convection term in Eq. (44) and, thus, require numerical solution of differential equations for the concentration along particle trajectories.

Equation (46) emphasizes that the particle trajectories immediately outside the "inner layer" may be nearly parallel to the reactor walls. This is to be expected when the opposing thermophoretic and hydrodynamic forces acting on the particle nearly balance each other.

C. STATUS

The mathematical development described in this section has been incorporated into a code (MPDEU) which couples to the boundary layer (GENMIX) code. Unfortunately time has not allowed its use.

V. DESCRIPTION OF THE GENMIX-MPDEU CODE FOR SOLUTION OF THE SILICON TRANSPORT EQUATION

A. MPDEU CODE STRUCTURE

Figure 12 shows the structure of the newly developed code MPDEU for the description of silicon particle transport in the developing tubular flow encountered in the downstream reactor section. Since Eq. (39) is a nonlinear partial differential equation, the well-known PDECOL[32] is utilized advantageously for its solution. In Appendix A the particle transport equation, Eq. (39), is recast into a form suitable for solution using PDECOL. The main advantage of using PDECOL, as opposed to a conventional finite difference procedure, is its superior computational efficiency. It also incorporates variable step size control and variable order integration procedures that help it cope with numerical "stiffness" problems. A listing of MPDEU is given in Appendix B.

79-184

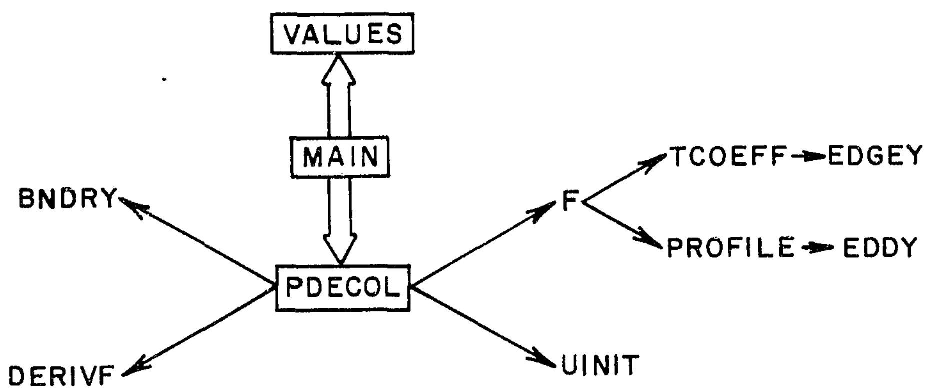

FIGURE 12 REPRESENTATION OF THE STRUCTURE OF THE PARTICLE CODE, MPDEU

The roles of the various subprograms that constitute MPDEU are described below:

MAIN

a. Reads list of input parameters.

b. Reads from random file DATA the results generated by the boundary

layer code regarding the various dependent variable profiles, etc. at several x-stations along the reactor (i.e., streamwise history) stored in ARRAY.

c. Generates input parameters for PDECOL and satellite subroutines.

d. Checks on input through WRITE statements.

e. Calls VALUES for giving results at specified stations. These results include the non-dimensional mass fraction profile and the dimensional profiles along the tube radius.

PDECOL

This is the partial differential equation solver based on the method of lines approach developed by Madsen and Sincovec.[32] It uses a finite element collocation scheme for discretization of the spatial cross stream variable as it integrates a set of ODE with x as independent variable. A full description of PDECOL is available in Ref. 32.

BNDRY

This is a subroutine in the PDECOL package, needed for specifying the boundary conditions on the partial differential equation being solved (i.e., the particle equation, in this case). In this case one specifies the two boundary conditions--at the wall and at the species layer edge. The one at the wall specifies zero mass fraction there while the one at the species layer is specified according to the method given in Section IV.

UINIT

This is also a subroutine in the PDECOL package. It specifies the initial conditions on the partial differential equation being solved. These initial conditions must be at an initial x point (which is not x = 0), typically a small distance downstream from the leading edge of the boundary layer, in this case XD(1).

F

A subroutine in the PDECOL package which specifies the differential equation being solved. In this case one specifies the particle transport equation in the non-dimensional form:

$$\frac{\partial \tilde{Y}_i}{\partial \tilde{x}} = -\left(\frac{L}{\delta_m \tilde{u}}\right)(\tilde{v} - \tilde{v}_s)\frac{\partial \tilde{Y}_i}{\partial \tilde{r}} + \left(\frac{L\, D_{ie}}{\delta_m{}^2 u_E \tilde{u}}\right)\tilde{D}_{eff}\frac{\partial^2 \tilde{Y}_i}{\partial \tilde{r}^2} + \tilde{\Phi}/\tilde{u}$$

$$= A\frac{\partial \tilde{Y}_i}{\partial \tilde{r}} + B\frac{\partial \tilde{Y}_i}{\partial \tilde{r}} + C\left(1 - 2\left\{(Y_{i_m} - Y_{i_w})\tilde{Y}_i + Y_{i_w}\right\}\right)$$

$$\frac{\partial \tilde{Y}_i}{\partial \tilde{r}} + D\frac{\partial^2 \tilde{Y}_i}{\partial \tilde{r}^2} + E\left[\left\{\tilde{Y}_i(Y_{i_m} - Y_{i_w}) + Y_{i_w}\right\}\left\{1 - \tilde{Y}_i\right.\right.$$

$$\left.\left.(Y_{i_m} - Y_{i_w}) - Y_{i_w}\right\}\right] \tag{47}$$

where A, B, C, D, E are coefficients whose values are specified in Appendix A. The values of these coefficients are computed in subroutine TCOEFF while subroutine PROFILE is called to establish the velocity and temperature profiles at the x-station of interest. These profiles are needed in the evaluation of the coefficients, at points along the tube radius.

DERIVF

A dummy subroutine that is required by PDECOL (see Ref. 32 for details).

TCOEFF

This subroutine computes the coefficients A, B, C, D, E of the particle equation at a given (x, γ) location within the tube. Prior to evaluation of the coefficients, however, it is necessary to compute the particle Damkohler number (see Appendix A), the suction terms due to variable properties, and the Soret effect and the "effective diffusivity" (sum of the Brownian and eddy diffusivities). Using cross-stream profile information on the abovementioned quantities at a given x-station, one interpolates to establish values for a given γ station. This subroutine calls EDGEY to find the boundary layer edge concentration value.

EDGEY

The first task this subroutine performs is to find the mass transfer boundary layer thickness (DELM), using the specified Lewis number and thermal layer thickness. The latter half of this subroutine computes the particle mass fraction YM at the outer edge of the boundary layer. This subroutine codes the solution of the degenerate particle transport equation (Eq. (47)).

EDDY

This subroutine computes the eddy diffusivity based on the Lin et al[15] formulae which describe the variation of the diffusivity discretely in the laminar sublayer, the buffer layer, and the turbulent outer layer.

PROFILE

This subroutine computes the cross-stream profiles at a given x-station by linear interpolation from the two nearest neighbor x-station profiles. Then the temperature gradient profile is established by numerical differentiation of the temperature profile (using subroutine DGT3). These quantities are utilized to establish the needed profiles of Damkohler number, suction velocity, effective diffusivity, and the pseudo-effective rate constant.

VALUES

A subroutine which is supplied with the PDECOL package for the computation of results, at specified gridpoints, using a spline interpolation technique.

B. COUPLING OF MPDEU CODE WITH THE GENMIX CODE

The solutions to the gas-phase momentum and energy equations are found using the modified GENMIX code (see Ref. 2). These solutions are stored on disk through the random I/O procedure available on the CDC computer. Writing these solutions on a disk file is accomplished by the WRITMS command. Once stored in the ARRAY vector these solutions may be read (via the READMS command) into a subsequent, independent run of another program. In this case, MPDEU utilizes these solutions to compute the silicon particle mass concentration field within the reactor. Special coupling statements are, therefore, present in both programs.

C. DESCRIPTION OF INPUT PARAMETERS FOR MPDEU

Two sets of input parameters are involved: (1) those that are direct input to PDECOL, and (2) those that are needed for the additional computations performed by PDECOL (e.g., as in subroutines TCOEFF, PROFILE, EDGEY, AND EDDY). The first category parameters are fully discussed in Ref. 32 and need not be repeated. In the second category the following parameters need to be input:

- YMO - Edge mass fraction at initial x-station.
- YW - Wall mass fraction.
- RW - Radius of tube.
- RMO - Radial location of boundary layer edge at initial x-station.
- KPOL - Degree of interpolation polynomial to be used in subprogram AITINT.
- NGRID - Number of radial gridpoints at which solution is stored by GENMIX.
- XLO - Reference length used to non-dimensionalize x coordinate.
- NXPT - Number of x-stations at which profiles are stored by GENMIX.
- PR - Prandtl number.
- SC - Schmidt number.
- AMUR - Reference viscosity.
- TEMPR - Reference temperature corresponding to reference viscosity.
- OMEG - Temperature exponent in viscosity law: $\mu/\mu_r = (T/T_r)^w$.
- DIR - Reference diffusivity.
- AND - Temperature exponent in diffusivity law: $D_i D_{i_r} = (T/T_r)^n$.
- ALPHA - Soret factor for given particle size.
- RUNIV - Universal gas constant
- NGAS - Molecular weight of carrier gas.
- ITURB - Index to indicate if laminar or turbulent flow is involved.
- ITEST - Index to obtain extra output (i.e., additional quantities) in case one wishes to check/test the program.
- ICOUNT - Index to count the number of times the species boundary layer thickness is computed in sub EDGEY. It is used to distinguish the computation of the edge concentration at the first x-station from subsequent computations.
- YI(I) - Input mass fraction profile at first x-station to serve as initial condition in the solution of the particle equation.

D. DESCRIPTION OF INPUT PARAMETERS FOR GENMIX (MODIFIED FOR THE PRESENT Si REACTOR SIMULATION)

In the version of GENMIX commonly used the input is provided through "arithmetic FORTRAN statements" embedded within the body of the MAIN program. Due to the many different types of parameters involved (e.g., control indices, geometrical, physico-chemical, etc.) the authors of the program apparently found it more convenient to divide the MAIN program into several subsections (or chapters), with the input specified appropriately within each subsection. While this approach is useful for self-instruction purposes, it appears that once GENMIX has been suitably modified for a given problem it would be desirable to pull out these "arithmetic statements" and replace them by READ statements. Then all the necessary input can be specified separately on data cards and one saves the additional costs of recompilation of the program every time one or more of the input parameters change their values (e.g., as in a parametric study of the reactor performance).

This was done here too and the different READ statements provided appear under a series of input points (within the MAIN program) entitled INPUT 1, INPUT 2, etc. (A listing of the version of GENMIX used is given in Appendix C.) In what follows, these different input parameters are described:

INPUT 1

- LESSON - Index used to aid self-instruction in the use of the program. Does not affect the results.
- KASE - Index for self-instruction. Does not affect the results.
- NSTAT - Number of x-steps between output of single variables (e.g., pressure, etc.).
- NPROF - Number of x-steps between output of array variables, or "profiles" (e.g., temperature, etc.).
- NPLOT - Number of x-steps between output of plot of velocity, temperature profiles.
- ITEST - Index that controls "extra output" for program checking or testing purposes.
- IUTRAP - Controls action taken if negative velocities are calculated (see Ref. 2).
- MTEST - Number of x-stations from start of computation for which "extra output" (with ITEST $\neq$ 0) is desired.

NSMALL - Number of initial x-steps over which one wishes to safeguard against possible instability by retaining a small step size (1/10 of specified step size).

MASSAG - Index that controls the need to improve specified initial conditions by making them continuous profiles. It was not found necessary in the present calculations to modify the uniform initial conditions specified at the tube entrance.

IREC - Index that controls record number on which computations at a given x-station are to be stored (on disk file DATA) for later use by the MPDEU program. Set IREC = 0 initially.

INPUT 2

ICUNIF - Index that controls whether uniform or polynomial initial conditions are going to be used (see Chapter 5 of program).

NFRAC - A fraction less than unity used in case polynomial initial conditions are specified. It specifies the wall value of the dependent variable related to concentration (see Chapter 5 of program).

NWALL - Number of radial gridpoints from tube centerline up to which a uniform I.C. profile holds and beyond which a polynomial I.C. profile is specified.

ICURR - Index used to alter the values of the dependent variables at gridpoints next to the boundaries. ICURR = 0 does not alter them from the original GENMIX formulation.

POHLIC - Pohlhausen parameter used in the specifications of polynomial I.C.s in Chapter 6 of the program.

ICBET - Index that controls whether it is necessary to improve I.C.s (see Chapter 6) at all.

IMPROV - Index that is used in case improved (polynomial) I.C.s are needed (see Chapter 6).

RERR - Error tolerance in the computation of the tube wall streamline radius (used in Chapter 6).

Note: The abovementioned INPUT 2 parameters do not play an important role in the program if it is found that adequate solutions result from uniform initial conditions alone, as was the case in the reactor study described in Section III.

INPUT 3

N - Number of cross-stream intervals (between radial gridpoints) to be used.

XULAST - x-location at which integration is to terminate.

LASTEP - Number of steps in x-direction after which integration is to be stopped.

XOUT - Distance x (meters) to end of outer confining duct.

XEND - Distance x (meters) to end of central pipe.

FRA - Ratio of step length to total grid width, DX = FRA*Y(NP3).

ULIM - Constant used in calculating entrainment.

TAN - Tangent of semi-angle of duct.

PEILIM - Maximum allowable increase in the quantity $(\psi_e - \psi_I)$, per step.

AFAC - Factor multiplying area change term.

AEXDLM - Maximum desired value of dimensionless area excess/2π (i.e., dimensionless AEX).

KRAD - Control index for plane or axisymmetric geometry.

CSALFA - Duct geometry parameter (i.e., cos α) which indicates if walls are inclined or not.

KIN - Index to specify nature of I boundary.

KEX - Index to specify nature of E boundary.

POWER - Exponent used in prescribing the grid spacing in terms of the normalized stream function w.

INPUT 4

OM(1) - ω value at tube centerline.

OM(NP3) - ω value at tube wall.

ISTEP - Number of integration steps completed.

IEND - Number of steps to end of central pipe, otherwise IEND = 10000 (the latter applies here).

IAX - Number of steps to position where I boundary meets symmetry axis, otherwise IAX = 10000.

IOUT - Number of steps to end of outer confining duct, otherwise IOUT = 10000.

XU - Upstream distance, x.

DX - Integration step size, DX = XD - XU.

IFIN - Index that controls when calculations should terminate ($IFIN \neq 0$ terminates).

EWALL - Constant in logarithmic velocity profile formula.

INPUT 5

MASSTR - Index to indicate if considered flow has uniform or variable composition.

NOVEL - Index to dictate if velocity computation is required.

NEQ - Number of differential equations to be solved.

INPUT 6 (SI units are to be used here)

GASCON - Universal gas constant.

CFU - Specific heat of fuel.

COX - Specific heat of oxidizer.

CPR - Specific heat of product

CMIX - Specific heat of mixture.

WFU - Molecular weight of fuel.

WOX - Molecular weight of oxidizer.

WPR - Molecular weight of product.

WMIX - Molecular weight of mixture.

VISFU - Viscosity of fuel.

VISOX - Viscosity of oxidizer.

VISPR - Viscosity of product.

VISMIX - Viscosity of mixture.

HFU - Enthalpy of formation of fuel.

AENER - Activation energy of gas divided by the universal gas constant.

PREEXP - Pre-exponential factor in chemical reaction rate law[5]:

$$\dot{w}_{fuel} = F\, p^2\, m_{fu} m_{ox} \exp(-E/R^{\circ}T)$$

OXDFU - Molar ratio of oxidizer to fuel in reactants.

MODEL - Index to show whether flow is laminar or turbulent.

INERT - Index showing whether the considered mixture is chemically reacting or not.

PRO - Value of laminar Prandtl number (assignable in terms of a profile with distance from the wall).

PREFO - Value of turbulent "effective" Prandtl number (assignable in terms of a profile with distance from the wall).

Note: Several of the parameters in this section pertain to a chemically reacting system as envisioned in Version 4A of GENMIX. However, in the present study, we consider a chemically inert flow within the "downstream" reactor tube section. As such, many of these input parameters have to be assigned suitable "dummy" values in order to reduce the available generality to the specific problem of interest here. A typical set of input parameters (given later) illustrates this.

INPUT 7

H	- Recovery factor.
AK	- Mixing length constant K (von Karman's), see Ref. 5.
ALMG	- Mixing length constant, λ.
FR	- Constant used to calculate minimum velocity gradient.
UFAC	- Constant used to calculate lower limit to $\ell\left\|\frac{du}{dy}\right\|$.

INPUT 8

UA, UB, UC, UD	- Velocities of A, B, C, D streams.
TA, TB, TC, TD	- Temperatures of A, B, C, D streams.
TWALL	- Wall temperature.
RA, RB, RC, RD	- Inner radii of A, B, C, D streams viewed as tubes.

INPUT 9

F2A, F2B, F2C, F2D	- "Fuel" concentration in A, B, C, D streams.
OXA, OXB OXC, OXD	- "Oxidizer" concentration in A, B, C, D streams.

Note: In INPUTS 8 and 9 reference is made to four incoming streams of reactants (A, B, C, and D) according to the general configuration treated in Ref. 5. However, for the present problem of a single stream, containing silicon in a "carrier gas" having H_2, Ar, NaCl as the main constituents, one needs to again resort to certain "dummy" values for these input parameters in order to

simulate the problem of interest here (see the typical values assigned to these parameters) shown later.

INPUT 10

PRESS - Pressure.

DPDDX - Pressure gradient, dp/dx.

TREF - Reference temperature used in viscosity law.

$$\frac{\mu}{\mu_r} = \left(\frac{T}{T_r}\right)^{\omega}$$

VISREF - Reference viscosity of gas corresponding to TREF.

VISEXP - Temperature exponent in viscosity law.

VPB - Pre-exponential constant appearing in Si vapor pressure law.

VPA - Constant appearing in the argument of the exponential in the Si vapor pressure law:

$$Y_{Si_w} = \frac{M_{Si}(VPB)}{M_{mix}\ p} \exp\left(-\frac{VPA}{T_w}\right)$$

INPUT 11

NINT - Number of intervals used for Simpson's integration to establish collection efficiency.

KPOL - Degree of polynomial used for interpolation in the above integration.

NPTS - Number of points (≠NINT+1) considered in abovementioned Simpson's integration.

E. TYPICAL INPUT PARAMETER VALUES FOR THE SILICON REACTOR SIMULATION WITH GENMIX

INPUT 1

LESSON	=	0
KASE	=	11
NSTAT	=	100
NPROF	=	100
NPLOT	=	100
ITEST	=	0
IUTRAP	=	2
MTEST	=	2
NSMALL	=	100
MASSAG	=	0
IREC	=	0

INPUT 2

ICUNIF	=	1
WFRAC	=	0.5
NWALL	=	10
ICURR	=	0
POHLIC	=	7.0
ICBET	=	0
IMPROV	=	0
RERR	=	0.01

INPUT 3

N	=	77
XULAST	=	9.0
LASTEP	=	10000
XOUT	=	9.0
XEND	=	0.0
FRA	=	0.05
ULIM	=	0.05
TAN	=	0.0

INPUT 3 (cont'd)

PEILIM	=	0.01
AFAC	=	0.1
AEXDLM	=	0.01
KRAD	=	1
CSALFA	=	1.0
KIN	=	3
KEX	=	1
POWER	=	1

INPUT 4

OM(1)	=	0.0
OM(NPS)	=	1.0
ISTEP	=	0
IEND	=	0
IAX	=	0
IOUT	=	10000
XU	=	0
DX	=	0
IFIN	=	0
EWALL	=	9

INPUT 5

MASSTR	=	1
NOVEL	=	2
NEQ	=	3

INPUT 6		
GASCON	=	8314
CFU	=	1375
COX	=	1375
CPR	=	1375
CMIX	=	1375
WFU	=	28.09
WOX	=	25.58
WPR	=	2
WMIX	=	25.58
VISFU	=	0.00005
VISOX	=	0.00005
VISPR	=	0.00005
VISMIX	=	0.00005
HFU	=	0
AENER	=	0
PREEXP	=	0
OXDFU	=	0
MODEL	=	2
INERT	=	1
PRO	=	0.7
PREFO	=	0.86

INPUT 7		
H	=	0.9
AK	=	0.435
ALMG	=	0.09
FR	=	0.033
UFAC	=	0.01

INPUT 8		
UA	=	20
UB	=	20
UC	=	20
UD	=	20

INPUT 8 (cont'd)		
TA	=	3500
TB	=	3500
TC	=	3500
TD	=	3500
TWALL	=	1700
RA	=	0
RB	=	0
RC	=	0
RD	=	0.075

INPUT 9		
F2A	=	0.1
F2B	=	0.1
F2C	=	0.1
F2D	=	0.1
OXA	=	0
OXB	=	0
OXC	=	0
OXD	=	0

INPUT 10		
PRESS	=	101325
DPDDX	=	0
TREF	=	3000
VISREF	=	0.00005
VISEXP	=	0.65
VPB	=	7.3166E10
VPA	=	46710

INPUT 11		
NINT	=	49
KPOL	=	2
NPTS	=	100

VI. THE CHEMPART CODE: MODELS

One of the major accomplishments of this research program has been the development of the CHEMPART code, a much modified and augmented version of the AeroChem Low Altitude Plume Program (the LAPP code).[3] The CHEMPART code is an axisymmetric marching (parabolic) model which, in addition to containing the non-equilibrium finite rate chemistry routines of the LAPP code, includes a number of new routines which treat two-phase flow phenomena, including: (i) the exchange of momentum and energy between a particulate phase and the gas, (ii) the formation of this particulate phase, i.e., nucleation, and (iii) the growth of the particulate phase via both heterogeneous condensation/evaporation and via agglomeration. Another major improvement included in the CHEMPART code has been the addition of routines which allow the treatment of enclosed flows (in addition to the free jet expanding flows originally treated by LAPP).

In this section we will describe the numerous models which have been incorporated into this code. The structure of the code, the preparation of input data, the operation of the code, and the output information obtained from it will be discussed in following sections. Finally, we will discuss the application of the code to Na/$SiCl_4$ silicon reactors. Throughout the discussion of the CHEMPART code, frequent reference will be made to actual FORTRAN variables and subroutines contained within the code. This will be done to enable readers of this report to modify the numerous models contained within the code to better fit their purposes and to allow users of the code to correct errors which they may find have been incorporated within it. In any large code such as CHEMPART, many options are available to the user with regard to both the preparation of input data and the particular phenomena which may be treated. Not all these options have yet been tested and, therefore, errors undoubtedly exist within the code which will only be corrected as it is used over a wide range of problems. Our aim here is, therefore, to present the reader sufficient information to allow him some facility in finding his way through the code, to augment or improve those models which he finds inadequate, and to correct any errors which may exist within the code. To help the reader who wishes to modify the code, Appendix D gives an explanation of the important FORTRAN variables used in the code. Appendix E contains a listing of the code.

A. GOVERNING EQUATIONS

For gas-phase systems in which no particulate phase exists, the following equations describe the free shear layer turbulent or laminar mixing of the co-flowing axisymmetric streams undergoing chemical reactions. For turbulent flows all properties are interpreted to be the mean (time-averaged) values. The effective (molecular + eddy) viscosity, μ, is described by one of the phenomenological expressions given in Section VI.C (below). Nomenclature is tabulated in the front of this report.

Global Continuity

$$\frac{\partial}{\partial x}(\rho u) + \frac{1}{r}\frac{\partial}{\partial r}(\rho v r) = 0 \tag{48}$$

Conservation of Species

$$\rho u \frac{\partial F_i}{\partial x} + \rho v \frac{\partial F_i}{\partial r} = \frac{1}{r}\frac{\partial}{\partial r}\left(\frac{Le}{Pr}\,\mu r\,\frac{\partial F_i}{\partial r}\right) + \dot{w}_i \tag{49}$$

Conservation of Momentum

$$\rho u \frac{\partial u}{\partial x} + \rho v \frac{\partial u}{\partial r} = -\frac{dp}{dx} + \frac{1}{r}\frac{\partial}{\partial r}\left(\mu r\,\frac{\partial u}{\partial r}\right) \tag{50}$$

Conservation of Energy

$$\rho u \frac{\partial H}{\partial x} + \rho v \frac{\partial H}{\partial r} = \frac{1}{r}\frac{\partial}{\partial r}\left(\frac{\mu r}{(Pr)}\frac{\partial H}{\partial r}\right) + \frac{1}{r}\frac{\partial}{\partial r}\left[\left(1-\frac{1}{Pr}\right)\mu r\,\frac{\partial}{\partial r}\left(\frac{u}{2}\right)^2\right]$$

$$+ \frac{1}{r}\frac{\partial}{\partial r}\left[\sum_{i=1}^{NS}\left\{\frac{\mu}{Pr}(Le-1)\,r\,h_i\,\frac{\partial}{\partial r}(F_i)\right\}\right] \tag{51}$$

State

$$\rho = \frac{pW}{RT} \tag{52}$$

The conservation equations are solved subject to the following initial and boundary conditions:

$$x = 0: \quad u = u(r), \quad F_i = F_i(r), \quad T = T(r)$$

$$r = 0: \quad \frac{\partial u}{\partial r} = \frac{\partial T}{\partial r} = \frac{\partial F_i}{\partial r} = 0$$

For free jets:

$$r \rightarrow \infty: \quad u \rightarrow u_e, \; F_i \rightarrow (F_i)_e, \; T \rightarrow T_e \tag{53}$$

For enclosed flows:

$$r = r_w: \quad u = 0.1 \text{ cm s}^{-1}, \quad F_i \rightarrow (F_i)_w \text{ or } \frac{\partial F_i}{\partial r} \rightarrow 0^*, \quad T \rightarrow T_w \tag{54}$$

For a free jet expansion, pressure may be specified in the axial direction according to,

$$p = c_0 + c_1 x + c_2 x^2 + c_3 x^3 \tag{55}$$

It is convenient to transform the equations into a streamline coordinate system and utilize the stream function, Ψ, as the radial coordinate. The transformation from cylindrical (x, r) coordinates to streamline (x, Ψ) coordinates (which automatically satisfies global continuity, Eq. (48)) is defined by:

$$\Psi \frac{\partial \Psi}{\partial r} = \rho u r \tag{56a}$$

$$\Psi \frac{\partial \Psi}{\partial x} = - \rho v r \tag{56b}$$

From Eqs. (56a) and (56b) we obtain,

$$\left(\frac{\partial}{\partial r}\right)_x = \frac{\rho u r}{\Psi} \left(\frac{\partial}{\partial \Psi}\right)_x \tag{57a}$$

$$\left(\frac{\partial}{\partial x}\right)_r = \left(\frac{\partial}{\partial x}\right)_\Psi - \frac{\rho v r}{\Psi} \left(\frac{\partial}{\partial \Psi}\right)_x \tag{57b}$$

Introducing Eqs. (57a) and (57b) into Eqs. (49), (50), and (51), gives:

<u>Species</u>

$$\frac{\partial F_i}{\partial x} = \frac{1}{\Psi} \frac{\partial}{\partial \Psi}\left[\left(\frac{Le}{Pr}\right) \frac{\mu \rho u r^2}{\Psi} \frac{\partial F_i}{\partial \Psi}\right] + \frac{\dot{w}_i}{u \rho} \tag{58}$$

---

* $(F_i)_w$ is specified by the equilibrium vapor pressure of the species at the wall temperature, T_w, if the ith species is condensible. Otherwise the radial derivative is set to zero at the wall.

Momentum

$$\frac{\partial u}{\partial x} = - \frac{1}{\rho u}\frac{dp}{dx} + \frac{1}{\Psi}\frac{\partial}{\partial \Psi}\left[\frac{\mu\rho u r^2}{\Psi}\frac{\partial u}{\partial \Psi}\right] \tag{59}$$

Energy

$$\frac{\partial H}{\partial x} = \frac{1}{\Psi}\frac{\partial}{\partial \Psi}\left[\left(\frac{1}{Pr}\right)\frac{\mu\rho u r^2}{\Psi}\frac{\partial H}{\partial \Psi}\right] + \frac{1}{\Psi}\frac{\partial}{\partial \Psi}\left[\left(1 - \frac{1}{Pr}\right)\frac{\mu\rho u r^2}{\Psi}\frac{\partial}{\partial \Psi}\left(\frac{u^2}{2}\right)\right]$$

$$+ \frac{1}{\Psi}\frac{\partial}{\partial \Psi}\left[\sum_{i=1}^{NS}\left(\frac{1}{Pr}\right)(Le - 1)\frac{\mu\rho u r^2}{\Psi} h_i \frac{\partial F_i}{\partial \Psi}\right] \tag{60}$$

The governing set of parabolic partial differential equations, (Eqs. (58), (59), and (60)), are rewritten in finite difference form and then solved using standard forward marching techniques.[3,33] The chemistry terms (see below), $\dot{w}_i$, in the species continuity equations are evaluated via implicit differences[3]; the diffusion terms in the species continuity equations are evaluated via explicit differences.[33]

B. FINITE RATE CHEMISTRY MODEL

1. Kinetics Model

Five possible reaction types are currently included in the program:

Reaction Type

(1)	$A + B \rightleftarrows C + D$
(2)	$A + B + M \rightleftarrows C + M$
(3)	$A + B \rightleftarrows C + D + E$
(4)	$A + B \rightleftarrows C$
(5)	$A + M \rightleftarrows C + D + M$

In Reactions (2) and (5) M is an arbitrary third body. In this program, all species are assumed to have equal third-body efficiencies; thus, in evaluating $\dot{w}^{(j)}$, $F_M = (W)^{-1}$. The net rates of production for all reactions are written below, in the form $\dot{w}^{(j)} = RP^{(j)} - RM^{(j)}$.

(1) $$\dot{w}^{(j)} = k_f \rho^2 F_A F_B - \frac{k_f \rho^2 F_C F_D}{K_p}$$

(2) $$\dot{w}^{(j)} = \frac{k_f \rho^3 F_A F_B}{W} - \frac{k_f \rho^2 F_C}{K_p WRT}$$

(3) $$\dot{w}^{(j)} = k_f \rho^2 F_A F_B - \frac{k_f \rho^3 F_C F_D F_E RT}{K_p}$$

(4) $$\dot{w}^{(j)} = k_f \rho^2 F_A F_B - \frac{k_f \rho^3 F_C}{K_p RT}$$

(5) $$\dot{w}^{(j)} = \frac{k_f \rho^2 F_A}{W} - \frac{k_f \rho^3 F_C F_D RT}{K_p W}$$

To reduce round-off and truncation errors, forward and reverse rates $RP^{(j)}$ and $RM^{(j)}$, are computed separately for each reaction. All contributions to the molar rate of production of a given species are then computed and added algebraically to form $\dot{w}_i$ (WDOT(J)) in subroutine CHEM.

The forward rate coefficient, k_f, is expressed in the form

$$k_f = AT^{-N} \exp(B/RT) \tag{61}$$

and K_p is determined from,

$$\ln K_p = -\Delta G/RT \tag{62}$$

The rate coefficients are currently divided into seven types:

Rate Coefficient Type

(1) $k_f = A$

(2) $k_f = AT^{-1}$

(3) $k_f = AT^{-2}$

(4) $k_f = AT^{-1/2}$

(5) $k_f = A \exp(B/RT)$

(6) $k_f = AT^{-1} \exp(B/RT)$

(7) $k_f = AT^{-3/2}$

2. Thermodynamic Data

The thermodynamic properties (specific heat, Gibbs free energy, and enthalpy) for each species are input to the program as

c_{p_i}, $-\left(\frac{g_i - h_{298_i}}{T}\right)$ and $(h_i - h_{298_i})$ in tabular form as a function of temperature. Linear interpolation is used to define thermodynamic properties at the local temperature. Such data can, for many species, be found in the JANAF Thermochemical Tables.[34] Where no such source exists, these quantities should be estimated in the best way available. (It should be kept in mind that any reasonable estimate is almost certainly better than exclusion of a species from the reaction scheme.)

C. TURBULENT EDDY VISCOSITY MODELS*

The following eddy viscosity models[35-38] are incorporated into the program via subroutine TURB.

Model 1 (Ferri)[35]

Initial region,†

$$\mu_t = \rho\,\varepsilon = \alpha 0.00137\ x\ |\rho_o u_o - \rho_e u_e| \tag{63a}$$

Developed region,

$$\mu_t = \rho\,\varepsilon = \alpha K\ b_{1/2}\ |\rho_o u_o - \rho_e u_e| \tag{63b}$$

where $b_{1/2}$ is the value of r where $\rho u = (\rho_o u_e + \rho_e u_e)/2$ and K is the eddy viscosity coefficient, usually taken to be 0.025.§

Model 2 (Ting/Libby)[37]

$$\mu_t = \rho\,\varepsilon = \alpha K\ \bar{r}_{1/2}|u_o - u_e|\ \rho\left(\frac{\rho_o}{\rho}\right)^2\left(\frac{\eta}{r}\right)^2 \tag{64}$$

where

$$\eta^2 = 2\int_o^r (\rho_o/\rho)\ r'\ d\ r' \tag{65}$$

---

*For enclosed flows only Model 6 (Donaldson-Gray) or the laminar model may be chosen.

† Defined as region upstream of axial position where $(u_o - u_e)/(u_j - u_e) = 0.95$.

§ Most of the models contain a numerical coefficient K which must be determined empirically. The value K = 0.025, taken from Schlicting,[36] has been incorporated directly into the program. This can be changed by the program input data via an appropriate value for the additional constant, α, Eqs. (63) - (69).

and $\bar{r}_{1/2}$ is the value of η where $u = (u_o + u_e)/2$.

Model 3

Initial region,

$$\mu_t = \rho\,\varepsilon = \alpha 0.00137\, x\, \rho_o |u_o - u_e| \tag{66a}$$

Developed region,

$$\mu_t = \alpha K\, r_{1/2}\, \rho_o |u_o - u_e| \tag{66b}$$

where $r_{1/2}$ is the value of r where $u = (u_o - u_e)/2$.

Model 4

Initial region,

$$\mu_t = \rho\,\varepsilon = \alpha 0.00137\, x\, \rho_e\, |u_o - u_e| \tag{67a}$$

Developed region,

$$\mu_t = \rho\,\varepsilon = \alpha K\, r_{1/2}\, \rho\,\varepsilon |u_o - u_e| \tag{67b}$$

Model 5*(Ting/Libby)[37]

Initial region,

$$\mu_t = \rho\,\varepsilon = \alpha 0.00137\, x\, |u_j - u_e|\, \rho\left(\frac{\rho_j}{\rho}\right)^2 \tag{68}$$

Developed region,

$$\mu_t = \rho\,\varepsilon = \alpha K\, \bar{r}_{1/2}\, |u_o - u_e|\, \rho\left(\frac{\rho_o}{\rho}\right)^2 \left(\frac{\eta}{r}\right)^2 \tag{64}$$

Model 6 (Donaldson/Gray[38]

Initial region,

$$\mu_t = \rho\,\varepsilon = \alpha\bar{K}(r_{1/2} - r_{in})\, \rho |u_o - u_e|/2 \tag{69a}$$

---

* In the CHEMPART program, the specification of Model 5 means that Eq. (68) will be used in the initial region and Model 2 (Eq. (64)) will be used in the developed region. This is important for re-starting a problem in the developed region for which Model 5 was selected to run from x = 0.

$$\begin{aligned} \text{For}\quad M_{1/2} &\leq 1.2 \quad \overline{K} = 0.0468 + M_{1/2}\left[-0.0460\, M_{1/2} + 0.0256\, M_{1/2}^{2}\right] \\ M_{1/2} &> 1.2 \quad \overline{K} = 0.0248 \end{aligned} \tag{70}$$

where $M_{1/2}$ is the value of the Mach number where $u = (u_o + u_e)/2$ (i.e., the half radius). The speed of sound at the half radius, $a_{1/2}$ is expressed by,

$$a_{1/2} = \left[\frac{c_p}{c_p - (R/W_{1/2})} \; \frac{RT_{1/2}}{W_{1/2}}\right]^{1/2} \tag{71}$$

where $W_{1/2}$ and $T_{1/2}$ are evaluated at the half radius. In Eq. (69a), r_{in} is the inner mixing zone radius and is defined as the value of r where $(u_o - u_e)/(u_j - u_e) = 0.95$.

Developed region,

$$\mu_t = \rho\, \varepsilon = \alpha\overline{K}\, r_{1/2}\, \rho\left|u_o - u_e\right|/2 \tag{69b}$$

<u>Laminar Flow</u>

The temperature dependent viscosity of each gaseous species is included as part of the input to the code and the viscosity obtained from them. The individual species viscosities are in the form

$$\mu_i = \mu_i^o \left(\frac{T}{T_o}\right)^{\Omega} \qquad i = 1,\ldots,NS \tag{72}$$

The viscosity is then

$$\mu_g = \sum_{i=1}^{NS} F_i\, W\, \mu_i \tag{73}$$

D. GAS/PARTICLE DYNAMICS

Small particles will (i) follow the gas streamline as they are carried along and (ii) adjust rapidly to the temperature of the surrounding gas (although phase changes such as fusion may result in sizeable transfers of energy to or from the gas). Thus little exchange of momentum or energy will occur (with the notable exception of phase change just mentioned). Large particles, on the other hand, will slip in the gas and may find themselves at a temperature significantly different from the surrounding gas. Thus, to

treat flows in which heavy particle loadings result in large gas/particle interaction, it is necessary to modify the gas momentum and energy equations to include this interaction and to introduce the momentum and energy equations of these larger particles. The following terms (74) and (75) must thus be added to the momentum and energy equations, respectively, (Eqs. (59) and (60)) to account for this momentum and energy exchange. For cases examined to date, particles with Kn $\approx$ 2 are found to have substantially the same temperature and velocity of the gas. Therefore, in the present version of CHEMPART, small particles are considered to be those for which the Knudsen number, Kn, is greater than 2.

Momentum

$$- 9/(2\mu) \sum_{j}^{NPG} \frac{F_{p_j} \, f_{p_j} \, \mu_g m_i}{\rho_p \, r_j^2} \left(u - u_{p_j}\right) \tag{74}$$

Energy*

$$9/(2\mu) \sum_{j}^{NPG} \frac{F_{p_j} \, f_{p_j} \, \mu_g m_i}{\rho_p \, r_j^2} \left[\left(u - u_{p_j}\right)^2 + 2/3 \, \frac{C_p}{Pr} \, \frac{g_{p_j}}{f_{p_j}} \left(T_{p_j} - T\right)\right] \tag{75}$$

The indicated sums are over the particle mass classes.

The species equations for each particle mass class can be written in a form similar to Eqs.(49) and (58), i.e., in (x, r) coordinates:

Particle Species

$$\rho \, u_{p_i} \frac{\partial F_{p_i}}{\partial x} + \rho \, v_{p_i} \frac{\partial F_{p_i}}{\partial r} = 1/r \, \frac{\partial}{\partial r} \left(\frac{Le}{Pr} \, \mu_{p_i} r \, \frac{\partial F_{p_i}}{\partial r} \right) + \dot{w}_{p_i} \tag{76}$$

The equations describing the energy (including radiation to the wall) and momentum of the particles themselves are the following:

---

* The condensation (evaporation) of particulate material releases (absorbs) latent heat. The heat is assumed to be transferred immediately to the gas phase. The resulting change in gas temperature is calculated in subroutine AGGLOM.

Particle Momentum

$$\frac{\partial u_{p_i}}{\partial x} = \frac{9}{2} \frac{f_{p_i} \mu_g}{\rho_p r_i^2} \left(u - u_{p_i} \right) \tag{77}$$

Particle Energy

$$u_{p_j} C_{p_p} \left(\frac{d T_{p_j}}{dx} \right) = - \frac{3 \mu_g g_{p_j}}{\rho_p r_j^2} \frac{C_p}{Pr} \left(T_{p_j} - T \right) - \frac{3 \varepsilon \sigma}{r_j \rho_p} \left(T_{p_j}^4 - T_w^4 \right) \tag{78}$$

Equations (76), (77), and (78) are solved explicitly for F_{p_i}, u_{p_i}, and T_{p_i}, respectively. In CHEMPART, terms and Eqs. (74) - (78) are evaluated and used only for particle mass classes for which $Kn_j \leq 2$. Particle classes with larger Knudsen numbers are treated as gases having the gas temperature and velocity and contributing to the gas density, enthalpy, heat capacity, etc. For small particles ($Kn_j \geq 2$), radiation is assumed to cool the gas, rather than the individual particles and a further term

$$- \sum_{j (Kn_j \geq 2)}^{NPG} 4\pi\varepsilon^{\sigma} \left(T^4 - T_w^4 \right) r_j^2 \frac{F_{p_j} m_i}{u} \tag{79}$$

is added to the energy equation (Eq. (60)).

The terms f_{p_j} and g_{p_j} are defined as follows[39]: For $Re_{p_j} < 0.5$, $f_{p_j} = 1.0/SCF_j$. For $0.5 < Re_{p_j} < 10$,

$$f_{p_j} = [1 + 0.376\, Re_{p_j} + 0.225\, (Re_{p_j})^2 \ln(Re_{p_j})]/SCF \tag{80}$$

For $Re_{p_j} > 10$

$$f_{p_j} = 0.033\, Re_{p_j}/SCF_j \tag{81}$$

The factor g_{p_j} is given by

$$g_{p_j} = (1 + 0.336\, Re_{p_j}^{0.55}\, Pr^{0.33})/[Kn_j \times (1 + 0.336\, Re_{p_j}^{0.55}\, Pr^{0.33} + Pr/Kn_j)] \tag{82}$$

The factor SCF_j in Eqs. (80), (81) is the Stokes-Cunningham correction factor[40]

$$SCF_j = 1 + 1.26\ Kn_j + 0.4\ Kn_j\ \exp(-1.1/Kn_j) \qquad (83)$$

In Eq. (82), Pr is the laminar Prandtl number. The source terms $\dot{w}_{p_i}$ in Eq. (76) will be discussed below in the sections on nucleation and particle growth.

The calculations described in this section are performed in subroutines GPINT and PARTC in CHEMPART.

E. PARTICLE SOURCES

1. Nucleation

In systems in which very refractory species with large surface energies are found and in which large supersaturation ratios occur, such as those of interest here, it is attractive to employ a nucleation model[41] in which a limited series of simple gas-phase addition reactions are written which result in a "critical nucleus" above which growth to particle species with bulk properties is rapid. Such a model recommends itself because (i) it fits naturally into the gas-phase chemical kinetics format of the CHEMPART code, (ii) it avoids the use of "liquid drop" models which utilize bulk surface tensions which, for small n-mers ($n \approx 10$-10^2 atoms), are difficult to justify, and (iii) it avoids the crucial assumption of classical nucleation theory that the nucleation step is rate-limiting--an assumption which will often be false if very high supersaturation ratios are encountered. Such a model has recently been proposed and used to treat iron particle nucleation in shock-tube studies in which $Fe(CO)_5$ was thermally decomposed.[41]

The model used to treat particle nucleation is one which treats the series of Si n-mer reactions

$$Si_k + Si_n + M \underset{}{\overset{k_{n+k}}{\rightleftharpoons}} Si_{n+k} + M \qquad (84)$$

The model allows the forward and reverse rate coefficients for Reaction (84) to be estimated for all n. Using these rate coefficients it is possible to obtain a gas-kinetically determined critical size (as opposed to one based on classical liquid drop concepts) and a nucleation rate.

Examination of processes like Reaction (84) leads one to write a realistic detailed mechanism for them as

$$Si_k + Si_n \underset{\kappa_{n+k\to n}}{\overset{\kappa_{n\to n+k}}{\rightleftharpoons}} Si^*_{k+n} \tag{85a}$$

$$Si^*_{k+n} + M \xrightarrow{\kappa_{s,k+n}} Si_{k+n} + M \tag{85b}$$

where Reaction (85a) leads to an excited cluster which may either decompose into its original constituents or may be stabilized by collision with another molecule via Reaction (85b). The overall forward rate coefficient for the overall Reaction (84) is then given by the following equation for k_{n+k} in terms of the rate coefficients for Reaction (85a and b).

$$k_{n+k} = \frac{\kappa_{s,n+k}\ \kappa_{n\to n+k}}{\kappa_{n+k\to n}} \cdot \frac{1}{1 + \dfrac{\kappa_s}{\kappa_{n+k\to n}}[M]} \tag{86}$$

The forward rate for Reaction (84) is then

$$\frac{d}{dt}[Si_{n+k}] = k_{n+k}\,[Si_n]\,[Si_k]\,[M] \tag{87}$$

Following the model development of Bauer and Frurip,[41] we estimate the values of $\kappa_{s,\ n+k}$, $\kappa_{n\to n+k}$ and $\kappa_{n+k\to n}$ as follows: $\kappa_{n\to n+k}$ is assumed to be gas kinetic (each collision yields Si^*_{n+k}) so that

$$\kappa_{n\to n+k} = \pi(r_{n+k})^2\ v_{rel,n,k} \tag{88}$$

where r_{n+k} is the radius of a spherical molecule containing (n + k) atoms. (The bulk liquid density is used to obtain this radius.) The ratio $\kappa_{n\to n+k}/\kappa_{n+k\to n}$ is the equilibrium constant for Reaction (85a); its value is given by

$$\kappa_{n\to n+k}/\kappa_{n+k\to n} = 4\pi\int_{r_{n+k}}^{\infty} dr\ r^2 \exp\left(-\frac{U_{n,k}}{k_B T}\right) \tag{89}$$

where $U_{n,k}$ is an interaction potential between the n-mer and the k-mer and k_B is Boltzmann's constant. The stabilization rate coefficient, κ_s, is also assumed gas kinetic and is given by

$$\kappa_s = \pi(r_{n+k} + r_M)^2 \, v_{rel,n+k,M} \tag{90}$$

where r_M is the radius of the bulk gas molecules and $v_{rel,n+k,M}$ is the average relative velocity of cluster and bulk gas molecules. Using Eqs. (88), (89), and (90) the overall forward rate coefficient $k_{n\to n+k}$ is obtained once the interaction potential $U_{n,k}$ is found. $U_{n,k}$ is estimated by Frurip and Bauer by a Lennard-Jones potential

$$U_{n,k}(r) = 4\,\varepsilon_{n,k}\left[\left(\frac{r_{n+k}}{r}\right)^{12} - \left(\frac{r_{n+k}}{r}\right)^{6}\right] \tag{91}$$

where $\varepsilon_{n,k}$ is a function of the heats of formation of the n-mers

$$\varepsilon_{n,k} = \left\{ |\Delta H^\circ_{n+k}| - |\Delta H^\circ_n| - |\Delta H^\circ_k| \right\}/2 \tag{92}$$

and

$$\Delta H^\circ_n = -\,n\left\{ L(1 - n^{-1/4}) + \Delta H^\circ_1 \right\} \tag{93}$$

where L is the latent heat of vaporization.

The overall reverse rate, $k_{n+k\to n}$, for Reaction (84) may be determined from the forward rate once the Gibbs free energies of formation, ΔG°, of the n-mers are specified. The enthalpies of formation necessary to derive ΔG° are estimated using Eq. (93). The entropies associated with the formation of n-mers from Si atoms are also obtained from Ref. 41 and are given by

$$\Delta S^\circ_n = R\left\{ -\frac{14n^3}{3n^2} + (n-1)\ln 2 + \frac{2}{3}\sum_{j=1}^{n-1} \ln j \right\} \tag{94}$$

for $n \geq 10$. For $n \leq 10$, the configuration terms, on the RHS of Eq. (94) (the second two terms) are replaced by values obtained from the graph (Fig. 7)

of Ref. 41. Using these estimates, the free energies are given by

$$\Delta G^\circ_n = \Delta H^\circ_n - T\Delta S^\circ_n + n\,\Delta G^\circ_1 \tag{95}$$

The reverse rate coefficients are given by

$$k_{n+k\to n} = k_{n\to n+k}\, RT \exp\left[\frac{\Delta G^\circ_n + \Delta G^\circ_k - \Delta G^\circ_{n+k}}{RT}\right] \tag{96}$$

The rate coefficients of Table IV were calculated using this model. It can be seen that the forward rate coefficients rise fairly rapidly with increasing n while the reverse coefficients decrease rapidly, reflecting the greater stability of the excited clusters with increasing n.

For $n \leq 10$, the reverse rate coefficients range up to $\approx 10^{-7}$ ml molecule^{-1} s^{-1}. For a simple two-body reaction between neutral, small molecules such rate coefficients are unreasonably large (by > 2 orders of magnitude). Their large size here reflects the fact that, at the high temperatures involved, the excited clusters of Reaction (85a) usually undergo decomposition as they are formed, before collision with another molecule can stabilize them. Larger ($n > 10$) clusters live longer due to their ability to channel excitation energy into the many available bonds and thus for these, realistic two-body reverse rate coefficients are formed for the overall Reaction (84).

In order to use this model to obtain rates of particle formation it is necessary to define a critical size cluster analogous to the critical size nucleus obtained from liquid drop nucleation theory. In the kinetic nucleation model used here this critical size is determined by establishing where the "bottleneck" in the series of reactions represented by Reaction (84) occurs. This is done by finding that n-mer for which the rates of reactions creating it are most nearly equal to the rates destroying it. The critical size determined in this fashion is compared to that obtained from liquid drop theory in Table V. To determine the number of Si atoms in the liquid drop critical nucleus, the Kelvin equation is used for computing the critical radius, r^*,

$$r^* = \frac{2\gamma W_{Si}}{RT\rho_p \ln S} \tag{97}$$

TABLE IV

COMPUTED RATE COEFFICIENTS FOR Si POLYMERIZATION

$$Si + Si_n + M \rightleftharpoons Si_{n+1} + M \qquad (M = Ar)$$

T = 2400 K, P = 1 atm

n	Forward Rate Coefficient (ml^2 $molecule^{-2}$ s^{-1})	Reverse Rate Coefficient (ml $molecule^{-1}$ s^{-1})
1	4.45 (-30)[a]	4.59 (-7)
2	1.01 (-29)	4.46 (-8)
3	1.53 (-29)	4.33 (-8)
4	1.97 (-29)	1.57 (-8)
5	2.35 (-29)	1.68 (-8)
6	2.68 (-29)	3.90 (-9)
7	2.97 (-29)	9.57 (-10)
8	3.24 (-29)	7.32 (-10)
9	3.48 (-29)	6.90 (-10)
10	3.71 (-29)	2.46 (-10)
15	4.68 (-29)	1.78 (-10)
20	5.32 (-29)	9.18 (-11)
25	6.16 (-29)	5.72 (-11)
30	6.78 (-29)	3.97 (-11)
35	7.36 (-29)	2.96 (-11)
40	7.80 (-29)	2.31 (-11)
45	8.42 (-29)	1.87 (-11)
50	8.90 (-29)	1.55 (-11)

[a] The notation A(-B) implies $A \times 10^{-B}$.

TABLE V

COMPARISON OF CRITICAL CLUSTER SIZES

FOR GAS KINETIC AND LIQUID DROP NUCLEATION MODELS

T (K)	P(Si) (atm)	Supersaturation Ratio	r^* (nm) Liquid Drop Model	r^* (nm) Gas Kinetics Model
1800	0.001	325	0.44	1.19
1800	0.01	3247	0.32	0.93
1800	0.05	16230	0.26	0.79
2400	0.1	45.7	0.16	1.11

where γ is the surface tension, W_{Si} the molecular weight of silicon, ρ_p the droplet density, and S the supersaturation ratio. The number of Si atoms, n^*, is obtained using W_{Si}, ρ_p, r^*, and Avogadro's number N_A, from

$$n^* = 4/3\ \pi(r^*)^3 \rho N_A / W_{Si} \tag{98}$$

The surface tension of liquid Si is obtained from Ref. 42.

$$\gamma = 720 \left[1.67 - 0.67\ (T/1685) \right]^{1.2}\ (\text{dyne cm}^{-1}) \tag{99}$$

The density of liquid Si used is given in Ref. 43.

$$\rho_p = 3.0247 - 0.355 \times 10^{-3}(T - 273.15) \tag{100}$$

The supersaturation, S, is computed using JANAF thermochemical data[34] for silicon equilibrium vapor pressures for Si(g), Si_2(g), and Si_3(g) above Si(ℓ).

From Table V it can be seen that the kinetic model used selects a critical size larger than the liquid drop model predicts. For these large supersaturations the liquid drop model predicts nuclei radii which are on the order of one Si atom radius (0.17 nm) if one uses the surface tension of bulk Si(ℓ) in Eq. (97)

(e.g., γ = 681 dynes cm^{-1} at 1800 K). The use of such a value for γ is clearly meaningless here. Thus the selection of larger critical sizes by the present model is physically more realistic for cases where very large supersaturations are encountered.

The nucleation model just described does, however, have several deficiencies. The first of these is incorporated in Eq. (94) which describes the entropy of formation of the n-mers from Si atoms. The expression given in Eq. (94) does not converge toward the bulk liquid entropy as n increases; therefore free energies of the n-mers do not, in general, converge to the free energy of formation of the bulk liquid as n becomes large. In order to rectify this situation the free energy of large n-mers is found by interpolating between the free energy obtained by the model just described and the sum of the free energy of the bulk liquid and the surface free energy of the n-mer, assuming the bulk surface energy value, i.e., we interpolate between the model just described and the classical surface tension model for the free energy of the n-mers. Thus, ΔG°_n is given by the following equation:

$$\Delta G^\circ_n/n \;=\; F_n(\Delta H^\circ_n - T\Delta S^\circ_n + n\Delta G^\circ_1)/n + (\Delta G^\circ_\ell + 4\pi N_A \gamma r_n^2/n)\;(1 - F_n) \qquad (101)$$

where the fraction F_n given by

$$F_n \;=\; (500/n)/(500/n + n/500) \qquad (102)$$

From Eqs. (101) and (102) it can be seen for n-mers much smaller than 500 the model just described will specify the free energy of formation. For n-mers with many more than 500 constituents the free energy of formation will be specified by the classical expression involving the surface energy of the bulk liquid. Equations (101) and (102) insure that, as $n \to \infty$, the free energy of formation will indeed approach that of the bulk liquid.

Actual calculations performed in subroutine NTHERM of the CHEMPART code are a simplified version of the model just described. A major simplification involves an abbreviation of the reaction mechanism described in Eq. (85). The code as it is currently written considers reactions only between identical n-mers, i.e., k = n in Eq. (85). Furthermore, three-body mechanisms described by Eq. (85) are simplified so that, only for the initial reaction between two monomers, does the third body explicitly play a role. Reactions between higher n-mers are considered to be two-body reactions. Further simplication is made by employing the approximate formulas for the forward reaction rate

by Frurip and Bauer,[41] i.e., if $n < 100$, $k_{n\to n+k} = 1 \times 10^{-10} (n + k)^{1.8}$. If $n \geq 100$, $k_{n\to n+k} = 1 \times 10^{-11} (n + k)^{2.6}$. The three-body rate constant for the reaction between monomers is chosen to be 1×10^{-30}. The nucleation model therefore considers a series of reactions of the type given in Eq. (85), leading to the formation of a maximum n-mer size chosen by the user. Above this maximum size, the condensing material is considered to have formed a bulk particulate size. The smallest particle mass class in this particulate phase has a mass which is somewhat less than the mass of the largest n-mer formed in the nucleation model. In each step of the program, as the largest n-mer is formed via the nucleation model, it is converted into the smallest and next smallest particle using the following three equations:

$$\dot{w}^N_{p_1} = Q \, \dot{F}_{nmax} \, \rho \, N_A \tag{103}$$

$$\dot{w}^N_{p_2} = (1 - Q) \, \dot{F}_{nmax} \, \rho \, N_A \tag{104}$$

where

$$Q = (m_2 - W_{nmax}/N_A)/(m_2 - m_1) \tag{105}$$

(In these equations the subscript nmax refers to the number of constituent atoms in the largest n-mer.)

2. Agglomeration

The particle agglomeration model incorporated into CHEMPART (subroutine AGGLOM) considers (i) Brownian agglomeration, (ii) turbulence-enhanced agglomeration, and (iii) agglomeration via inertial capture. To formulate the model, particles are divided into mass classes $\{m_i\}_{i=1,r}$ where

$$m_i = \xi^{i-1} \, m \tag{106}$$

The factor ξ should be as small as possible for accuracy; because of calculation time considerations it will probably be set at 10 which results in a rather minor overestimation[44] of the rate of growth of the particles. The rate of formation of particles of mass m_i via coagulation is given by

$$\dot{w}^A_{p_i} = -\sum_{j=1}^{r} K_{ij} \, \rho^2 \, F_{p_i} \, F_{p_j} + \sum_{j=1}^{i} S_{ij} \, K_{ij} \, R_{ij} \, \rho^2 \, F_{p_i} \, F_{p_j} + \sum_{j=1}^{i-1} S_{i-1,j} \, K_{i-1,j} \, (1-R_{ij}) \rho^2 \, F_{p_i} \, F_{p_j} \tag{107}$$

The fraction R_{ij}, required to insure mass conservation, is given by

$$R_{ij} = \frac{m_{i+1} - (m_i + m_j)}{m_{i+1} - m_i} \tag{108}$$

S_{ij} is a factor which insures correct counting when particles of the same mass collide

$$S_{ij} = \begin{cases} 1/2 & i = j \\ 1 & i \neq j \end{cases} \tag{109}$$

The rate coefficients for agglomeration, K_{ij}, are sums of coefficients representing the various operative mechanisms, i.e., Brownian diffusion, turbulence-enhanced agglomeration, and agglomeration due to particle-particle impaction.

$$K_{ij} = K_{ij}^{Br} + K_{ij}^{turb} + K_{ij}^{im} \tag{110}$$

Brownian Agglomeration[45]

$$K_{ij}^{Br} = 4\pi(r_i + r_j)(D_i + D_j) \left\{ \frac{r_i + r_j}{r_i + r_j + \delta_{ij}} + \frac{4(D_i + D_j)}{(r_i + r_j)G_{ij}} \right\}^{-1} \tag{111}$$

where D_i is the particle diffusion coefficient[40]

$$D_i = \frac{k_B T}{6\pi \mu_g r_i} \left[1 + 1.26 \frac{\lambda}{r_i} + 0.4 \frac{\lambda}{r_i} \exp\left(- \frac{r_i}{1.1 \lambda_g} \right) \right] \tag{112}$$

G_{ij} is the mean relative particle velocity

$$G_{ij} = \left[\left(\frac{1}{m_i} + \frac{1}{m_j} \right) \frac{8 k_B T}{\pi} \right]^{1/2} \tag{113}$$

δ_{ij} is a particle mean free path

$$\delta_{ij} = (\delta_i^2 + \delta_j^2)^{1/2} \tag{114}$$

$$\delta_i = \frac{2^{1/2}}{48} \frac{\pi G_i}{D_i r_i} \left[\left(2 r_i + \frac{8 D_i}{\pi G_i} \right)^3 - \left(4r_i^2 + \left(\frac{8 D_i}{\pi G_i} \right)^2 \right)^{3/2} \right] \tag{115}$$

The following simplified expression is employed for certain cases: For large particles with Kn_i, $Kn_j \leq 0.01$

$$K_{ij}^{Br} \approx \frac{2}{3}\,\frac{k_B T}{\mu_g}\,(r_i + r_j)\left(\frac{1}{r_i} + \frac{1}{r_j}\right) \tag{116}$$

For Kn_i or $Kn_j > 10$

$$K_{ij}^{Br} \approx \pi(r_i + r_j)^2\, G_{ij} \tag{117}$$

Turbulence-Enhanced Agglomeration[46]

$$K_{ij}^{turb} = \pi\,\frac{\rho_p}{\rho}\,\frac{E_0{}^{3/4}}{\nu^{5/4}}\,(r_i^2 + r_j)\,|(r_i^2 - r_j^2)|\;\beta_{ij} + (E_0/\nu)^{1/2}\,(r_i + r_j)^3\,\beta_{ij} \tag{118}$$

where E_0, the turbulent energy dissipation rate per unit mass, is modeled by

$$E_0 = \mu_t\left(\frac{\partial u}{\partial r}\right)^2\Big/\,\rho \tag{119}$$

and μ_t is the (eddy viscosity - molecular (laminar) viscosity). The factor β_{ij} is the probability that a small particle approaching a larger particle will actually collide with and stick to the larger particle. This factor is a function of the Stokes number, St_{ij}, and is given by the formula

$$\beta_{ij} = 1 + 0.92/St_{ij} + 0.278/(St_{ij})^2 + 0.034/(St_{ij})^3 \tag{120}$$

obtained by fitting the (Re = 0) curve given in Ref. 47.

Particle-Particle Impaction

For particles with differing average velocities, a contribution to the coagulation rate exists which is given by

$$K_{ij}^{im} = \pi(r_i + r_g)^2\,|u_{p_i} - u_{p_j}|\,\beta_{ij} \tag{121}$$

3. Heterogeneous Condensation/Evaporation

Particle growth caused by the condensation of gas-phase species on the particles and particle shrinkage due to evaporation from particle surfaces

C-2

is treated using the following model. For large particles ($Kn_j \ll 1$) the rate of increase of particle mass is governed by Eq. (122)[48]

$$\dot{m}_i = 2\pi r_i\left(Y_{Si} - (Y_{Si})_{eq,i}\right) \rho\, D_{Si}(Sh_i)_{Kn\ll 1} \tag{122}$$

where $\dot{m}_i$ is the rate of increase of mass of a particle in the ith mass class and $(Sh_i)_{Kn\ll 1}$ is the Sherwood number for such a particle. $(Y_{Si})_{eq,i}$ is the Si mass fraction at the ith mass class particle surface which is taken to be the Si equilibrium pressure at the particle temperature (which is mass class dependent and different, generally, from the gas temperature). The gas density is ρ and D_{Si} is the diffusion constant for Si. The Sherwood number is a function of the particle slip (relative to the mean flow), Reynolds (Re), and Schmidt (Sc) numbers and is taken to be[48]

$$(Sh_i)_{Kn\ll 1} = 2(1 + 0.3\, Re_{p_i}^{1/2}\, Sc_i^{1/3}) \tag{123}$$

For very small particles (Knudsen number $\gtrsim$ 1) diffusion will be very fast over lengths comparable to the particle diameter and the rate of mass increase will be limited by the actual incorporation of material at the surface, i.e., for an accommodation coefficient of unity,

$$\dot{m}_i = \pi r_i^2 \left(Y_{Si} - (Y_{Si})_{eq,i}\right) \rho \left[\frac{8\, RT_{p,i}}{\pi\, W_{Si}}\right]^{1/2} \tag{124}$$

where W_{Si} is the molecular weight of Si.

The Sherwood number in this case comes directly from gas kinetics theory and is given by

$$(Sh_i)_{Kn\gtrsim 1} = \frac{1}{2}\left[\frac{8\, RT_{p,i}}{\pi\, W_{Si}}\right]^{1/2} r_i/D_{Si} \tag{125}$$

In order to compute the rate of mass increase throughout the broad particle size range desired, we will interpolate between the two regimes, using

$$Sh_i = (Sh_i)_{Kn\gtrsim 1}\,(Sh_i)_{Kn\ll 1} \Big/ \left[(Sh_i)_{Kn\gtrsim 1} + (Sh_i)_{Kn\ll 1}\right] \tag{126}$$

and

$$\dot{m}_i = 2\pi r_i \left(Y_{Si} - (Y_{Si})_{eq,i}\right) \rho\, D_{Si} Sh_i \tag{127}$$

Condensation and evaporation lead to a redistribution of particles among the various mass classes. This is accomplished by the following algorithm:

For condensation ($\dot{m}_j$, $\dot{m}_{j-1} > 0$)

$$\dot{w}^C_{p_j}/\rho = F_{p_{j-1}} \dot{m}_{j-1}/(m_j - m_{j-1}) - F_{p_j} \dot{m}_j/(m_{j+1} - m_j) \quad (128)$$

For evaporation ($\dot{m}_j$, $\dot{m}_{j-1} < 0$)

$$\dot{w}^E_{p_j}/\rho = F_{p_j} \dot{m}_j/(m_j - m_{j-1}) - F_{p_{j+1}} \dot{m}_{j+1}/(m_{j+1} - m_j) \quad (129)$$

In Eqs. (128) and (129) the factors involving m_j, m_{j+1}, m_{j-1}, $\dot{m}_j$, $\dot{m}_{j-1}$, and $\dot{m}_{j+1}$ are those needed to conserve particle number and total mass. They are similar in nature to the factors R_{ij} used in Eq. (107) and are easily obtained by setting the sums of the particle mass after deposition ($m_j + \dot{m}_j dt$) equal to fractional parts of a particle in the jth mass class and the (j+1)th mass class (for condensation) or (j-1)th mass class (for evaporation).

As in the other "particle chemistry" models described above, this model rigorously conserves particle number. The code corrects the concentration of the condensing or evaporating vapor so that mass is also conserved. The latent heat liberated or absorbed by the change phase is assumed to be transformed immediately to the gas at each step of the program and the gas temperature is adjusted (explicitly) accordingly in subroutine AGGLOM.

F. ENCLOSED FLOWS

A major problem encountered when considering enclosed flows is the calculation of the rate of transport of mass, momentum, and energy to the walls containing the flow. In order to do this a reasonable estimation of the turbulent transport (the eddy viscosity) must be obtained. In CHEMPART (subroutine TURB) the following simple mixing length governs the eddy viscosity used. The mixing length is related to the effective turbulent viscosity, μ_w, in the wall region via Eq. (130)

$$\mu_w = \mu_g + \rho\, \ell^2 \left|\frac{\partial u}{\partial y}\right| \quad (130)$$

where μ_g is the molecular viscosity and y is the distance to the wall,

$$y = r_w - r \tag{131}$$

The mixing length, ℓ, is a function of the distance from the wall as given by the following two equations[5a]:

$$\ell = K_w y \eta \qquad \text{for } y < \lambda_w y_\ell / K_w \tag{132}$$

$$\ell = \lambda_w y \ell \qquad \text{for } y > \lambda_w y_\ell / K_w \tag{133}$$

In Eq. (132) the factor η is the van Driest damping factor given by[49]

$$\eta = 1 - \exp(-y\rho u^*/A^+\mu_g) \tag{134}$$

The constants K_w and λ_w have values typically taken to be 0.44 and 0.99, respectively. The friction velocity, u^*, is $(\tau/\rho)^{1/2}$, where τ is the momentum flux to the wall (the wall stress). The boundary layer thickness is $y_{\tilde{\ell}}$. The empirical factor A^+ has a value which is a weak function of u^* and dp/dx and is typically ≈ 26.[9]

In the upstream regions of the reactor both boundary layer development and the spreading of an axially centered jet within the reactor must be modeled. In these upstream regions the following equation is used to describe the effective turbulent viscosity:

$$\mu = [\mu_j(r_w - r) + \mu_w(r - r_{1/2})]/(r_w - r_{1/2}) \tag{135}$$

In this equation μ_j is computed via the jet mixing model described in Section IV.C, while μ_w is the turbulent viscosity given by Eq. (130). These are averaged with weighting factors proportional to the distance from the wall and from the jet radius, $r_{1/2}$. When the jet radius exceeds half the distance between the initial jet radius and the wall, μ is set equal to μ_w.

Using the effective viscosity, μ, obtained with this model, the code computes the flux of condensible species, particulate matter, momentum, and energy across the outermost stream tube to obtain rates of pressure drop, mass, and energy deposition on the reactor walls. For particulate transport to the reactor walls a simple thermophoretic diffusion velocity is also computed. The reader is referred to the discussion of the modified GENMIX code (Section IV) for a rigorous description of calculations of this type.

The change of pressure with axial distance, dP/dx, is computed using substantially the method of Patankar and Spalding[5b] in which the change in pressure for a step, dx, is computed using the momentum flux to the wall, the gain or loss of material via wall condensation/evaporation, and the temperature change which occurred during the previous step. The pressure change is that required to maintain the cross-sectional area of the flow equal to the reactor cross-sectional area. Since, in a marching code such as CHEMPART, the pressure change, dP, must be computed using information obtained in the previous step (i.e., downstream information required to precisely calculate dP is not available), the flow area will not be the same as the reactor area, but instead continually "seeks" the reactor area.

G. GRIDPOINT DISTRIBUTION

For free jet expansions the radial gridpoint in ψ-space is uniform, i.e., the stream tubes defined by the gridpoints all carry the same mass flux. As the jet entrains gas from its edge, additional gridpoints are added. However, the code, at present, is limited to a maximum of 30 radial gridpoints. Hence, it is necessary, when this limit is reached, to redistribute the gridpoints throughout the jet and reduce the number of gridpoints. At present, when the maximum number of 30 gridpoints is reached, this redistribution is done so that the code proceeds with only 20 gridpoints which are then augmented as more mass is entrained.

For enclosed flows the amount of mass flowing through the system is constant (except for that condensing or evaporating at the walls of the system). Thus, throughout the calculation, a constant number of gridpoints is used and each stream tube defined by these gridpoints carries a constant amount of flow. For enclosed flow calculations, however, the spacing between the gridpoints is not uniform. Accurate calculation describing a number of phenomena occurring near the reactor walls requires that the spacing there be much finer than is, in general, needed within the core flow. Thus, the spacing (in ψ-space) of the first three gridpoints encountered as one proceeds inward from the wall is only 3.125% of that between gridpoints in the core. The spacing between successive gridpoints doubles as one proceeds inward until the 6th gridpoint is reached. The spacing is then even from the 6th point to the axis. In this way sufficient definition is obtained near the

walls to allow the calculation of reasonable values for mass, momentum, and energy fluxes to the walls.

H. STEP SIZE

Except for the first few steps, the step size used by the program is totally determined by mixing parameters, in particular the value of the eddy viscosity and by the grid spacing, i.e., by $(\Delta\psi)^2$. Specifically step size, dx, is governed by Eq. (136)

$$dx = \text{minimum}\ [\text{FDL} \times \Psi_i^2 d\Psi_i^2/(3\mu_i \rho_i \mu_i y_i^2)] \tag{136}$$

where FDL is an input parameter generally taken to be 1 and the subscript i denotes that values are examined at each gridpoint. For the initial fifteen steps taken in the calculation, a chemical kinetic criterion for step size is used in which the step size is taken to be a multiple of the molecular mean free path. Specifically,

$$dx^1 = \bar{\lambda} \times 2^{(\text{INTSTP} - 1)} \tag{137}$$

where λ is the average of the molecular mean free paths at the centerline and at the wall or edge and INTSTP is the integration step number.

VII. THE CHEMPART CODE: STRUCTURE

A. GENERAL CHARACTERISTICS

CHEMPART is written in standard FORTRAN IV. A listing of the code is included as Appendix E of this report. A simplified schematic of the program flows is shown in Fig. 13. The MAIN routine of CHEMPART governs the program flow. Within it numerous variables are initialized, routines for inputing and outputing data are called, and some of the major governing equations, i.e., the particle conservation equations, the momentum equation, and the energy equation are set up and solved. The initial routine called by the MAIN program is subroutine READIT. Within this routine the input information is read and many additional variables are initialized. The next routines called are subroutines INITL, RADIAL or NONRAD, which set up initial values for concentrations, temperatures, and velocities in the coordinate system used within the program. After this input and initialization stage, the next subroutine to be called is subroutine NTHERM. This routine computes the thermodynamic data required by the nucleation and condensation models contained in the program. After a final initialization step performed by another call to subroutine INITL, subroutine WALCON is called (if the flow is an enclosed flow) and in this routine the vapor pressures of the condensing species at walls is computed. The program then enters a large loop from which it does not exit until the problem is solved. Each passage through this loop marks the taking of a step downstream in the flow. Within this large loop one first computes the gas-phase density, the molecular viscosity, and the specific heat of the gases at each radial gridpoint across the flow. (There are MPSI of these gridpoints.) After converting between the actual radial coordinates and the stream or ψ (PSI) coordinate system actually used to solve the problem, the subroutine TURB is called. In this subroutine one or another of the zero-equation turbulence models chosen by the user is called and the effective turbulent (or laminar) viscosity (the "eddy" viscosity) is evaluated at each radial gridpoint. The next step is the calculation of the step size to be taken (DX). The MAIN program then solves the momentum and energy equations at each gridpoint. The equations are set up and solved implicitly for all gridpoints simultaneously. Subroutine GETH is used during this step to obtain the static enthalpy at each

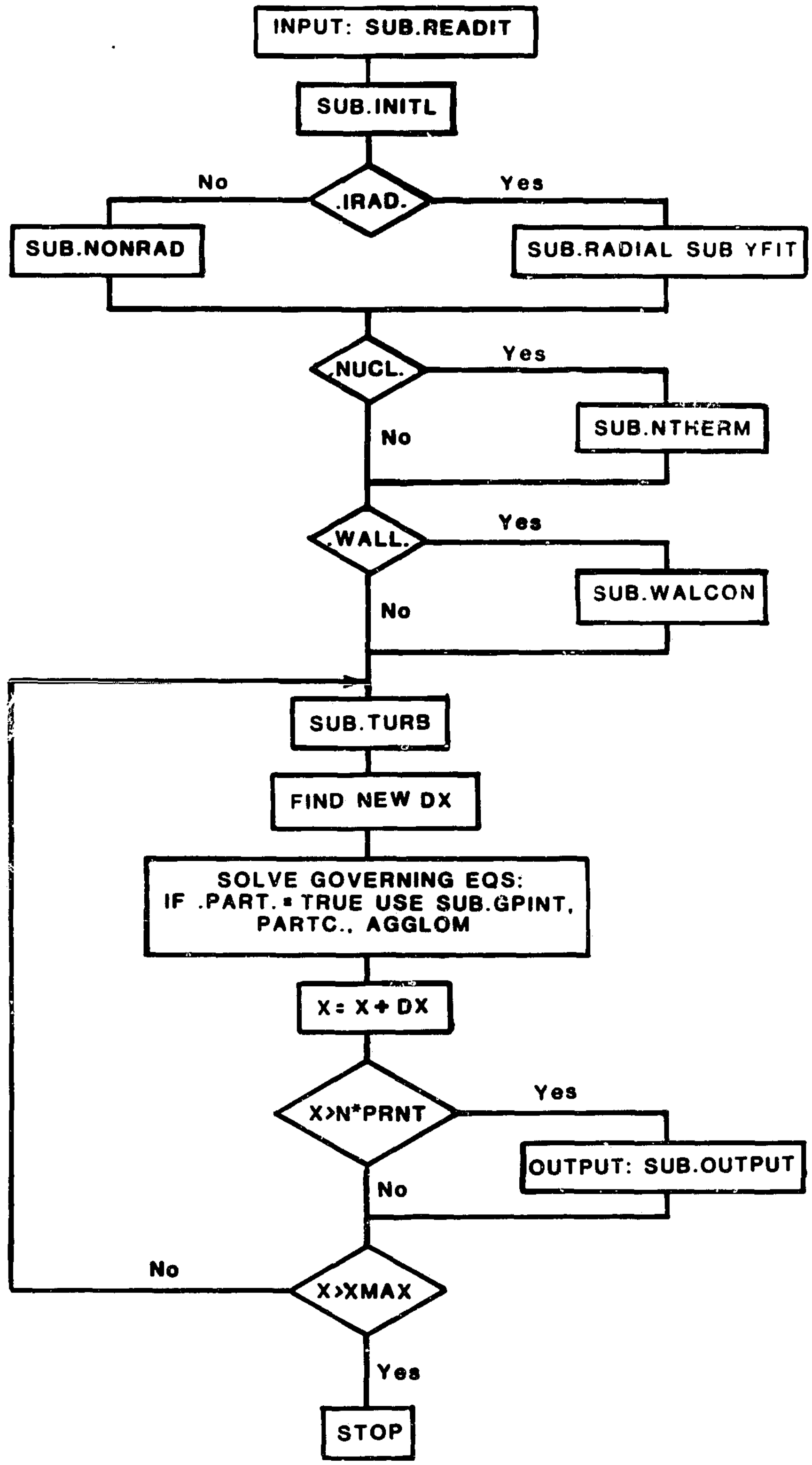

FIGURE 13 CHEMPART FLOW CHART

gridpoint and subroutine TRIDAG is used to solve the tri-diagonal matrix in order to obtain the new velocities and temperatures which result from taking the downstream step. The program calls subroutine TCHEM next. In this routine the species equations including chemical reaction source terms are set up and solved implicitly. MAIN then calls subroutine GPINT in which the contributions to the change in gas velocity and gas temperature due to the presence of particles moving through the gas at different velocities and temperatures are calculated. Subroutine AGGLOM is then called to compute the rates of particle agglomeration and particle growth via heterogeneous condensation. The particle conservation equations are then solved explicitly within MAIN and particle cloud densities are obtained for each particle mass class. Finally, subroutine PARTC is called and new values of particle temperatures and velocities are obtained using the momentum and energy exchange quantities found in subroutine GPINT. Subroutine NEGCHK is then called and the new downstream values for velocity, temperature, species concentration, and particle densities are scanned to determine whether a stable solution is being calculated (i.e., all these quantities are checked to see if any have become negative). If instability occurs, the step is repeated with a new step size (DX) which is one-tenth that taken initially. Subsequent steps then are gradually increased to that determined by Eq. (136). The above calculations are performed at each gridpoint at the end of which, if the flow is an enclosed one, subroutine FLUX is called from MAIN. Within subroutine FLUX the flux of energy, momentum, and condensible species to walls is computed and the pressure drop due to transport of momentum to the walls is computed. After return to MAIN, initialization required for taking the next step is performed, the program returns to the beginning of the large loop referred to above, and the next step is taken. This process is continued until the program has marched to the maximum downstream distance (XMAX) specified by the user.

B. PROGRAM INPUT

The preparation of input data for CHEMPART is described in Appendix F. A sample input card deck is given in Appendix G. The overall structure of the input data is governed to a large extent by the user's choice of values for the logical variables IRAD, IRADP, PART, NUCL, and WALL (see explanation of Card 2 in Appendix F). If the user chooses IRAD = .TRUE., then a set of

radial gridpoints Y(I), and values for gas species and particle concentrations, velocities, and temperatures at these gridpoints must be specified. If the user chooses IRAD = .FALSE., then the user must specify only axial and edge values for species and particle concentrations, velocities, and temperatures. For the latter case the radial dependence of the initial values of the quantities will be step functions where the axial values are taken for gridpoints up to the edge of the jet (RJ) and edge values are used for all gridpoints with radius greater than RJ. The logical variable PART specifies whether or not a particulate phase is (or may be formed) in the flow. If PART = .TRUE., then initial values for particle cloud density, particle velocity, and particle temperature must be specified. Whether they are specified only on axis and at the edge or at points, Y(I), across the flow is determined by the selection of IRADP to be either .TRUE. or .FALSE., respectively. The variable NUCL, if taken to be true, means that the code will include the nucleation model. If NUCL = .TRUE., then cards specifying the number of n-mers to be included in the nucleation mechanism and various thermodynamic properties of the bulk liquid must be included (see Appendix G). Modeling of particle growth via condensation and deposition of vapor on reactor walls is also controlled by the NUCL specification. If NUCL = .FALSE., these processes will not be considered. If WALL = .TRUE., then the flow calculation will be done for an enclosed flow and cards must be added to the input deck which give the reactor radius and the reactor wall temperature.

C. PROGRAM OUTPUT

The program output, a sample of which comprises Appendix H, begins with an identification of the program and an identification of the run (TITLE (I), I = 1,...36). Next follows information supplied by subroutine INOUT. This information includes the input pressure, the jet nozzle radius, the reactor radius (if an enclosed flow is being considered), and the initial and final axial coordinates (XINIT, XMAX). The print increment (PRNT) and the minimum step size (DXMIN) are then printed. The viscosity model being used is then given. Next follows a table which gives the temperature, velocity, and species mole fraction along the jet centerline and at the edge of the flow (at R = infinity if a free jet is being modeled and at a point just beyond the jet boundary if an enclosed flow is being modeled). If particles are to be included in the calculation (PART = .TRUE.), a table is given of the number

of particle mass classes, the mass of the particles in each class, the radius of the particle, the particle cloud density along the centerline, the particle temperature, and the particle velocity. Next the reaction mechanism is tabulated; each reaction is listed along with its rate constant. This list includes nucleation reactions which are constructed by the nucleation model in subroutine NTHERM. If particles are being treated in an enclosed flow (if PART = .TRUE. and if WALL = .TRUE.), the particle Schmidt numbers at the wall are then tabulated. The particle mass for each mass class is given along with the particle radius and the particle Schmidt number.

As integration proceeds, whenever the x coordinate becomes greater than an integral multiple of the print increment (PRNT), the following information is printed using subroutine OUTPUT: First, the value of the x coordinate is printed and the run labeling information is repeated. Next the non-dimensional value of x, the integration step size (DX) of the integration step immediately preceding the call to subroutine OUTPUT is printed, the pressure is printed, and the smallest and largest steps taken between print stations are printed. Next non-dimensional values for the jet radius (QQ100), the inner mixing zone radius (QQ200), and the Mach number at the jet radius (QQ300) are printed. Also, the mixing rate coefficient (QQ400) is printed if turbulence model 6 is used. Then the Prandtl number on the centerline is given. Next the non-dimensional coordinates of each gridpoint, the velocity, temperature, density, Mach number, static enthalpy, viscosity (eddy), and the value of the stream coordinate Ψ are given at each gridpoint. This is followed by a tabulation of the mole fractions of each species at each gridpoint. If particles are present in the flow, the particle cloud density, particle temperature, and particle velocity at each gridpoint are then given. Next a summary of important physical quantities integrated across the flow is given. This includes the total mass flow ($\pi\Psi^2$), the mass flow of gases, and the mass flow of particulate matter. The rate of change of the pressure and the total pressure change from the beginning of the calculation are printed. The total static enthalpy of the flow is then given followed by the total stagnation enthalpy of the flow. Changes in the mass flows are then listed: for total flow, gas flow, and particle flow. Next, changes in static and stagnation enthalpies and, if an enclosed flow is being modeled, the reactor radius and the reactor wall temperature are given, followed by values for the mass average temperature and the mass average velocity across the flow. The energy and the mass being deposited

per unit length at the wall are then printed. The boundary layer thickness (non-dimensional) is then given. In the above, non-dimensional lengths are obtained by dividing by the initial jet radius if free jet expansion is being modeled or by the reactor wall radius if enclosed flows are being treated.

The evaluation of integrated or averaged quantities across the flow is performed by making polynomial fits (subroutine POLFIT) to quantities which must be averaged or integrated and integrating the polynomials using function FINTGL. In order to obtain changes which occur and mass flow and enthalpy flow, it is necessary to subtract the values of the appropriate integral from the value of that integral obtained after the first integration step. It should be recognized that, early in the flow, the taking of differences between large, nearly equal numbers obtained by such procedures is apt to be inaccurate. For example, changes in mass flow of 0.1% or less due to (i) entrainment of gas in a free expanding jet, or (ii) deposition of particles or vapor on reactor walls, will not necessarily be accurately calculated by the procedure used.

A number of other output messages and output information will occasionally be given. These include messages concerning the presence of particles in the flow, a repetition of the particle Schmidt number information after the 100th integration step, and messages from subroutine NEGCHK if negative velocities, temperatures, species concentrations, or particle cloud densities are encountered. Other messages which may be encountered in the output tell the user that the program has reached the end of the jet inviscid core, or that the number of gridpoints has been cut by subroutine TUBCUT. Lastly, there exist a number of STOP commands which may halt the program if certain errors occur. These STOP commands are numbered and the computer day file may generally be used to locate the source of the error with the help of the program listing.

VIII. $SiCl_4/Na$ REACTION AND $Si(\ell)$ FUME FORMATION: SAMPLE CHEMPART CALCULATIONS

In order to illustrate the use of the CHEMPART code we describe here a number of calculations performed to describe $SiCl_4/Na$ flow reactors of the type similar to that being tested by Westinghouse.[1] Specifically, a series of calculations in which the input enthalpy is varied over a substantial range will be described. For low input enthalpy the heat transfer to the walls is found to reduce the temperature in the core flow sufficiently rapidly that particulate formation occurs. Radiation from the $Si(\ell)$ fume then reduces the temperature rapidly leading to even more fume formation and an accelerated temperature decrease. Calculations of this type test nearly all the models currently incorporated in the CHEMPART code; in fact, only the routines dealing with translation of the initial values from r-space to ψ-space remain untested at this time. In all the runs to be discussed in this section, step function initial conditions were employed.

In Table VI the important input parameters of the series of five runs of interest here are described. The table shows input parameters for four runs in which the input enthalpy is varied by assuming various degrees of dissociation of a constant amount of input hydrogen. In the fifth run, more hydrogen was added and total dissociation of the input hydrogen is assumed. In the first four runs an Si input (in the form of $SiCl_4$) of 28 kg h^{-1} is assumed; the fifth run assumes a flow of 45 kg h^{-1}. The H/Si input ratio is 4 in the first four runs and 12.5 in the last run. It is assumed that the arc heaters used by Westinghouse will supply between 0.3 and 1.9 MW in these runs. With these energy inputs, and starting with essentially room temperature reactants, adiabatic flame temperatures varying between 2880 K (for run 1) and 2750 K (for run 5) are encountered. (Run 5 represents a case in which the input parameters match most closely those which Westinghouse plans to use. The first four runs underestimate the amount of power to be added by arc heaters and the amount of hydrogen to be used.) Appendix G gives a listing of the input deck for run 1 of Table VI. The sample output shown in Appendix H is taken from the output of this computer run.

The results of this set of computer runs can be summarized with the use of Figs. 14-17. Figure 14 shows temperature profiles along a streamline

TABLE VI

SAMPLE TEST CASE - INPUT PARAMETERS

Reactor Diameter = 15 cm

Run	Si Input $kg\ h^{-1}$	Reactant Ratios[a] H/Si	Na/Si	Ar/Si	% of Input H_2 Dissociated	Initial[b] velocity $m\ s^{-1}$	Initial[b] temperature, K	Input[c] static enthalpy, $kcal\ s^{-1}$	Heat[d] added, MW
1	28	4.0	4.0	0.5	0	23.1	2820	29.1	0.31
2	28	4.0	4.0	0.5	6.2	23.6	2820	32.6	0.32
3	28	4.0	4.0	0.5	31	25.5	2860	47.4	0.38
4	28	4.0	4.0	0.5	62	27.9	2940	66.8	0.46
5	45	12.5	4.1	1.1	100	125.	3360	380	1.90

[a] Reactants in runs 1-4 are introduced as $SiCl_4(g)$, H_2, H, and Ar at 3700 K and Na(g) at 1400 K. In run 5 reactants enter as $SiCl_4(g)$ at 500 K, Ar and H at 4500 K, and Na(g) at 1400 K. Na(g) is introduced as a jet, r_i = 3.75 cm; $SiCl_4$, H, H_2, and Ar are introduced in an outer flow between the jet and the wall.

[b] Mass-averaged across the (initially) unmixed flow.

[c] This enthalpy includes heats of formation.

[d] The heat added is calculated by (i) assuming the H_2 and Ar must be heated to their input temperatures from 298 K, (ii) $SiCl_4(\ell)$ at 298 K must be vaporized and heated to its input temperature, and (iii) $Na(\ell)$ is supplied at 500 K and must be vaporized and heated to 1400 K.

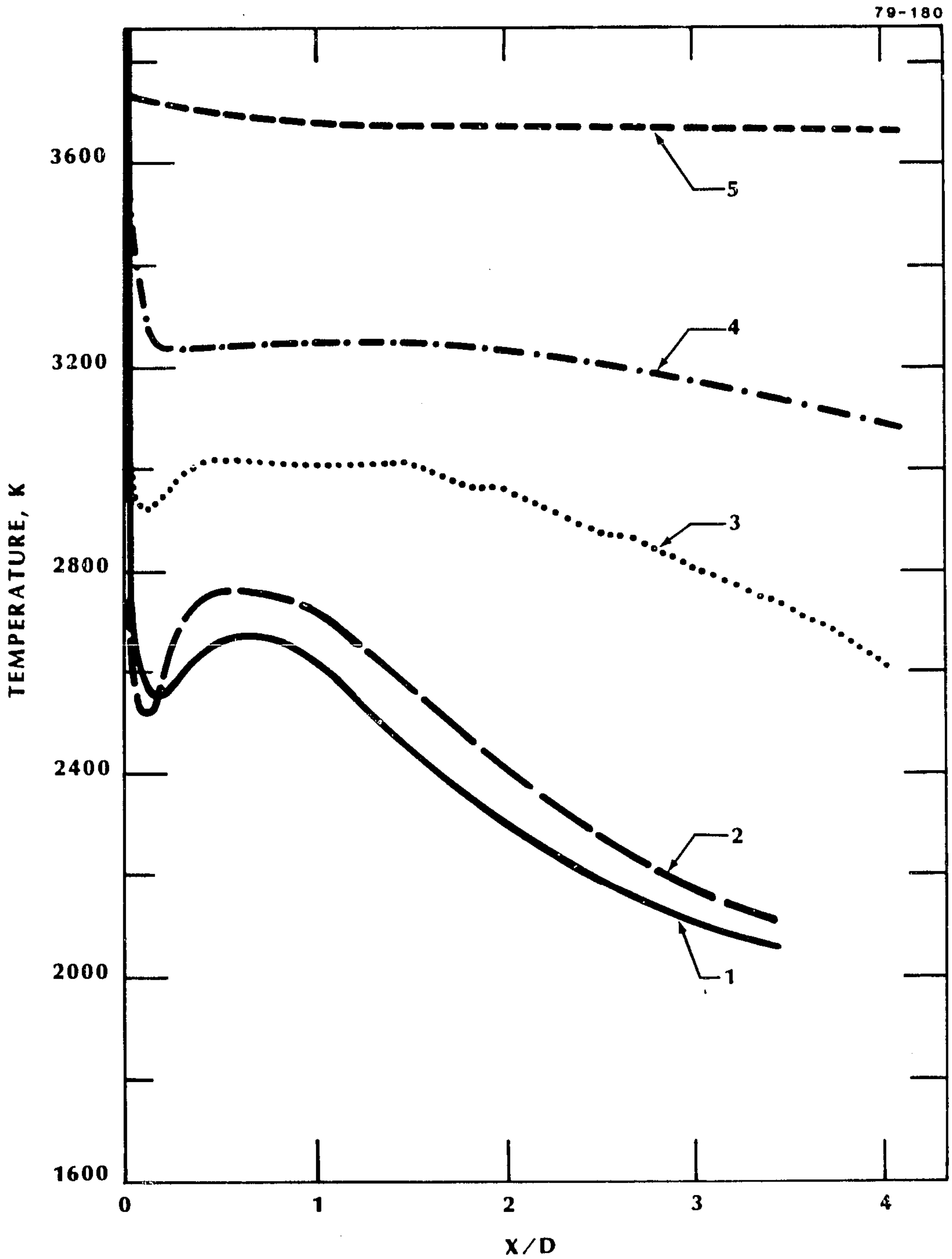

FIGURE 14 TEMPERATURE PROFILES

r/D ≈ 0.27; wall temperature = 1800 K.
Curve labels refer to run numbers.
Conditions are given in Table VI.

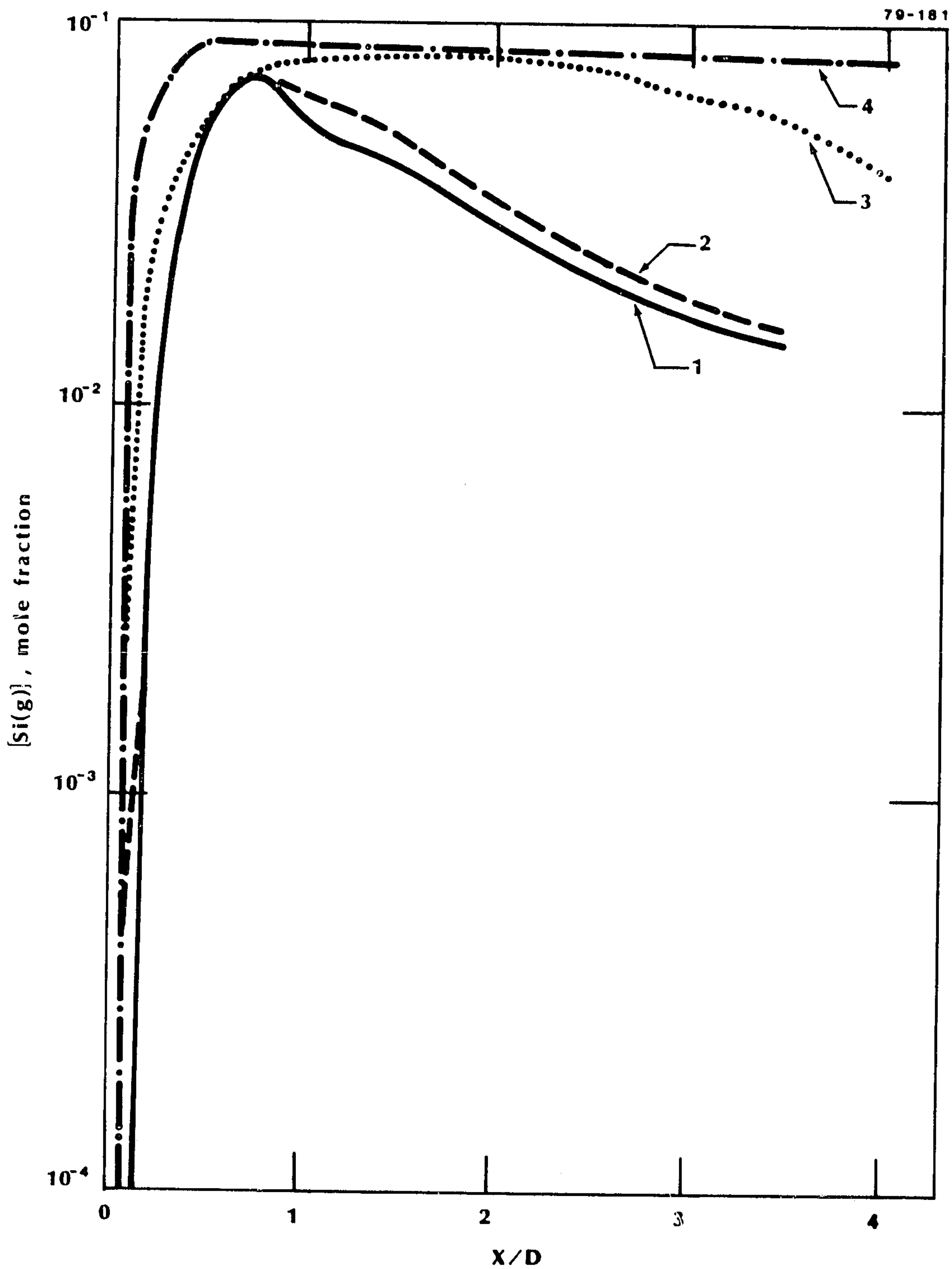

FIGURE 15 Si(g) PROFILES

r/D = 0.27.
Curve labels refer to run numbers.
Conditions are given in Table VI.

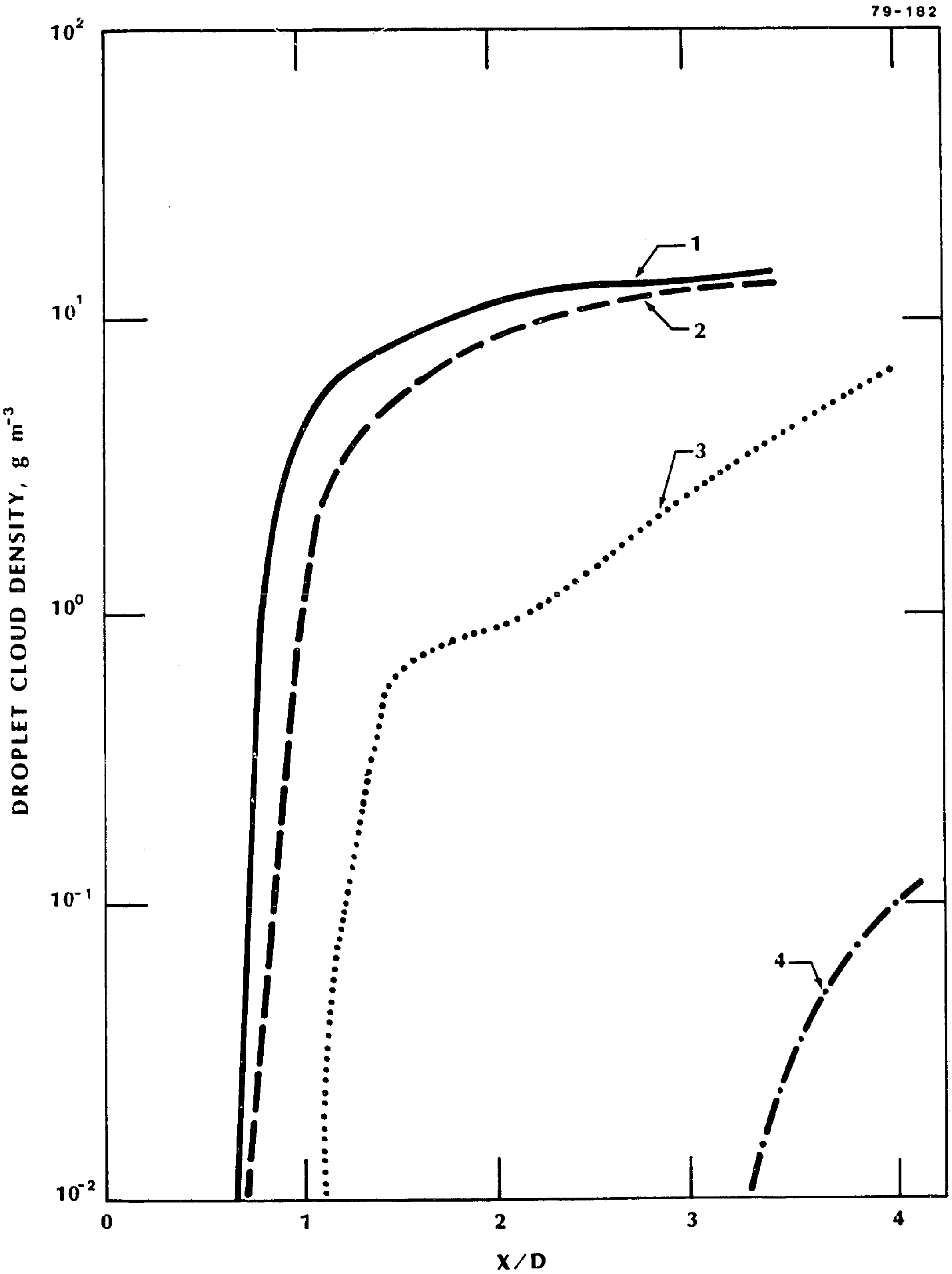

FIGURE 16 Si(ℓ) CLOUD DENSITY PROFILES

r/D = 0.27.
Curve labels refer to run numbers.
Conditions are given in Table VI.

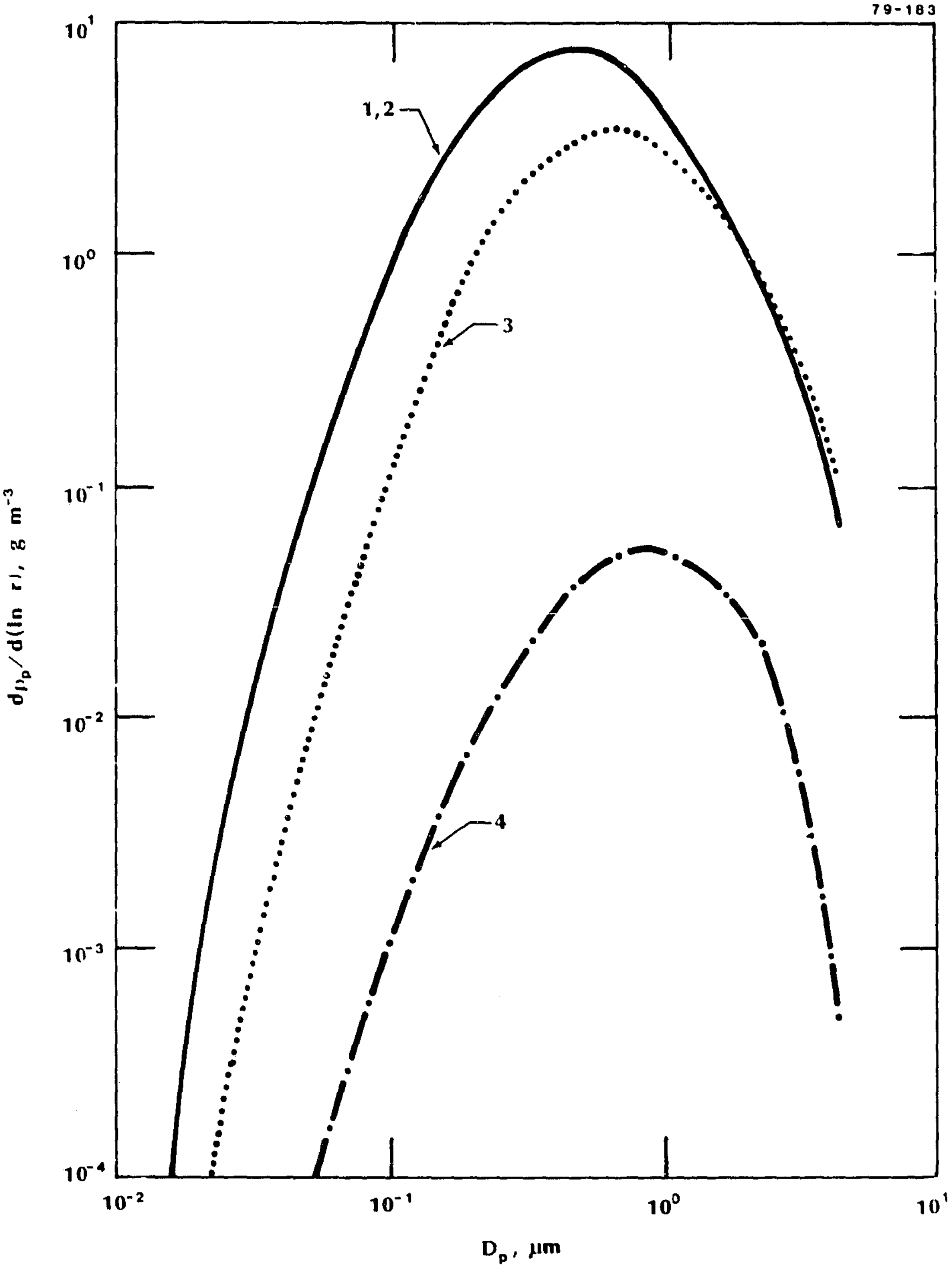

FIGURE 17 DROPLET SIZE DISTRIBUTIONS

x/D = 3.4; r/D = 0.27.
Curve labels refer to run numbers.
Conditions are given in Table VI.

just outside the initial jet radius. It is along this streamline that reaction between the 3.75 cm sodium jet and the outer $SiCl_4/H_2/H/Ar$ flow is greatest. As can be seen from Fig. 14, the computer runs to be discussed extend only 60 cm or so down the reactor. The reason for not continuing these runs to greater distances was simply one of cost. CHEMPART is an expensive code to run and the essential features of the flow were revealed in runs during the first 50 cm or so. The essential features of the temperature profiles shown in Fig. 14 are as follows: For all but the last case, there is a rapid drop in temperature from the 3700 K input temperature for the outer $SiCl_4/H_2/H/Ar$ flow as H and H_2 rapidly react with $SiCl_4$ to produce, principally, $SiCl_2$ and HCl. As sodium crosses the streamline being tracked, the reaction to yield NaCl(g) and Si(g) causes the temperature to rise; however, for runs 1 and 2 by x/D (where D is the reactor diameter) an Si(ℓ) fume is formed which radiates strongly to the walls and is principally responsible for the decrease in temperature noted in these two low enthalpy runs.* In run 3 condensation does not occur until $x/D \approx 1.5$. For the higher enthalpy run 4, particulate formation is not evident until $x/D \approx 3$ and even at $x/D \approx 4$, there is not a large amount of Si(ℓ) fume. However, even for run 4 an accelerating temperature decrease may be noticed due to the small amount of fume present between $3 \leq x/D \leq 4$. For the fifth run, no fume is formed and the temperature shows no sign of decay over the distance examined. In Fig. 15 the concentration of gaseous Si is plotted for runs 1-4 along the same streamline used in Fig. 14. In runs 1 and 2 the decrease of Si(g) as Si(ℓ) forms is very noticeable. For run 3 this decrease occurs later and is less drastic and for run 4 the decrease due to particulate Si formation is just noticeable by $x/D = 4$. [Si(g)] for run 5 is not shown; it is essentially constant and equal to 0.051. Figure 16 shows the Si(ℓ) cloud mass density along the same streamline. The rapid formation of particulate material in runs 1 and 2 at $x/D < 1$ is notable. For these runs, at $x/D = 3$ about 3/4 of the available silicon has been incorporated in the particulate

---

* The model currently assumes that radiation occurs through an optically thin droplet cloud. For runs 1-3, the cloud is definitely thick optically, with an (absorption + scattering) coefficient $\approx 1\ cm^{-1}$. Thus the temperature drop will not actually be as pronounced as indicated.

silicon. For the higher enthalpy runs, the formation of the particulate phase is still rather rapidly evolving even at x/D = 4.

Figure 17 shows droplet Si(ℓ) size distributions at the streamline used for the previous figures and at x/D = 3.5. As would be expected from the results shown in Fig. 16, the particle density distribution calculated in runs 1 and 2 shows considerably more particles present at this point in the flow than do the higher temperature runs 3 and 4. However, a more interesting feature is that the particle sizes present in the latter two runs tend to be larger than in the lower temperature runs. The particle size distribution one obtains is expected to be dependent on the competition between the nucleation process which generates new particles and the condensation of Si(g) on particles already formed. Thus, in the higher temperature runs, fewer particles are formed and condensation on these particles tends to lead to larger particle sizes. In other words, the longer one is able to maintain the flow at relatively low supersaturations, the larger the resultant particles. The droplet sizes being calculated are relatively large. Particle diameters in all four cases are considerably greater than 0.1 μm, and in run 4 the peak particle size approaches 1 μm. Indeed, the results shown in Fig. 17 hold promise of pointing to conditions at which particles substantially larger than 1 micron might be produced by operating very close to the Si dew point. It should be recognized, of course, that because the size distribution is quite obviously a function of the competing rates of nucleation and particle growth via condensation (on the time scales involved in Figs. 14-17 particle agglomeration plays no role), it is important that the nucleation process be modeled reasonably accurately. The simple model used in CHEMPART is believed to yield considerably more reasonable results than would be obtained using a classical nucleation model with its assumptions of rate limitation by the nucleation step and the use of surface tension concepts. The rate constants chosen for the nucleation reactions are deliberately picked to be unreasonably large so that errors which may occur will tend to yield more, smaller particles than would be calculated if smaller rate constants were chosen. Nonetheless, the nucleation rates computed are slow enough that particles approaching 1 micron in size are predicted. Perhaps coincidentally, experimental evidence from experiments using $SiCl_4$/Na flames at AeroChem, and even for seemingly unrelated silicon production processes such as the Union Carbide Free Space Reactor process

(an SiH_4 decomposition process), do seem to lead to particles with sizes in the 0.1-1.0 μm size range. Certainly, more work to determine the sensitivity of the nucleation model to changes in the nucleation reaction rate constants is needed. Also, experimental work which would yield values for rates of nucleation in $SiCl_4$/Na flames is required before truly reliable results can be computed.

IX. CONCLUSIONS AND RECOMMENDATIONS

A. CODE DEVELOPMENT

In the research program described in this report, two extremely useful tools have been developed for studying and predicting the performance of high-temperature, two-phase flow reactors. The first, the combined GENMIX-MPDEU code, is suited for economically examining the development of the flow as it passes through the reactor and the transport of heat, condensible vapor, and particulate matter through the boundary layer to the reactor walls. The second, the CHEMPART code, treats the detailed chemical kinetics, particle formation, and particle growth processes needed to adequately describe processes as complex as those occurring in, e.g., the $SiCl_4$/Na reactor of Ref. 1. These codes complement one another in the following ways: (i) GENMIX-MPDEU is not capable of performing detailed chemical kinetics including nucleation and particle growth calculations. However, by neglecting these time-consuming operations, it can, using a more detailed grid, perform its boundary layer calculations with more precision and economy than can CHEMPART. (ii) CHEMPART, on the other hand, because it treats many more potentially important processes than does GENMIX-MPDEU will, particularly in the core flow of the reactor, produce a much more complete picture of what can be expected to occur. The price paid for this is that a coarser grid must be used, with an accompanying loss of accuracy near the walls and, of course, increased run time and expense.

Development of a computer code the size of CHEMPART is necessarily a multi-year project. It was noted earlier that many options for running the code and many types of systems can be treated by the code. To date, only a small number of these possibilities have been explored. It would be anticipated that, should the code find reasonably wide use, it will be substantially modified in the future. At the present time, a number of possibilities for further improvement in the code exist. Also, the GENMIX-MPDEU code is as yet untested in its current form. In view of these points, the following recommendations are made:

1. A sensitivity analysis of the nucleation model in CHEMPART should be performed. This should be done both by varying n-mer reaction rate constants and by specifying different numbers of n-mers (i.e., varying the size of the n-mer at which one treats the cluster as a particle of bulk material rather than a large molecule).

2. There are a number of widely available integration routines specifically built to handle the type of stiff equations that must be solved in CHEMPART. Some of these stiff equation solvers should be tried in place of the mixed implicit-explicit integration schemes now being used in the code.

3. The GENMIX-MPDEU code needs to be exercised so that accurate rates of particle transport to walls can be obtained for use in checking results obtained with CHEMPART and, in its own right, as a useful predictive tool for systems such as that of Ref. 1.

B. CODE APPLICATION

During this program the codes have been used to perform rather preliminary estimates of the behavior of flows in $SiCl_4$/Na reactors of the general design of that described in Ref. 1. The results of the calculations may be summarized by noting:

1. In flows with temperatures above the dew point of Si, velocities of less than 50 m s^{-1} are required to allow collection of more than 50% of the Si on the reactor (8 m long, 15 cm diam) walls.

2. The calculations described in Section VIII show that large input enthalpies are required to suppress the formation of Si(ℓ) droplets. The formation of a particulate phase at the high temperatures (> 2500 K) prevailing in such flows is of particular consequence since the intense radiation from the droplets to the reactor walls represents a significant (actually dominant) mechanism of heat transfer. This is not unimportant with regard to mass transport to the walls, since, in order for thermophoresis to be effective in allowing the particulate phase to penetrate the laminar sublayer at the wall, a larger temperature gradient is desirable. Rapid heat loss due to radiation will reduce this gradient.

3. In order to insure that sufficient enthalpy is introduced to prevent Si(ℓ) droplet formation, large quantities of atomic hydrogen must be supplied via, in the reactor of Ref. 1, arc heaters. This results, for a given $SiCl_4$ input, in an increased flow rate which in turn may lead to a loss in collection efficiency for velocities $\gtrsim$ 50 m s^{-1}. The alternative is to decrease the $SiCl_4$ input, i.e., to decrease the production rate of silicon. One therefore concludes that conditions must be sought which will allow the reactor to operate with the minimum input enthalpy per kg of $SiCl_4$ input (chiefly in the form of H atoms) which permits negligible fume formation at flow velocities $\lesssim$ 50 m s^{-1}.

A series of calculations describing the Westinghouse reactor is therefore needed in which the enthalpy is varied over a wide range, the H/Si ratio is varied over a reasonable range of about 4 to about 20, and the Si input rate is varied over a range of $\approx$ 25 to $\approx$ 200 kg h^{-1}. Calculations over several meters of the flow tube are needed to (i) check for the onset of Si(ℓ) fume formation and (ii) determine wall collection efficiencies (the rate of Si deposition at the wall). GENMIX-MPDEU could be used to assure that wall deposition rates (for heat and mass) are being performed accurately and to scan a wider range of conditions economically. Such a series of runs should provide an excellent prediction of conditions under which such reactors may be operated with greatest silicon production rates at optimum collection efficiencies. Other useful information, such as the rates of heat transfer to walls, pressure drop, and composition throughout the reactor would also be obtained.

X. NEW TECHNOLOGY

No reportable items of new technology have been identified.

XI. REFERENCES

1. Fey, M.B., "Development of a Process for High Capacity Arc Heater Production of Silicon for Solar Arrays," Westinghouse Electric Corp., Quarterly Report, DOE/JPL 954589-78/6, April-June 1978.

2. Spalding, D.B., GENMIX: A General Computer Program for Two-Dimensional Parabolic Phenomena, HMT Series, Vol. 1 (Pergamon Press, New York, 1977).

3. Mikatarian, R.R., Kau, C.J., and Pergament, H.S., "A Fast Computer Program for Nonequilibrium Rocket Plume Predictions," Final Report, AeroChem TP-282, AFRPL-TR-72-94, NTIS AD 751 984, August 1972.

4. Launder, B.E., "Heat and Mass Transport," in Turbulence, Vol. 12, Topics in Applied Physics, P. Bradshaw, Ed. (Springer-Verlag, Berlin, 1976).

5. Patankar, S.V. and Spalding, D.B., Heat and Mass Transfer in Boundary Layers (Intertext Books, London, 1970); (a) pp. 19-22, (b) pp. 117-120.

6. Stephenson, P.L., "A Theoretical Study of Heat Transfer in Two-Dimensional Turbulent Flow in a Circular Pipe and between Parallel and Diverging Plates," Int. J. Heat Mass Transfer 19, 413 (1976).

7. Bankston, C.A. and McEligot, D.M., "Turbulent and Laminar Transfer to Gases with Varying Properties in the Entry Region of Circular Ducts," Int. J. Heat Mass Transfer 13, 319 (1970).

8. Crawford, M.E. and Kays, W.M., "STAN-5, A Program for Numerical Computation of Two-Dimensional Internal/External Boundary Layer Flows," Thermosciences Div. Mechanical Engng. Dept., Stanford University, Report No. HMT-23, 1975.

9. Reynolds, W.C., "Computation of Turbulent Flows," Ann. Rev. Fluid Mech. 8, 183 (1976).

10. Van Driest, E.R., "On Turbulent Flow Near a Wall," J. Aero. Sci. 23, 1007 (1956).

11. von Mises, R., "Bemerkungen zur Hydrodynamik," Z. Angew. Math. Mech. 7, 425 (1956).

12. Srivastava, R. and Rosner, D.E., "A New Approach to the Correlation of Boundary Layer Mass Transfer Rates with Thermal Diffusion and/or Variable Properties," Int. J. Heat Mass Trans. (in press).

13. Srivastava, R. and Rosner, D.E., "Falsification of Particle Size Distribution for Capture by Simultaneous Brownian Motion and Thermophoresis," Int. J. Heat Mass Trans. (to be submitted).

14. Rosner, D.E., "Thermal (Soret) Diffusion Effects on Interfacial Mass Transport Rates," J. Physicochemical Hydrodynamics 1, No. 1 (in press).

15. Lin, C.S., Moulton, R.W., and Putnam, G.L., "Mass Transfer between Solid Wall and Fluid Streams," Ind. Eng. Chem. 45, 636 (1953).

16. Chapman, S. and Cowling, T.G., The Mathematical Theory of Non-Uniform Gases (Cambridge University Press, Cambridge, 1952).

17. Svehla, R.A., "Estimated Viscosities and Thermal Conductivities of Gases at High Temperature," NASA Tech Rept. R-132, 1962.

18. Grew, K.W. and Ibbs, T.C., Thermal Diffusion in Gases (Cambridge University Press, Cambridge, 1952).

19. Hidy, G.M. and Brock, J.R., Dynamics of Aerocolloidal Systems (Pergamon Press, New York, 1970).

20. Millikan, R.A., Phys. Rev. 22, 1 (1923).

21. Einstein, A., Ann. Physik 17, 549 (1905); see also Investigations on the Theory of Brownian Movement, R. Furth, Ed., (Dover, New York, 1956).

22. Bird, R.B., Stewart, W.E., and Lightfoot, E.N., Transport Phenomena (John Wiley, New York, 1960).

23. Hirschfelder, J.O., Curtiss, C.F., and Bird, R.B., Molecular Theory of Gases and Liquids (John Wiley, New York, 1954).

24. Phillips, W.F., "Motion of Aerosol Particles in a Temperature Gradient," Phys. Fluids 18, 144 (1975).

25. Waldmann, L. and Schmitt, K.H., "Thermophoresis and Diffusiophoresis of Aerosols," Aerosol Science, C.N. Davies, Ed. (Academic Press, New York, 1966) Chap. VI.

26. von Karman, Th., "The Analogy between Fluid Friction and Heat Transfer," Trans. ASME 61, 705 (1939).

27. Graetz, L., Ann. Phys. Chem. 25, 337 (1885).

28. Walker, K.L., Homsy, G.M., and Geyling, F.T., "Thermophoretic Deposition of Small Particles in Laminar Tube Flow," J. Colloid Interface Sci. 69, 138 (1979).

29. Goren, S.I., "Thermophoresis of Aerosol Particles in the Laminar Boundary Layer on a Flat Plate," J. Colloid Interface Sci. 61, 77 (1977).

30. Rosner, D.E. and de La Mora, J.F., "Recent advances in the Theory of Salt/Ash Deposition in Combustion Systems," Proceedings DOE/EPRI Conference on Advanced Materials/Alternate Fuel Engines (Castine, ME, in press, 1979).

31. Lapidus, L. and Schiesser, W.E., Numerical Methods for Differential Systems: Recent Developments in Algorithms, Software and Applications (Academic Press, New York, 1976).

32. Madsen, N.K. and Sincovec, R.F., "PDECOL: General Collaction Software for Partial Differential Equations," Lawrence Livermore Laboratory, PREPRINT/UCRL-78263 (Rev. 1), July 1977.

33. Carnahan, B., Luther, H.A., and Wilkes, J.O., Applied Numerical Methods (Wiley, New York, 1969).

34. JANAF Thermochemical Tables (Dow Chemical Company, Midland, MI, continuously updated).

35. Ferri, A.J., "Review of Problems in Applications of Supersonic Combustion," J. Roy. Aeron. Soc. 68, 575 (1964).

36. Schlichting, H., Boundary Layer Theory (Pergamon Press, New York, 1955).

37. Ting, L. and Libby, P.A., "Remarks on the Eddy Viscosity in Compressible Mixing Flows," J. Aero. Sci. 27, 797 (1960).

38. Donaldson, C. duP. and Gray, K.E., "Theoretical and Experimental Investigation of the Compressible Free Mixing of Two Dissimilar Gases," AIAA J. 4, 2017 (1966).

39. Soo, S.L., Fluid Dynamics of Multiphase Systems (Blaidell, Waltham, MA, 1967) Chap. 2.

40. Fuchs, N.A., The Mechanics of Aerosols (Macmillan, New York, 1964) p. 27.

41. Bauer, S.H. and Frurip, D.J., "Homogeneous Nucleation in Metal Vapors. A Self-Consistent Kinetic Model," J. Phys. Chem. 81, 1015 (1977).

42. Keck, P.H. and Van Horn, W., "Surface Tension of Liquid Silicon and Germanium," Phys. Rev. 91, 511 (1953).

43. Glasor, M.V., Liquid Semiconductors (Plenum Press, New York, 1969).

44. Hwang, B.C. and Gould, R.K., "Rocket Exhaust Ground Cloud/Atmospheric Interactions," Final Report, AeroChem TP-362, NASA CR-145255, 1977.

45. Zebel, G., "Coagulation of Aerosols," Aerosol Science, C.N. Davies, Ed. (Academic Press, New York, 1966) Chap. 2.

46. Saffman, P.G. and Turner, J.S., "On the Collision of Drops in Turbulent Clouds," J. Fluid Mech. 1, 16 (1956).

47. Friedlander, S.K., Smoke, Dust and Haze (Wiley, New York, 1977) p. 107.

48. Fuchs, N.A., The Mechanics of Aerosols (Macmillan, New York, 1964) pp. 204-212.

49. Hinze, J.O., Turbulence, 2nd Ed. (McGraw-Hill, New York, 1975). p. 622.

APPENDIX A

DEFINITION OF THE PARTICLE TRANSPORT EQUATION

The particle transport equation, in primitive variables, has the form:

$$u \frac{\partial Y_i}{\partial x} + (v - v_s) \frac{\partial Y_i}{\partial r} = D_{eff} \frac{\partial^2 Y_i}{\partial r^2} + \frac{r_i'''}{\rho} \tag{A1}$$

where, for the axisymmetric flow geometry,

$$v_s \equiv \frac{1}{r} D_{eff} + \frac{1}{\rho} \frac{\partial}{\partial r} \left\{ \rho \, D_{eff} \right\} + D_i \, \alpha_i (1 - 2Y_i) \left(\frac{1}{T} \frac{\partial T}{\partial r} \right) \tag{A2}$$

(pseudo suction velocity

$$r_i''' \equiv \rho \, K \, Y_i (1 - Y_i) \qquad \text{(pseudo volumetric reaction rate)} \tag{A3}$$

with the pseudo specific rate constant given by

$$K \equiv \left[\left\{ \frac{1}{r} D_i \alpha_i + \frac{1}{\rho} \frac{\partial}{\partial r} (\rho \, D_i \alpha_i) \right\} \frac{1}{T} \frac{\partial T}{\partial r} + D_i \alpha_i \frac{1}{T} \left\{ \frac{\partial^2 T}{\partial r^2} - \frac{1}{T} \left(\frac{\partial T}{\partial r} \right)^2 \right\} \right] \left(\frac{\delta_m^{\,2}}{D_{i_e}} \right) \tag{A4}$$

After the equations above are non-dimensionalized according to the following scheme:

$$\tilde{Y}_i \equiv (Y_i - Y_{i_w}) / (Y_{i_M} - Y_{i_w}) \tag{A5a}$$

$$\tilde{u} \equiv u/u_E \tag{A5b}$$

$$\tilde{v}_{eff} \equiv v_{eff}/u_E, \quad \text{where } v_{eff} \equiv v - v_s \tag{A5c}$$

$$\tilde{r} \equiv (r - r_w)/(r_M - r_w) \tag{A5d}$$

$$\mathcal{D} \equiv K \, \delta_m^{\,2}/D_{i_e} \tag{A5e}$$

one obtains the following definitions for the five coefficients that appear in the particle transport equation:

$$A \equiv \left(\frac{L}{\delta_m \, \tilde{u} \, u_E}\right) (-v) \tag{A6a}$$

$$B \equiv \left(\frac{L}{\delta_m \, \tilde{u} \, u_E}\right) (v_{s_1}) \tag{A6b}$$

$$C \equiv \left(\frac{L}{\delta_m \, \tilde{u} \, u_E}\right) (v_{s_2}) \tag{A6c}$$

$$D \equiv \left(\frac{L}{\delta_m^{\,2} \, \tilde{u} \, u_E}\right) D_{eff} \tag{A6d}$$

$$E \equiv \mathcal{D}\left(\frac{L \, D_{i_e}}{\delta_m^{\,2} (Y_{i_m} - Y_{i_W}) \, \tilde{u} \, u_E}\right) \tag{A6e}$$

where

$$v_{s_1} \equiv \frac{1}{r} D_{eff} + \frac{1}{\rho} \frac{\partial}{\partial r} (\rho \, D_{eff}) \tag{A7a}$$

$$v_{s_2} \equiv D_i \alpha_i \left(\frac{1}{T} \frac{\partial T}{\partial r}\right) \tag{A7b}$$

$$D_{eff} \equiv D_i + \varepsilon_p \tag{A7c}$$

Appendixes B through H are published in a separate supplementary volume, DOE/JPL-954862-79/8A.